The determination of the momentum dependence of the ionisation loss of fast cosmic-ray particles in neon

Jones, D.G.

THE DETERMINATION OF THE MOMENTUM DEPENDENCE OF THE IONISATION LOSS OF FAST COSMIC-RAY PARTICLES IN NEON

A thesis submitted to the University of Durham

for the Degree of Doctor of Philosophy

by

D.G. Jones, B.Sc.

July, 1961

PREFACE

This thesis describes two projects. The first concerns the Author's share of the design, construction and operation of the Durham High Energy Cosmic Ray Spectrograph. This consisted in the development of an automatic momentum analyser and its operation over a period of several months during which time some 250,000 particles were recorded. The development of a momentum selector with which very high energy particles may be selected is also described.

The second project is concerned with an experiment using the spectrograph in a measurement of the ionisation loss of relativistic μ-mesons in neon. This experiment was the responsibility of the Author alone. The design and construction of the proportional counters and ancillary electronic equipment used in the experiment are described and preliminary results are given of the variation with momentum of the ionisation loss of fast μ -mesons in neon.

This work was carried out at the University of Durham under the supervision of Dr. A.W. Wolfendale.

Some of the results of the work with the spectrograph have been published by the Author and his colleagues; Ashton et al, 1960.

CONTENTS

12.4. Conclusions

CHAPTER 1

INTRODUCTION

1.1. General features of the Cosmic Radiation

The primary cosmic ray flux at the top of the atmosphere has been shown to consist predominantly of protons with smaller numbers of alpha particles and heavier nuclei. On entering the atmosphere the primary particles interact with the nuclei of the air molecules with a mean free path of about 125 gm cm^{-2}. Thus most of the interactions take place in the first few hundred gm cm^{-2} of the atmosphere, i.e. at heights above about 10 km.

Although the flux of primary particles falls with increasing energy, in many cases the energies involved in the collisions are considerably above the threshold for π -meson production. The π -mesons are unstable particles with a mass of about 270 electron masses and are produced in both neutral and charged states. The neutral π^0-meson has a half life $< 5 \times 10^{-16}$ sec. and decays into two photons. The charged $\pi^{\pm}$-meson has a half life of 2.56×10^{-8} sec. and decays into a $\mu^{\pm}$ -meson and a neutrino. As a consequence of the very short half life of the π^0 -meson the photons are formed very close to the point of collision whereas the $\pi^{\pm}$-mesons have some probability of interacting before decay, especially when their velocity is high enough for time dilation to be important. At a depth of a few hundred gm cm^{-2} however, the air density is so low

that only the very fast $\pi^{\pm}$-mesons (energy > 100 GeV) have an appreciable chance of interacting before they are essentially 'removed' by π-μ decay.

The photons produced when a π^{0}-meson decays interact strongly with the electromagnetic fields of the air nuclei and produce electron-pairs. Some fast electron production also occurs by the Compton effect. These fast electrons lose energy by ionisation and, to a greater extent, by Bremsstrahlung radiation. Thus further photons are produced which, in turn, produce more electron pairs. The result is that an electron-photon cascade is built up which is propagated through the atmosphere. If the energy of the initial particle is sufficiently high a significant number of electrons may penetrate to sea level, constituting an 'extensive air shower'; for example a primary cosmic ray of energy 10^{14} eV produces a shower of about 2,000 electrons at sea level.

In the vast majority of interactions however, the π -mesons are emitted with comparatively low energy and after very few generations the energies of the individual photons fall below that necessary for pair-production, and other non-multiplicative processes complete the energy degradation. These small showers die out in the upper levels of the atmosphere.

As mentioned already, the charged $\pi^{\pm}$-meson decays into a $\mu^{\pm}$-meson (of mass 206 m_e) and a neutrino. Of these particles the $\mu^{\pm}$-meson is of greater importance in so far as development of the cosmic radiation is concerned, since, although the neutrino

carries off an appreciable fraction of the energy of the $\pi^{\pm}$ -meson, its cross-section for interaction with nuclei is only $\sim 10^{-45}$ cm^2 and therefore vanishingly small. The μ -meson is a far more stable particle than the $\pi^{\pm}$ -meson having a half life against decay of 2.22×10^{-6} sec. Its interaction with nuclei is very weak and, at energies below about 10^{12} eV, the most important source of energy loss is due to ionisation which, for a high energy μ -meson in air, amounts to about 2 Mev/gm cm^{-2}, i.e. about 2 GeV for traversal of the whole atmosphere. Many of the μ -mesons therefore reach sea level and the more energetic particles even penetrate far underground. The μ -mesons which decay do so into an electron and two neutrinos. These decay electrons undergo some slight cascade multiplication and are responsible for some of the electron-photon component at sea level. The remainder is due to electrons which have been knocked on by fast μ -mesons and those electrons and photons which reach sea level from cascades initiated by π°-mesons.

The cosmic ray flux at sea level therefore consists predominantly of μ -mesons, electrons and photons with smaller numbers of protons, neutrons and π -mesons. There is also a very small component of unstable mesons of higher masses and other strange particles.

1.2 The Sea Level Spectrum

Significance of the Spectrum

In order to obtain information on both the oualitative and quantitative aspects of Cosmic Rays, measurements of the momentum spectrum have been made at various altitudes and below ground. The work to be described is concerned with measurements of the sea level spectrum. A precise knowledge of this spectrum is important for a variety of reasons. Apart from its own intrinsic worth it is possible by comparison with other data to obtain information on several aspects of Cosmic Radiation. These may be conveniently listed:

(1) A comparison with the depth-intensity curve provides information on the energy loss of very high energy μ -mesons.

(2) A comparison with the spectrum at different depths underground yields similar information, but in this case as the spectra can be compared at different momenta a comparison with the spectrum obtained at one point underground is equivalent to several measurements on the depth intensity curve.

(3) A comparison with the sea level spectrum predicted from a knowledge of the primary cosmic ray spectrum and the diffusion equations of the various components is an indirect source of information on very high energy nucleon-nucleon interactions.

(4) A study of the time-variation of the sea level spectrum, its energy dependence and its correlation with terrestial or extraterrestial phenomena may provide information on the sources of cosmic radiation.

Previous measurements

A review of the technique and instruments used by previous workers is given in Chapter 2. The most precise measurements have been made with magnetic spectrographs, notably those at Manchester, Hyams et al (1950), and Sydney, Caro et al (1951). The Manchester group have measured the spectrum from 0.5 to 20 GeV/c, making measurements on some 20,000 particles. Later modifications of the Manchester Spectrograph extended the upper limit of measurement to 300 GeV/c (Holmes et al, 1955) and a preliminary analysis by Rodgers (1957), based on 1000 particles of momenta >20 GeV/c, has yielded some interesting results. Using the method of item 1 above, an unexpectedly high value for the energy loss of very high energy μ -mesons was found. Also, an increasing difference between the predicted and experimental sea level spectra with increasing energy appeared to indicate a large contribution to the fast μ -meson flux at sea level from sources other than the decay of π -mesons.

Future measurements

The spectra determined by the instruments at Manchester and Sydney are not in very good agreement in the common momentum region <20 GeV/c. This may be due to the differing experimental bias in

the two instruments, but further precise measurements are required both to decide the issue and to improve the statistics.

The work of Rodgers has shown the importance of measurements of the spectrum at momenta >100 GeV/c, but more results are required and an extension to higher momenta.

The study of the time variation of the sea level spectrum as opposed to the total flux offers considerable scope for future work.

In order to carry out this programme an instrument is required which has not only a high maximum detectable momentum, but also a high rate of particle collection, without which good 'statistics' will take time to attain. The Durham Spectrograph has been built to satisfy these requirements and has a maximum detectable momentum $\sim 10^{12}$ eV/c with an overall collection rate of 3.5/min. and a rate above the maximum detectable momentum of rather less than 1/day. The Spectrograph will be considered in detail in Chapter 2.

Automatic Analysis of Particle Momentum

A number of methods have been employed for the determination of particle momenta in magnetic spectrographs. Probably the simplest is that used by Hyams et al (1950), and described by Owen (1950), where the counters discharged by the ionising particle are recognised by a hodoscope arrangement. The magnetic deflection is then found by a simple calculation. Another method has been used by Caro et al (1951) in which the hodoscope is replaced by a punched card system. Both methods suffer from the disadvantage that the data produced directly by the instrument is not the quantity actually required,

viz, the magnetic deflection, and further analysis of the data is required. At high rates this problem is serious and some form of automatic analysis is required. The punched card system lends itself to automatic analysis, but the cost is rather great, and the system is rather inflexible. A purely electronic system would obviously be advantageous.

Owen (unpublished) has used an analogue pulse circuit in which the pulses are added simultaneously to permit the rather coarse division of particles into groups of high and low momenta. A refined version of this circuit has been developed for use in conjunction with the Durham Spectrograph.

1.3 Measurements On High Energy μ-Mesons

Two types of experiments can be carried out with cosmic ray spectrographs. The first type concern measurements of spectra, positive-negative ratio etc., and their comparison with other cosmic ray measurements. In the seond type the spectrograph is used as a source of high energy particles of known momentum and sign; the particles being predominantly μ-mesons. The interactions of these particles with atomic electrons and nuclei can therefore be studied. It is experiments of this type that are the special concern of the author.

The study of the behaviour of strongly interacting particles, protons, π-mesons etc., is the province of the accelerating machines, at least for energies below about 30 GeV. The position

with regard to μ-mesons is otherwise. On account of the comparatively long life time of fast π-mesons the generation of pure beams of μ-mesons is difficult and at the present time there appear to have been no machine experiments carried out with μ-mesons of energy above one GeV. Experiments with high energy μ-mesons are therefore still in the province of the cosmic ray physicist.

1.4. Statement of work to be described

The work to be described concerns the construction of the Durham Cosmic Ray Spectrograph, in particular the design, construction and operation of the apparatus associated with the automatic analysis of the particle momenta. The first part of this thesis is devoted to a description of this apparatus together with a brief summary of the results which have been obtained.

The second part of the thesis is concerned with a specific experiment with the spectrograph; the measurement of the ionisation loss of μ-mesons in a gas. The momentum of the μ-meson is determined by the spectrograph and the ionisation loss measured using neon filled proportional counters placed in the particle 'beam'.

CHAPTER 2

THE MEASUREMENT OF COSMIC RAY MOMENTA

2.1. Introduction

It has been pointed out that measurements of the momenta of sea level cosmic rays are useful and some discussion will be given of the various methods available.

The momentum or energy of a charged particle can be determined by observing its behaviour when acted upon by either electromagnetic or nuclear forces. The theory of electromagnetic interactions is well developed and forms a self consistent whole whereas nuclear forces have proved much more difficult to investigate, both experimentally and theoretically. So far as measurements on μ-mesons are concerned, the methods used to measure momentum or energy have been electromagnetic in nature. The methods are based on measurement of range, scattering or magnetic deflection.

2.2. Range measurements

The flux of cosmic rays from a given direction is selected by some form of telescope, usually comprising two or three sets of geiger counters connected in coincidence, and the flux measured with different thicknesses of absorber above the apparatus. This yields the integral range spectrum.

Two modifications of this basic apparatus are also used. One is concerned with the direct measurement of the differential spectrum. This spectrum can be obtained from the results which gave the integral

spectrum, but this is unsatisfactory from a statistical standpoint. The modification consists in placing a further absorber below the telescope and counting only those particles whose range is greater than the thickness of the upper absorber and less than the combined thickness of the two absorbers. This is done by using another detector connected in anticoincidence with the other counters. The other modification is designed to deal with the shorter ranges, where the electron component becomes comparable with the μ -meson component, and it is necessary to distinguish between the two. This is carried out by using the apparatus designed for direct measurement of the differential spectrum, but only selecting these events in which a particle is brought to rest in the lower absorber and is followed by the delayed emission of an electron. The method is rather uncertain, especially for absolute measurements, as it is difficult to predict the detection efficiency for the decay electron.

The range method has been used by various workers to measure the range spectrum at sea level over a range of 10 to 10^4 gm cm^{-2} of air. Lead can be used as the absorber for the low ranges, but becomes impracticable for higher momenta and it is necessary to use naturally occurring absorbers; the experiments being performed either at different depths under water or underground.

2.3. Scattering measurement

Measurements of multiple coulomb scattering in a multi-plate cloud chamber, or in a nuclear emulsion, have been used to determine

the momenta of charged particles, usually under conditions where more satisfactory instruments could not be used: for example at the top of the atmosphere (emulsions) or far underground (emulsion and multi-plate cloud chambers).

The Multi-plate Cloud Chamber

The cloud chamber is controlled by geiger counters which cause it to operate when a particle passes through the sensitive region of the instrument. The statistical accuracy of the measurements is limited by the number of observations of the angle of scattering and therefore by the number of plates. Increasing the number of plates, however, aggravates the turbulence caused by convection currents in the chamber and the number of plates used is rarely more than 10. The uncertainty in momentum of a single particle is usually in the region of 30% or more.

This technique is of limited use in measuring the momentum spectrum of cosmic rays owing to the low upper limit of measurement ~ 5 GeV/c imposed by turbulence, and the poor statistical accuracy. It has been used to study the low momentum region (up to 1 GeV/c) of the spectrum underground (Nash & Pointon, 1956). Its main application, however, is in the study of the nature and momenta of particles produced in interactions in the plates, and in this connection it has been used, for example, to investigate the interactions of μ -mesons underground.

The Nuclear Emulsion

The procedure used in measurement is to divide the track up into convenient cells and either measure the mean inclination of each segment or, more usually, measure the co-ordinates of the cell boundaries with respect to some fixed line. The angular deviations are then found from the second differences of these co-ordinates.

The actual relationship between $p\beta$ (the product of the momentum and the particle velocity in units of c, i.e. v/c) and the angular deviation depends on the form that the measurements take and also on the cut-off criterion applied to large single scatters, but it can always be expressed in the form $p\beta = \frac{k}{\langle\theta\rangle}$ where k is a constant and $\langle\theta\rangle$ is the particular mean value of θ used. The maximum value of $p\beta$ that can be measured depends on the size of the grains of the emulsion, mechanical imperfections in the microscope stage, the length of the cell and the magnitude of distortions in the emulsion. The maximum length of cell is usually governed by statistical considerations of the number of cells available. The error to be attached to a measurement in the case of a long track is $\sim 5\%$ and the maximum value of $p\beta$ is ~ 10 GeV.

2.4. Magnetic Deflection Measurements

The early work was carried out using counter controlled cloud chambers with a uniform magnetic field applied transversely across the chamber. Blackett (1937) and Wilson (1946) using this technique measured the differential sea level spectrum up to 15 GeV/c.

Theory shows that the momentum of a charged particle with unit electronic charge is given by the relation:

$$p = 300\, H\rho$$

where p is in eV/c, H is in gauss and the radius of curvature of the trajectory ρ is in cm. The equation is relativistically invariant.

Consider a section of the trajectory of a charged particle in a uniform transverse magnetic field. Let the length of the chord be l and the sagitta be s. Then:

$$p \simeq 300\, H\, \frac{l^2}{8s} \qquad \text{if} \quad s \ll \rho$$

and the highest momentum that can be measured for a given value of H and l will depend on the uncertainty in s. The error in s will be the sum of the instrumental error due to finite track width, turbulence, etc. and the error due to multiple scattering. The error due to multiple scattering varies as $1/p\beta$, so that at high momenta the fractional error in the momentum tends to a constant value. On the other hand the instrumental error in s is independent of the momentum of the particle, and the fractional error in the momentum determination therefore increases as the momentum increases.

The instrumental error is determined by operating the chamber without magnetic field and measuring the mean of the apparent values of s for high energy particles, for which the error due to scattering is negligible. The corresponding value of momentum is known as the maximum detectable momentum.

A lower limit of momentum measurements is set by the multiple scattering which increases as the momentum decreases, but in spectrum measurements this limit is not reached as a cut off is imposed due to low momentum particles being deflected out of the system by the magnetic field.

The maximum detectable momentum can be increased by:

1. Increasing the value of H. This is limited by saturation in iron-cored magnets. Air-cored coils of the Helmholtz type have been used, but to surpass the performance of existing iron-cored magnets the power requirements would be of the order of megawatts.

2. Increasing the track length. This requires both a larger magnet and a larger cloud chamber. A larger cloud chamber means in general a longer cycling time, with a consequent increased loss of events; also the greater turbulence due to increased convection currents may cancel out any gain due to increased track length.

It seems likely that the limit has been reached with the magnet cloud chamber technique and other techniques are necessary in order to extend the range of investigation to higher momenta.

2.5. Magnetic Spectrographs

The optical arrangement for photographing the tracks in a magnet-cloud chamber are such that the full potentialities of the uniform field region of a given magnet are not realised, and the non-uniform field region is, of course, not used at all. Hyams

et al (1950) give a figure of 5% for the ratio of $\int HdV$ (V - volume) used to total value of $\int HdV$ for a typical magnet-cloud chamber.

A great advance in the magnetic deflection technique was made when instruments were devised which used almost all of the field region. In this method the direction of the particle trajectory before and after deflection is measured, the detecting elements lying outside the field region. Thus, besides making much fuller use of the magnetic field, the distance between location points can be increased independently of the magnet dimensions.

Several instruments employing this principle (spectrographs) have been operated. The first high energy spectrograph was the instrument at Sydney (Caro et al, 1951). A diagram of this spectrograph is shown in Fig. 2.5.1. Each of the three sets of geiger counters used to locate the particle trajectory consists of two overlapping layers of counters connected so as to be equivalent to a single layer of counters of one third the diameter. The magnetic field is produced by an electromagnet with appropriately shaped pole pieces. The maximum value of H is 13,500 gauss giving a value of $\int Hdl$ of 7.4×10^5 gauss-cm and a maximum detectable momentum of $\sim$100 GeV/c. The instrument has been used to measure the sea level spectrum at vertical incidence (Caro et al, 1951) and at angles to the vertical (Moroney & Parry, 1954).

A diagram of a later spectrograph, the Manchester instrument (Hyams et al, 1950) is shown in Fig. 2.5.2. Two magnets are used here with three sets of geiger counters to locate the particle

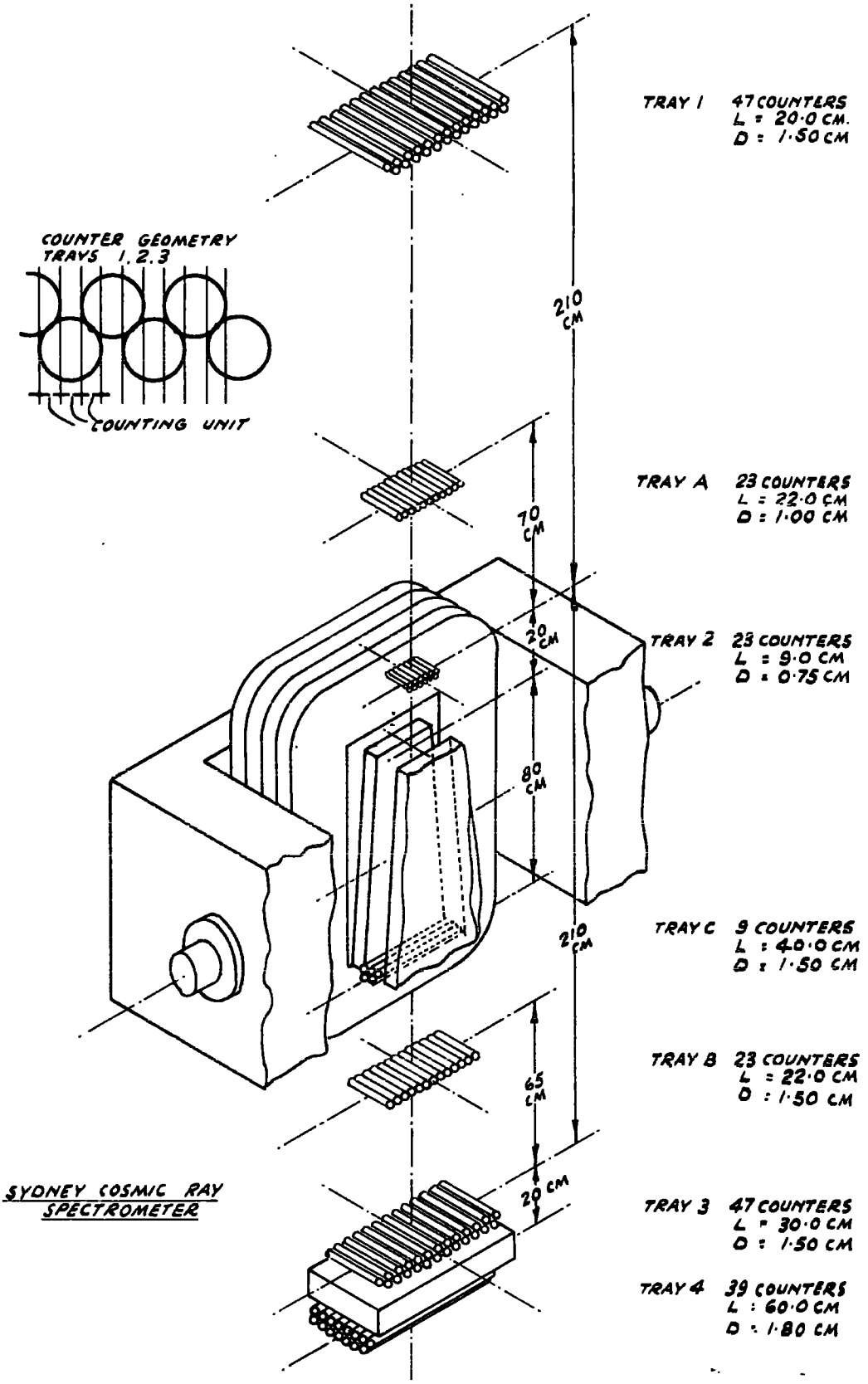

FIG. 2.5.1. THE SYDNEY SPECTROGRAPH

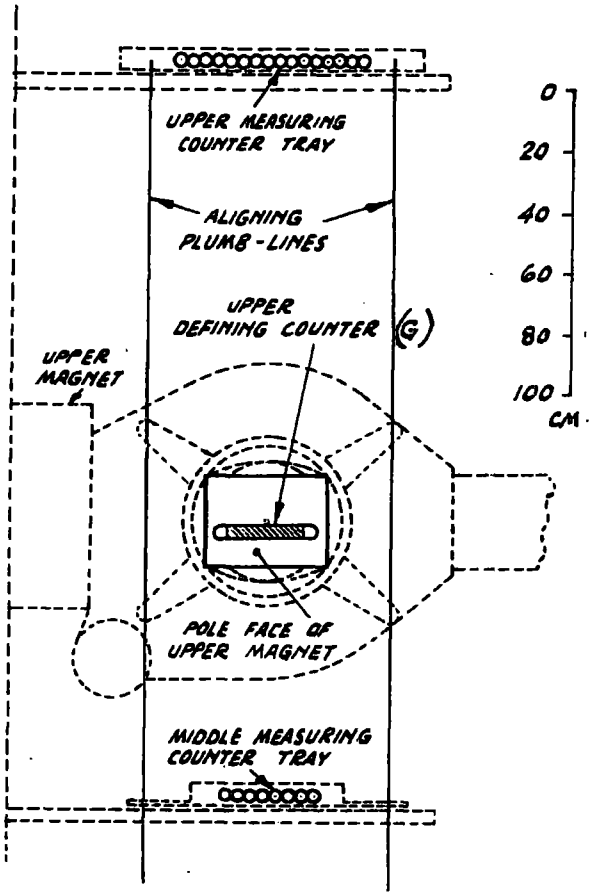

VIEW OF UPPER HALF OF INSTRUMENT WHICH IS SYMMETRICAL ABOUT MIDDLE COUNTER TRAY

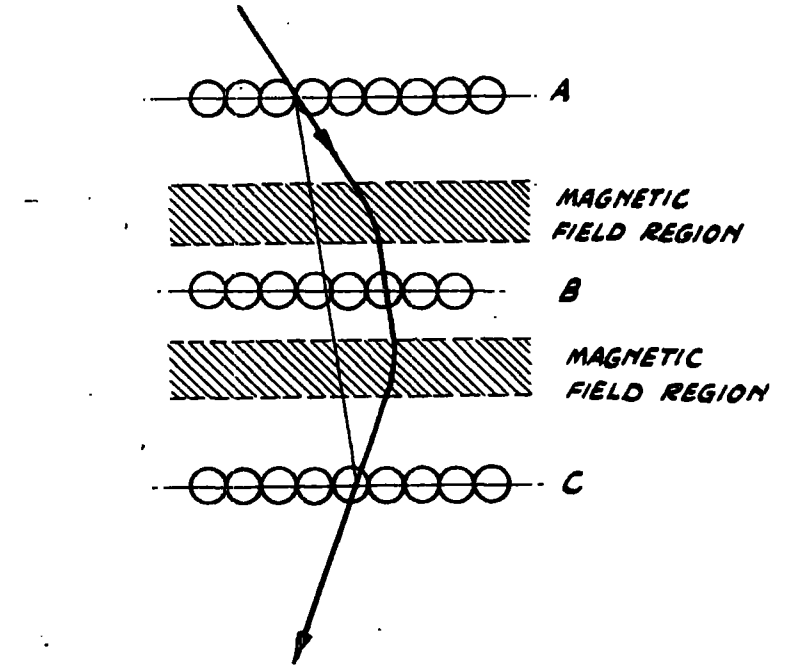

PARTICLE TRAJECTORY THROUGH INSTRUMENT

FIG. 2.5.2. THE MANCHESTER SPECTROGRAPH

trajectory. The counters designated G ensure that the particle actually passes through the air gaps of the two magnets and also reduces the number of spurious events. The two magnets are operated with their fields similarly directed and the total value of $\int Hdl$ at maximum field is $\sim 12.8 \times 10^5$ gauss cm yielding an m.d.m. (maximum detectable momentum) of ~ 20 GeV/c.

Geiger counters are not the only detectors that have been used in this type of spectrograph. Glaser et al (1950) used two cloud chambers one above and one below the magnet, attaining an m.d.m. of ~ 70 GeV/c by this method. This arrangement suffers, however, from two defects when compared with the two instruments described above.

1. The long cycling time of the cloud chambers limits the rate of particle collection.
2. The instrumental errors are not constant, so that the m.d.m. may vary over the period of the experiment.

Both of these defects apply wherever cloud chambers are used in spectrographs.

Cloud chambers have also been used in the Manchester Spectrograph to increase the m.d.m. to ~ 300 GeV/c (Rodgers, 1957). The modification to the Manchester instrument consisted in placing horizontal shallow cloud chambers just above each tray of geiger counters. The chambers were controlled by the five-fold coincidence

between the three trays of locating counters and the two sets of guard counters, and by photographing the tracks in all three cloud chambers simultaneously it was possible to locate the particle trajectory at each level to within $\pm$ 0.8 mm.

The work of Rodgers with the modified instrument has been outlined above. The rate of particle collection by this instrument is limited by the use of two magnets, and although the cycling time is not so important at high momenta, when a system of preliminary momentum selection is used, the other disadvantage of cloud chamber systems, the inconstancy of the m.d.m., is very important.

A spectrograph has been constructed at Durham with the aim of achieving a high rate of particle collection, coupled with a high m.d.m. This instrument also uses two forms of particle detection; Geiger counters for low momenta and neon flash-tubes (Conversi, 1955) for high momenta. In this case the m.d.m. is constant for a given arrangement, being set by the geometrical properties of the flash-tubes. The rate of particle collection is also improved over that of the Manchester instrument by using one magnet and detecting trays of large area.

CHAPTER 3

THE DURHAM COSMIC RAY SPECTROGRAPH

3.1. The geometrical arrangement

A schematic diagram of the instrument is shown in Fig. 3.1.1. The particle trajectory through the apparatus is defined by Geiger counters in the five levels designated A, B, C, D & G. The counters in A, B, C & D locate the position of the trajectory and the counters in G ensure that it also passes through the magnetic field.

The distance from the extreme counter trays to the centre of the magnetic field is 2.67 m and the solid angle subtended by these trays at the centre of the instrument is 8.0×10^{-2} sterad. 25 geiger counters are used in the trays A & D and 11 in each of the trays B & C. All the counters have internal diameter 3.6 cm and are spaced 3.8 cm apart in each tray. The counters in A & D are 60 cm long and those in B, C & G are 26 cm long. The entire system is aligned by two hanging wires to an estimated accuracy of 0.25 mm at each level.

3.2. The Magnetic Field

The magnet is an air-cooled Blackett-type electromagnet operating at a maximum current of 70 amps at 440 volts. The pole faces are 30 x 40 cm with the longer dimension horizontal. With the existing pole gap of 15 cm the maximum field strength is 12,010 gauss and the line integral, $\int Hdl$, for vertical trajectories through the centre of the field is 6.60×10^5 gauss-cm.

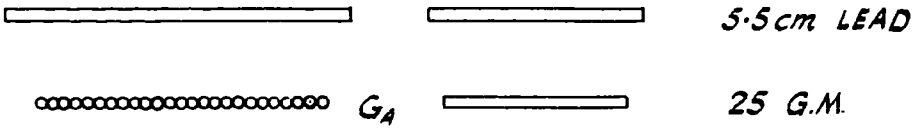

FIG. 3.1.1. THE DURHAM SPECTROGRAPH (COUNTER SECTION ONLY)

The value of the line integral $\int Hdl$ has been determined by two methods. Firstly by the indirect method of measuring the value of H at various points with a fluxmeter and evaluating the integral numerically, and secondly by using the deflected wire technique. The two methods give concordant results to within 1%.

3.3. Particle rates

The rate of particles through the spectrograph varies from 5.5 min^{-1} at zero field to 3.6 min^{-1} at maximum field. The decrease in rate with increasing magnetic field is due to the reduction in acceptance angle for particles of large deflection.

3.4. The accuracy of momentum measurement

Using the nomenclature of Fig. 3.4.1. the momentum of a particle is given by:

$$p = \frac{D}{(a-b) + (d-c)} \times 300 \int Hdl \quad eV/c$$

In practice the deflection (a-b) + (d-c) is measured in terms of geiger counter diameters and each particle is allotted to a momentum category n given by the relation

$$n = (n_A + n_D) - (n_B + n_C)$$

where n_A, etc. refers to the number of the counter discharged in layer A etc. The finite diameter of the counters imposes an instrumental limit on the accuracy of the momentum determination. Another limit is imposed by scattering in the instrument.

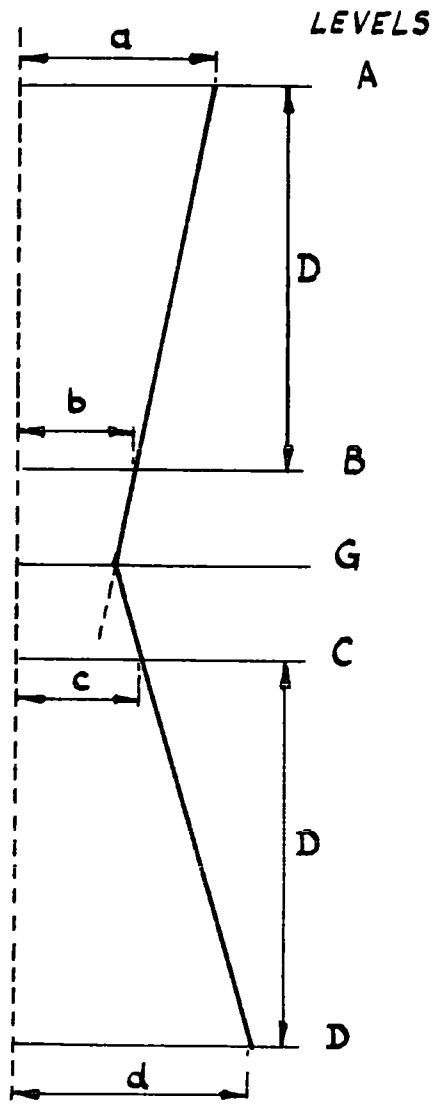

N.T.S.

FIG. 3·4·1

The Instrumental Limit

The uncertainty due to finite size of the geiger counters is given, for large category numbers, n, by the approximate relation

$$\delta p/p = \frac{0.3}{n}$$

At high moments, i.e. low category numbers, the error is not symmetrical and it is necessary to determine the complete momentum spectrum for particles within the category.

The momentum spectrum for a given category is found as follows. The acceptance function of the category is determined as a function of momentum (or, more precisely, the displacement of the particle trajectory). The product of this function and the intensity of the incident differential spectrum for given values of momentum then gives the required momentum spectrum for tho category. The acceptance function has been determined by making a series of trial measurements on a scale diagram of the spectrograph and has also been evaluated analytically.

As an example, the author used the sea level spectrum measured by the Manchester group and the acceptance function derived analytically by a colleague, Mr. J.L. Lloyd, to determine the momentum spectrum for categories n = 2 and n = 10. They are shown in Fig. 3.4.2. and Fig. 3.4.3.

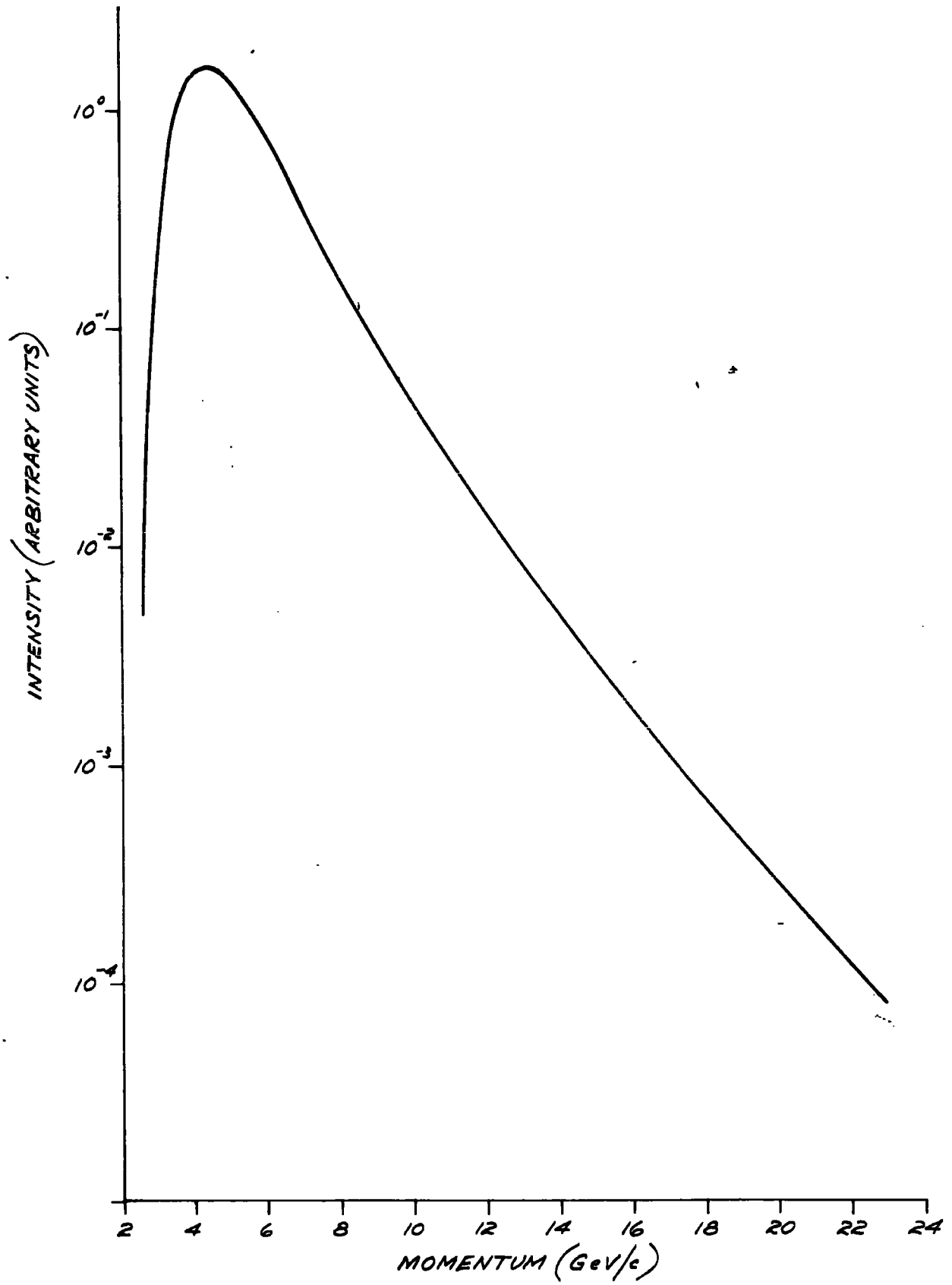

FIG. 3.4.2. THE MOMENTUM SPECTRUM FOR CATEGORY 2.

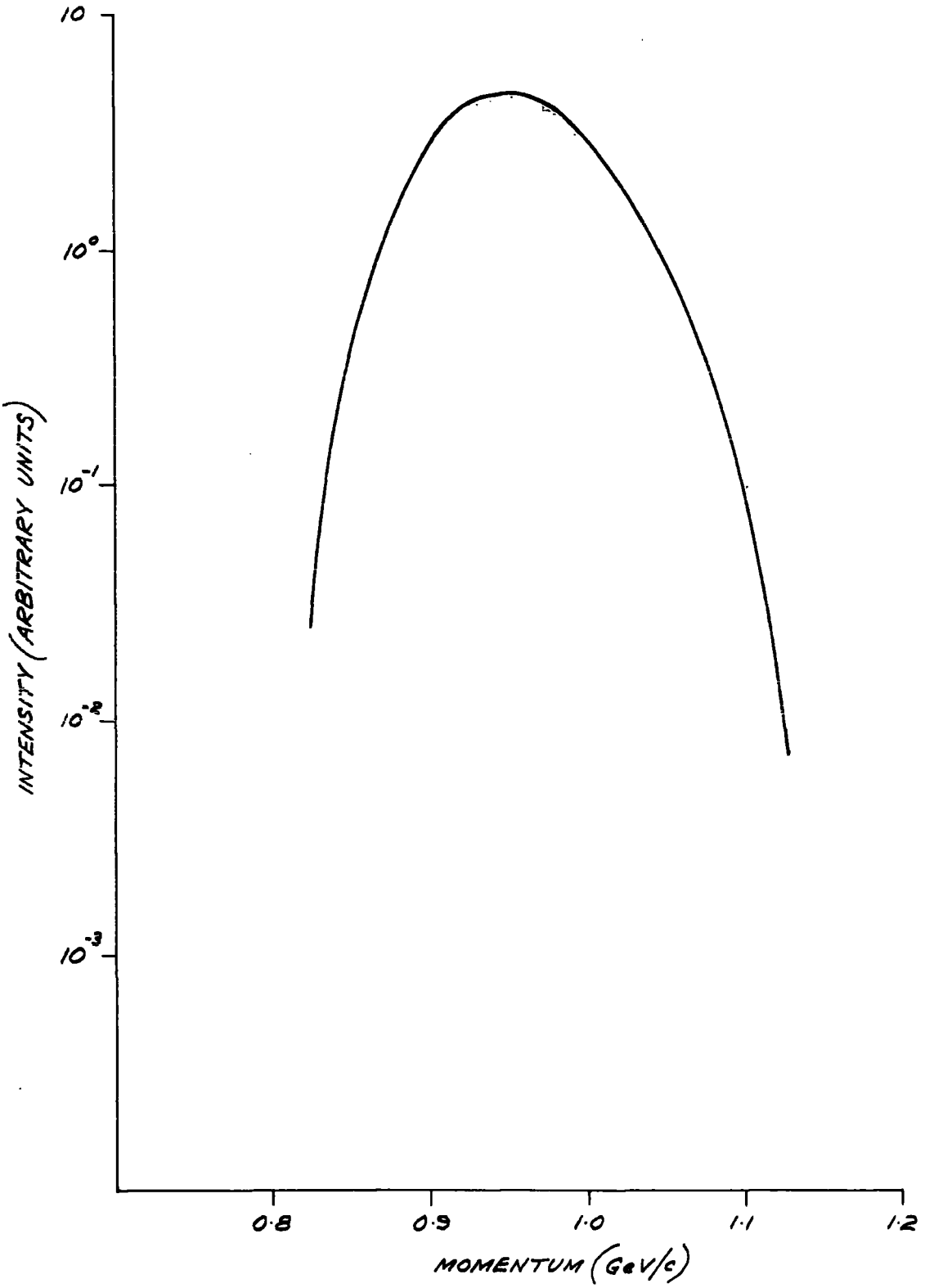

FIG. 3.4.3. THE MOMENTUM SPECTRUM FOR CATEGORY 10.

Scattering

The uncertainty in momentum due to scattering has been calculated. At maximum field strength and with the geiger counters alone the error amounts to 2.06%. When the neon flash tube assembly is inserted, in order to raise the limit of momentum measurement, the error is increased to 4.06%. When the ionisation measurements are made it necessarily increases the amount of material in the beam of the instrument still further giving a final error of 5.4%.

The principle of the scattering calculation will be illustrated by calculating the scattering introduced by the proportional counters and their container.

The simplifying assumption will be made that the scattering can be treated as if it took place at a series of discrete points rather than spread out over a series of finite distances. The initial scattering problem, i.e. before the proportional counters are inserted, then becomes as shown in Fig. 3.4.4.

The total r.m.s. angle of scattering in a given direction is given by

$$\sqrt{\overline{\theta^2}} = \left[\frac{\overline{\theta_1}^2 + \overline{\theta_2}^2 + \overline{\theta_3}^2}{2}\right]^{\frac{1}{2}} \qquad \text{or since } \overline{\theta_1}^2 = \overline{\theta_3}^2$$

$$\sqrt{\overline{\theta^2}} = \left[\frac{2\,\overline{\theta_1}^2 + \overline{\theta_2}^2}{2}\right]^{\frac{1}{2}}$$

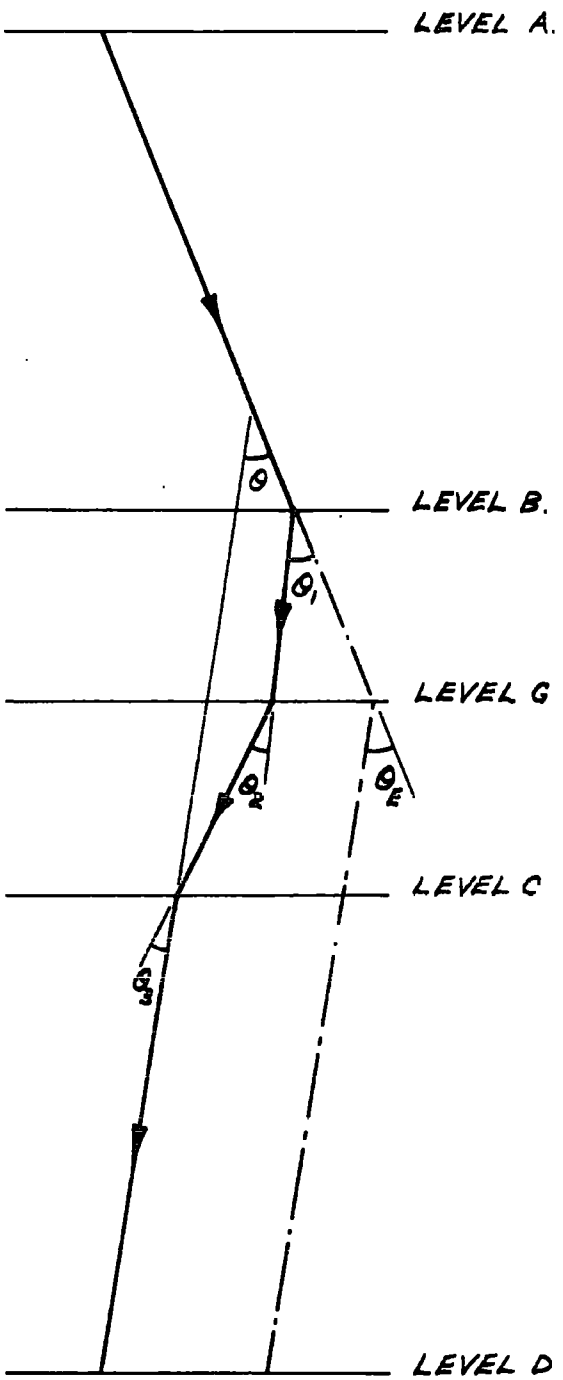

FIG. 3.4.4. SCATTERING IN THE SPECTROGRAPH.

BOTH THE TRAJECTORY SHOWN IN FULL LINE & THE TRAJECTORY SHOWN IN DOTTED BELONG TO THE SAME CATEGORY. IN THIS CASE θ_E, THE EQUIVALENT DEFLECTION AT THE CENTRE OF THE SYSTEM, IS EQUAL TO θ.

$\sqrt{\overline{\theta_1^2}}$ is the total r.m.s. angle of scattering in the G.M. counter and flash tube assembly in level B.

$\sqrt{\overline{\theta_3^2}}$ is the same for level C.

$\sqrt{\overline{\theta_2^2}}$ is the r.m.s. angle of scattering in the G.M. counters in level G .

The scattering introduced when the proportional counters are inserted into the spectrograph cannot be added to the initial scattering in quite the same straightforward manner, as the scattering in this case takes place not within the magnetic deflection region, but between two of the direction defining levels A and B. It is required therefore to replace an actual r.m.s. angle for scattering $\sqrt{\overline{\theta_4^2}}$ at a distance say l above level B by an equivalent r.m.s. angle of scattering $\sqrt{\overline{\theta_5^2}}$ at the centre of the system. Using the nomenclature of Figure 3.4.5. it can be seen that for small angles and for near vertical trajectories

$$\sqrt{\overline{\theta_5^2}} = \left(\frac{D-l}{D}\right)\sqrt{\overline{\theta_4^2}} \qquad \& \qquad \sqrt{\overline{\theta^2}_{total}} = \left[\frac{2\,\overline{\theta_1^2} + \overline{\theta_2^2} + \overline{\theta_5^2}}{2}\right]^{1/2}$$

Calculation of $\sqrt{\overline{\theta_4^2}}$

The r.m.s. angle of scattering is given, to sufficient accuracy, by the relation:

$$\sqrt{\overline{\theta^2}} = \frac{E_s}{p\beta}\left(\frac{x}{X_0}\right)^{1/2}.$$ (See for example Rossi, 1952)

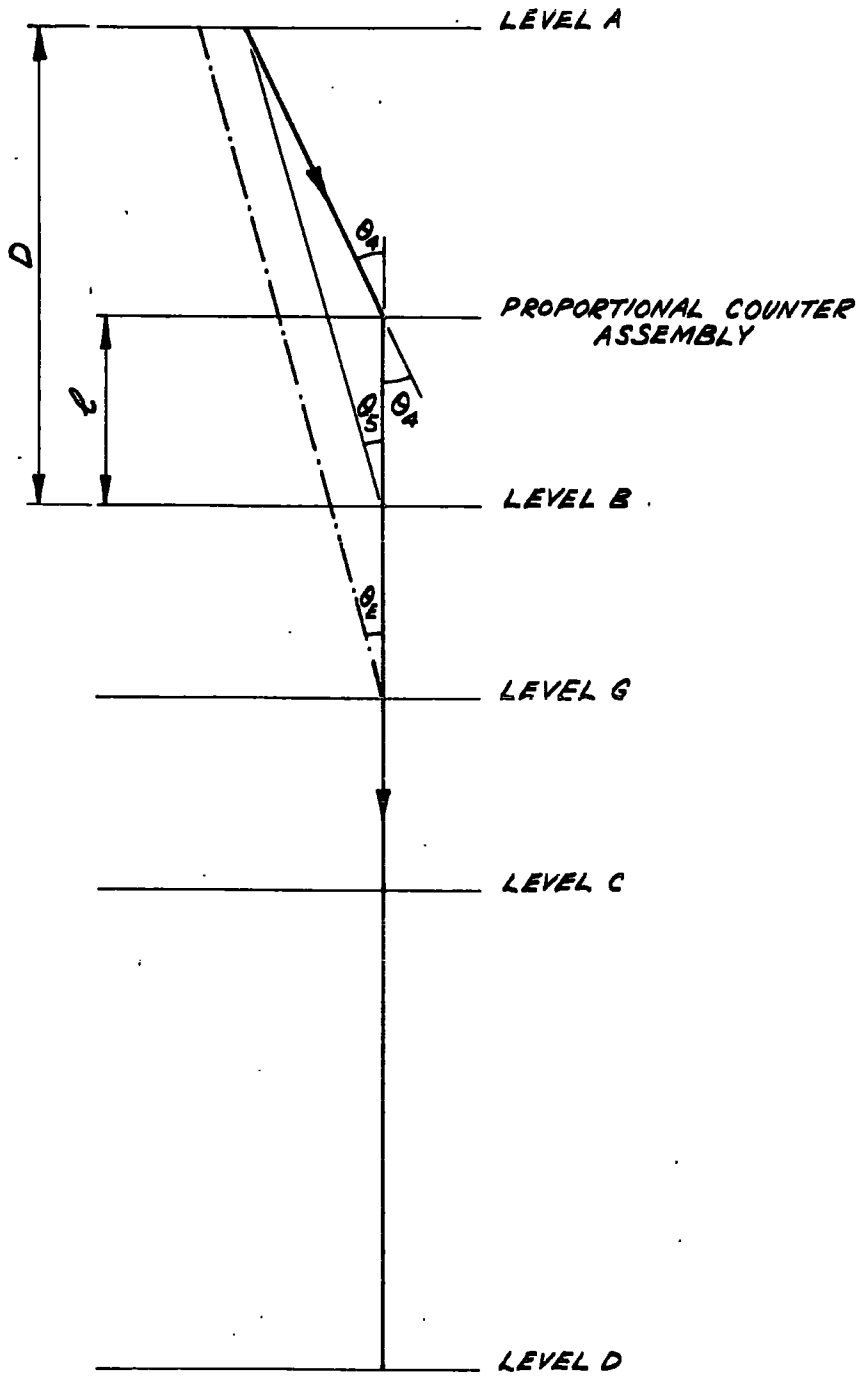

FIG. 3.4.5. SCATTERING IN THE PROPORTIONAL COUNTERS.

BOTH THE TRAJECTORY SHOWN IN FULL LINE & THE TRAJECTORY SHOWN IN DOTTED BELONG TO THE SAME CATEGORY. IN THIS CASE θ_2 (SEE FIG. 3.4.4), DOES NOT EQUAL θ_4 BUT IS EQUAL TO $\left(\frac{D-\ell}{D}\right)\theta_4$.

where E_s = 21 MeV, X_o is the radiation length of the scattering medium in units of gm cm^{-2}, and x is its thickness in gm cm^{-2}, and $p\beta$ is the product of momentum (in MeV/c) and velocity/c.

The relevant values for the proportional counter assembly are shown in table 3.4.1.

Table 3.4.1.

Material	X_o	Thickness (cm)	density (gm/c.c.)	x (gm cm^{-2})
Glass	32.34	0.60	2.5	1.50
Cu	13.3	0.40	8.9	3.56
Al	26.3	0.16	2.7	0.43

The magnetic deflection is given by $\theta = \frac{300 \int Hdl}{p}$

where $\int Hdl = 6.6 \times 10^5$ gauss-cm at max. current.

The percentage error due to scattering in the proportional counters then becomes:

$$\left(\frac{\bar{\theta}_5^2}{2}\right)^{1/2} \times \frac{100(\%)}{\theta} = \left(\frac{D - L}{D}\right) \frac{E_s}{p\beta}\left[\sum\left(\frac{x}{X_o}\right)\right]^{1/2} \frac{1}{\sqrt{2}} \quad \frac{p}{300 \int Hdl} \times 100\%$$

$$= 3.6\%$$

for high momentum particles where $\beta \simeq 1$.

This gives a total error due to scattering throughout the whole spectrograph of 5.4%.

By comparing this result with the uncertainty introduced by the finite size of the Geiger counters we see that equality is reached for $n \simeq 6$.

3.5. The Neon Flash Tube Assembly

The maximum detectable momentum of the spectrograph using geiger counters is ~ 20 GeV/c. In order to increase this to a figure of $\sim 10^{12}$ eV/c it is necessary to locate the particle trajectory with much greater accuracy. This is done by using additional detectors in the form of neon flash tubes.

These consist of glass tubes, filled with neon, which can be made to flash by applying a high voltage pulse within a few microseconds of the passage of an ionising particle. They were invented by Conversi's group at Pisa (Conversi et al, 1955) and developed for use in Cosmic Ray Spectrographs by the Durham Group (Gardener et al, 1957, Coxell et al, 1960).

In the spectrograph, 4 stacks of the tubes are used; one in close proximity to each of the 4 trays of geiger counters as shown in Fig. 3.5.1. Each stack consists of 8 layers of carefully staggered tubes. The tubes are 0.75 cm in diameter, and 62 cm long in the stacks adjacent to the extreme counter trays and 22 cm long in the two middle stacks. The system is aligned by two vertically hanging nylon threads which pass through holes drilled in graticules fixed at either end of each stack frame. In this way the system is

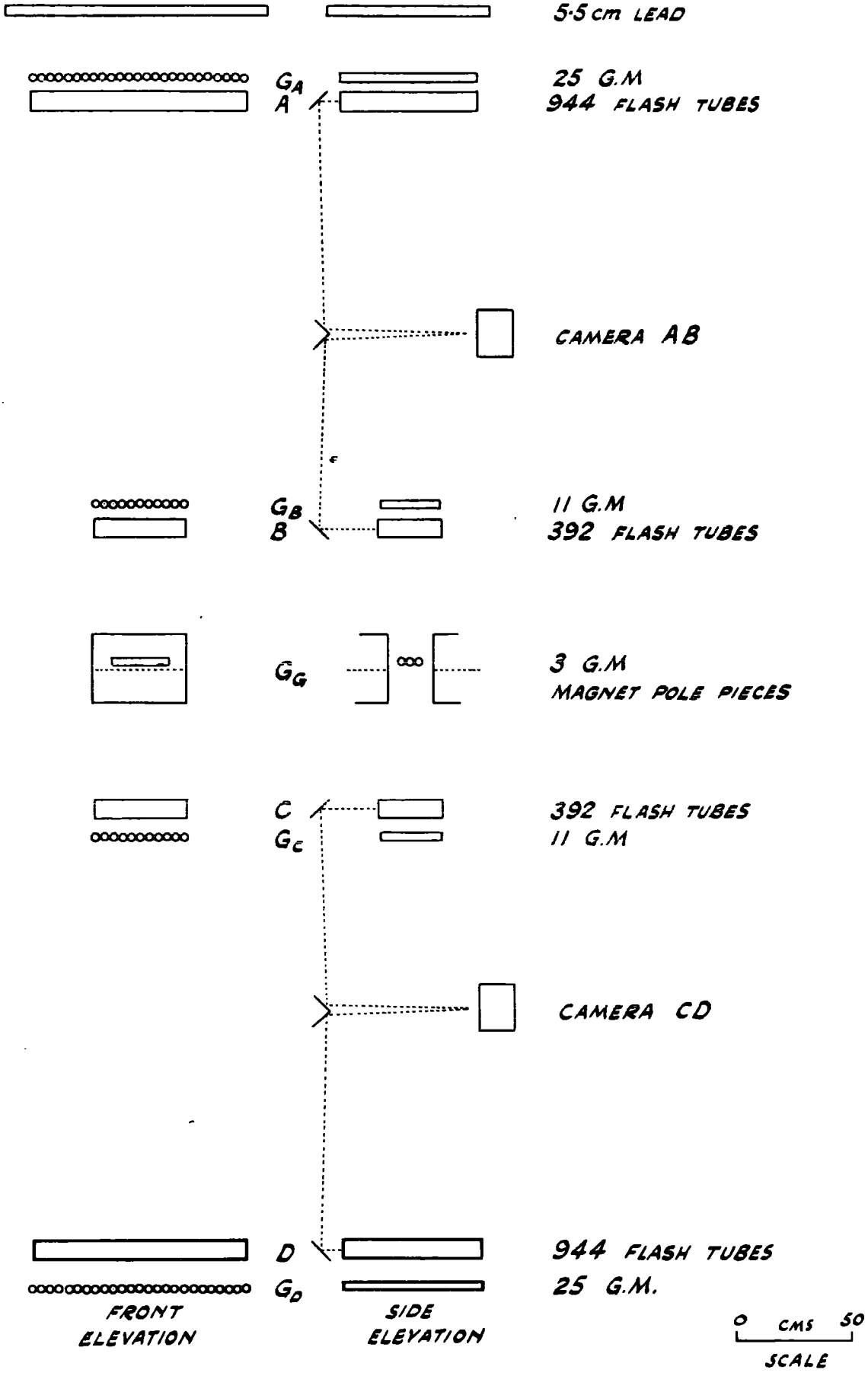

FIG. 3.5.1. THE COMPLETE DURHAM SPECTROGRAPH

aligned to $\pm$ 0.2 mm at each level and the accuracy of trajectory location at each level is $\pm$ 0.3 mm.

The high voltage is applied across a set of thin horizontal aluminium plates placed between the various layers of tubes. When a particle passes through the geiger counter trays a coincidence pulse triggers the high voltage pulsing unit and layers of flash-tubes are 'pulsed'. Most of the tubes through which the particle passed flash and photographs are taken of all the layers. Measurement of the reprojected photographs then gives an accurate determination of the deflection of the particle and thus its momentum.

Since the increased accuracy of particle location is only required for small category numbers, i.e. high momentum particles, a 'momentum selector' has been constructed. This comprises an electronic circuit which triggers the high voltage pulse generator only when a fast particle has traversed the spectrograph. In this way a considerable saving in time and film is affected.

The electronic circuits will next be described in some detail.

CHAPTER 4

THE AUTOMATIC MOMENTUM ANALYSER

4.1. Introduction

A block diagram of the apparatus for the automatic recording and analysis of the particle momenta is shown in Fig. 4.1.1. The overall appearance of the instrument is shown in Plate 4.1. The operation of this unit will be described first in general terms, then the individual units will be considered in some detail and finally an outline of the operating procedure will be given. Details of the performance of the apparatus and the results obtained using it will be given in Chapter 5 and a description of the unit that selects only the very high momentum particles in Chapter 6.

4.2. General Description

From the diagram (Fig. 4.1.1.) it is seen that each geiger counter is connected to a quenching unit and the outputs from the quenching units in any one tray are connected by a common line to one channel of a Rossi coincidence circuit. When a particle traversing the spectrograph gives rise to a 5-fold coincidence pulse by discharging a counter in each of the five layers A, B, C, D & G it is recorded.

In order to measure the deflection of the particles traversing the apparatus it is necessary to identify the counters which are discharged. This is done by assigning to each counter in trays

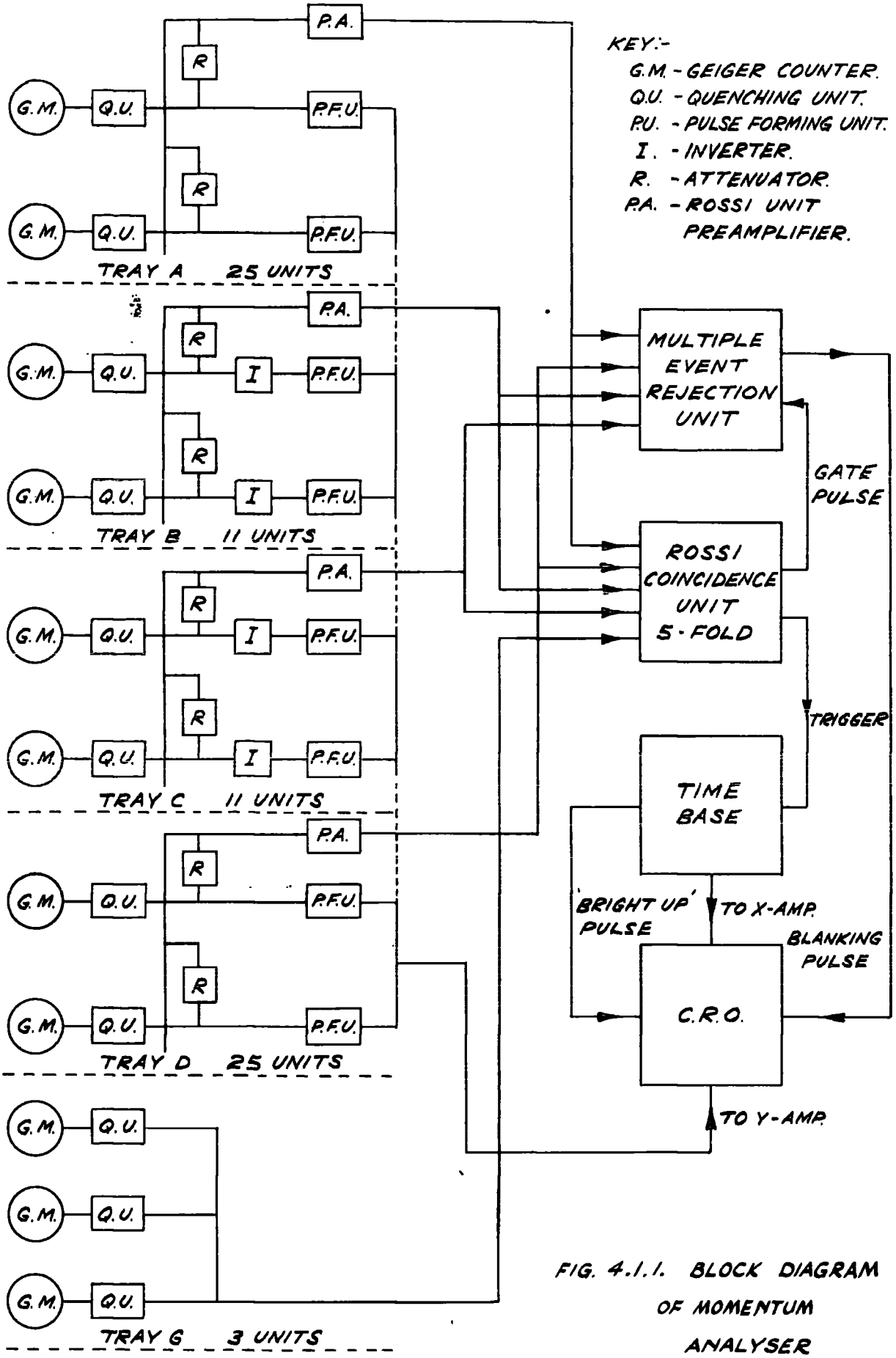

FIG. 4.1.1. BLOCK DIAGRAM OF MOMENTUM ANALYSER

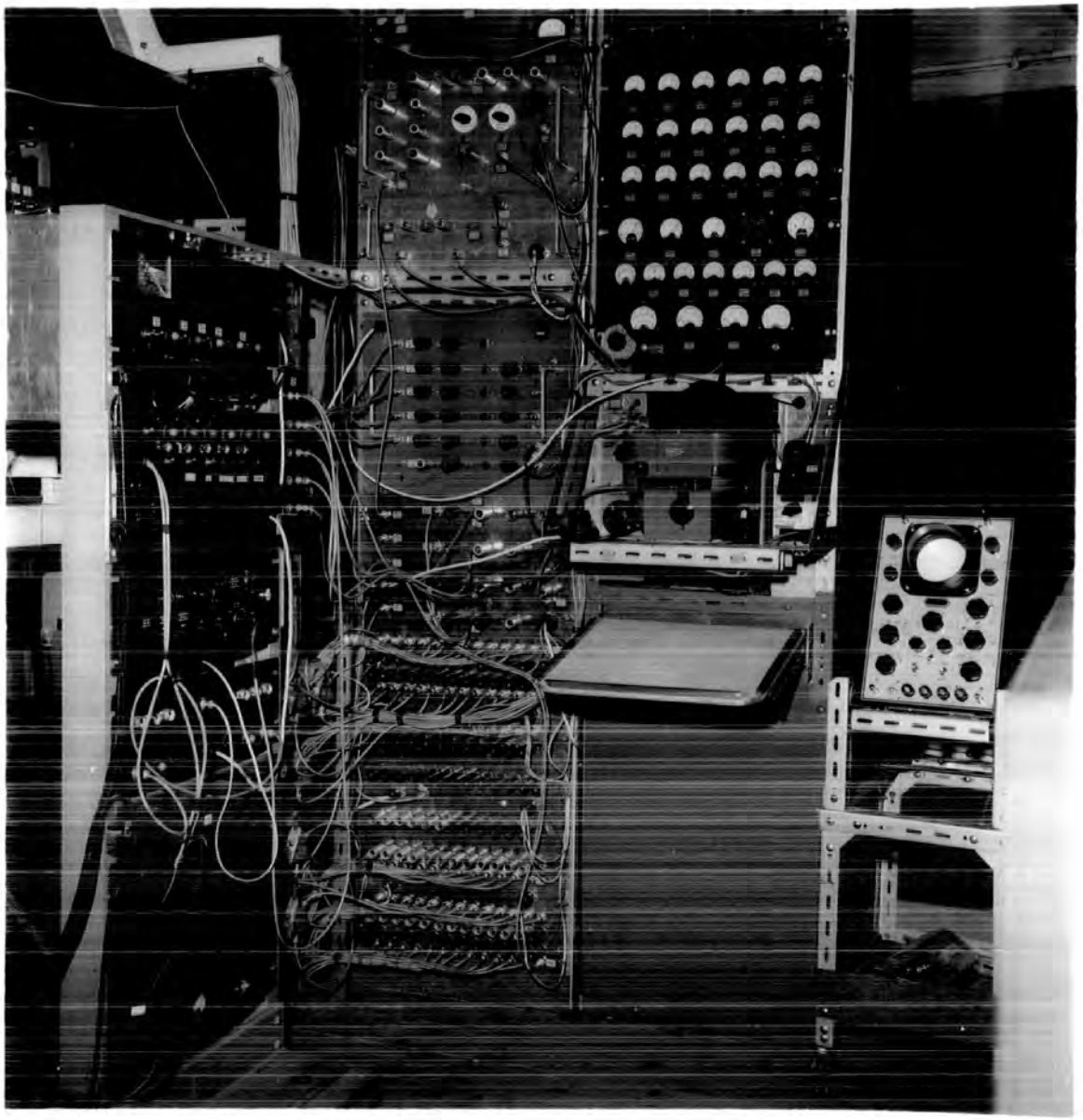

PLATE 4.1. THE MOMENTUM ANALYSER

A, B, C and D a pulse forming unit which is triggered each time a particle discharges the counter. The height of the output pulses from each of these units is related in a simple manner to the position of the corresponding counter in each tray, viz:

$$e_n = n\epsilon + k$$

where e_n is the output voltage, n is the number of the counter, i.e. its position in the tray, k and ϵ are constants.

The counters in the extreme top and bottom trays, i.e. A and D are each numbered from 1 to 25 and the counters in the two middle trays i.e. B and C are numbered in accordance with their position relative to the counters in A and D, i.e. since each of the B and C trays contains eleven counters, they are numbered from 8 to 18.

If now all the pulses associated with the outer A and D trays are of positive polarity and all those associated with the middle trays B and C of negative polarity, then addition of the pulses, one from each layer, will give a resultant pulse whose height is a measure of the deflection of the particle and hence its momentum.

Since:

$$\begin{aligned} e_o &= (e_A + e_B + e_C + e_D) \\ &= [(n_A\epsilon + k) + (-n_B\epsilon - k) + (-n_C\epsilon - k) + (n_D\epsilon + k)] \\ &= [(n_A + n_D) - (n_B + n_C)]\epsilon \\ &= n\epsilon \end{aligned}$$

where n, which gives the deflection in terms of the diameter of the counters, is the category number as defined in Chapter 3.

The resultant pulse is then displayed on a cathode ray oscilloscope and recorded photographically.

Only those pulses associated with a 5-fold coincidence correspond to a particle traversing the whole of the spectrograph and in order to select these pulses it is necessary to ensure either that the pulses are only produced when a 5-fold coincidence has been registered or that they are only recorded under these conditions. The former can be accomplished by gating the individual pulse forming units with the 5-fold coincidence pulse from the coincidence unit, and the latter by using the coincidence pulse both to trigger the time base of the recording oscilloscope and to brighten the trace. The latter method is in practice easier and has been adopted.

A modification of the same procedure is used to eliminate those events in which one or more additional particles traverse part or the whole of the apparatus at the same time as a particle registers a 5-fold coincidence.

The second particle may arise:

(a) As part of a shower.

(b) From a knock-on event produced by the first particle.

(c) By the chance passage of another particle within the resolving time of the system.

These spurious results associated with otherwise genuine 5-fold events are automatically blanked out and do not appear on the

photographic record. They are, however, counted in the total of 5-fold events, and also separately.

4.3. The Pulse Forming Units

The circuit is based on the Manchester design and is shown in Fig. 4.3.1. Under normal conditions V_1 is on, the potential at the point B is thus less than at C and V_2 is non conducting. If a positive going pulse is applied at A the potential of the point B rises until it is comparable with that at C and V_2 starts to conduct. Once this occurs any further rise in potential at B is limited since a continuing rise could only occur if current passed from A to B when the potential of the former was greater than that of the latter, i.e. when V_1 is biassed in the reverse direction. Thus if a positive pulse of magnitude greater than a certain amount is applied at A, V_1 is cut off, V_2 is turned on and the potential of the point C rises by an amount independent of the input pulse and determined only by the power supplies and the circuit parameters, associated with V_2.

The height of the voltage step at C is then given by

$$e_o = \frac{R_3}{(R_2 + R_3 + R_{diode})} \quad (E_{H.T.} - E_{Bias})$$

When the input pulse is removed the circuit reverts to its original state.

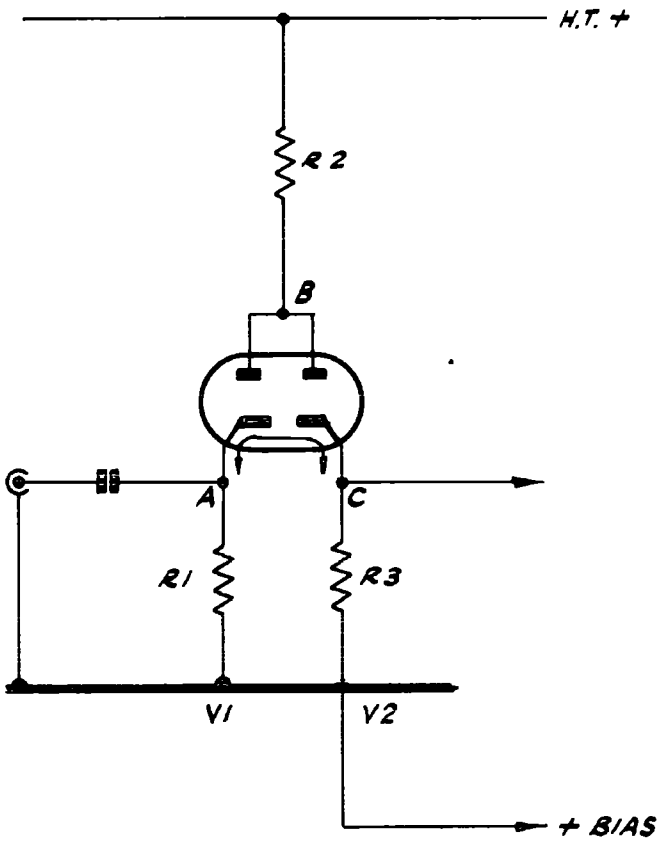

FIG 4.3.1. THE ANALOGUE PULSE GENERATOR (POSITIVE PULSES)

The voltage change at A necessary to achieve satisfactory operation must be greater than ($E_{B\ final} - E_{A\ initial}$) or approximately $E_{Bias} - E_{A\ initial}$ since with the circuit values employed here point B rises only slightly above E_{bias}.

The size of R_2, the common anode load, is chosen to be much greater than either R_3 or R_{diode}. The output pulse height then becomes almost independent of small changes in R_{diode} and at the same time variations in the output load resistor R_3 have little effect on the current flowing through it, so that the circuit behaves as a current pulse generator, a fact of some importance as explained below.

A small amount of capacitative coupling takes place between the input and output terminals via the interelectrode capacity of V_1 which is of the order of a few pF. Less than 1% of the input pulse height breaks through in this manner, however, since in operation the capacitative load across R_3 is several hundred pF and with R_3 ~1kn this pulse decays with a time constant less than a microsecond.

A similar circuit can be used to generate negative going pulses by replacing the positive power supplies by negative ones, interchanging the connections of anode and cathode, and applying a negative input pulse to operate the circuit.

It is also possible to construct a pulse forming unit of the required type around a single pentode or triode, but in this case the output pulse is very sensitive to valve characteristics and reliable operation over a long period would not be possible.

In the adopted circuit positive analogue pulses are generated using the double diode circuit (Fig. 4.3.1.) and negative ones by using the complementary circuit preceded by a simple inverter. The height of the output pulse from the pulse forming unit is controlled by varying R_2. The analogue pulse forming units for the counters in Tray A (or D) are connected together as shown in Fig. 4.3.2. and those for Tray B (or C) as shown in Fig. 4.3.3. The output pulses from all units appear across a common load resistance R_3 which consists of $R_{3A,D}$ and $R_{3B,C}$ in parallel, D.C. isolation being provided by suitable coupling condensers. The pulses are derived from a high impedance source, i.e. constant current sources, so that the current flowing into R_3 from a particular unit is unaffected by the current flowing into it from other units and their effects are additive.

The values of R_2 and R_3 were chosen to ensure sufficient accuracy of pulse height addition without making the pulse heights too small (see section 4.8.). The values chosen make $k = 0.4$ volts, and $\epsilon = 0.08$ volts in the equation $e_n = n\epsilon + k$ giving a range of pulses heights from 0.48 to 2.4 volts corresponding to $n = 1$ and $n = 25$.

4.4. The coincidence Circuit

It will be seen from Figs. 4.3.2. and 4.3.3. that the output from each quenching unit in a given tray, besides being connected to a pulse forming unit, is connected via a 100K resistor to a common line. Pulses on this line are amplified and fed into one of the channels of the Rossi coincidence circuit.

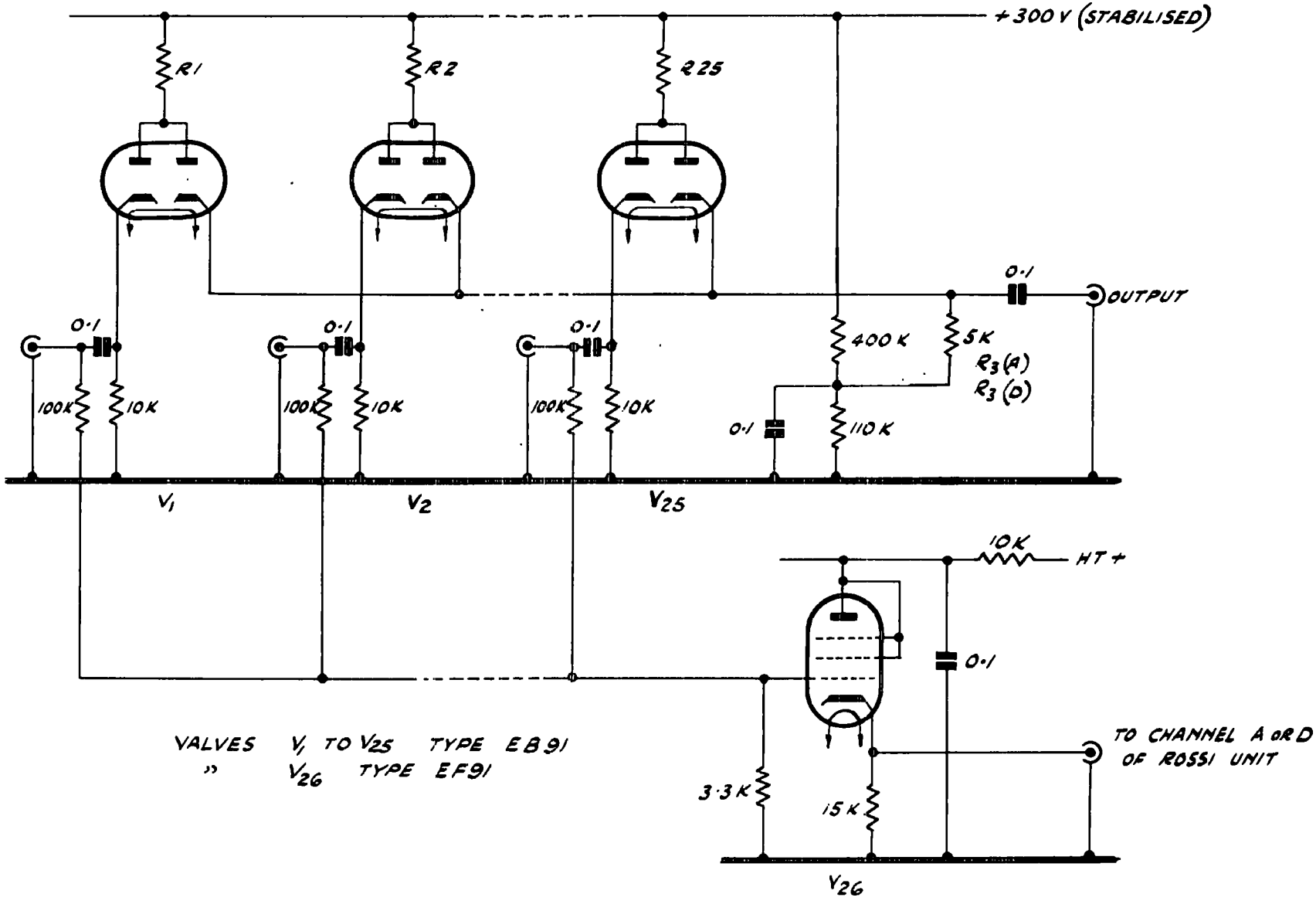

FIG. 4.3.2. THE ANALOGUE PULSE UNITS IN TRAYS A & D

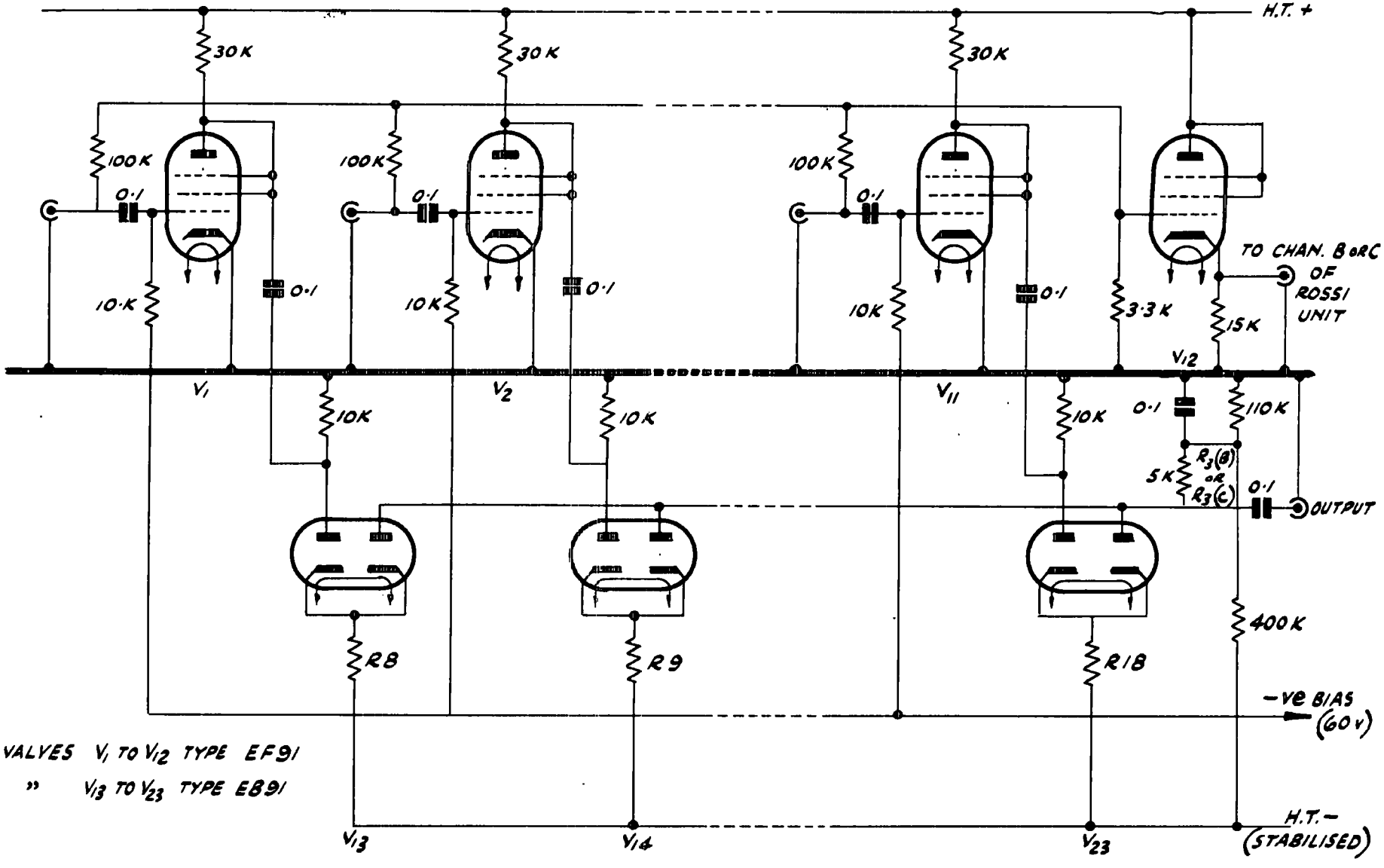

FIG. 4.3.3. THE ANALOGUE PULSE UNITS IN TRAYS B & C

The value of the resistor connecting the quenching unit to the common line was chosen to ensure that no interaction took place between the units. This method of coupling unfortunately means that an attenuated version of the quenching unit pulse appears on the common line and in order to operate the Rossi circuit efficiently the pulses must first be amplified. This is done by a grounded grid amplifier (V_1 in Figure 4.4.1.) which provides amplification without phase reversal. The positive output pulses from this then pass to the cathode followers V_2 and V_3.

The purposes of the double cathode follower arrangement V_2 and V_3 and its associated resistance network R_4 and R_5 are:

(a) To provide a low impedance source for the signal which has to be fed via a length of coaxial cable to the Rossi circuit. The low impedance source reduces the attenuation and distortion in the connecting link, and

(b) To prevent "grid-current-limiting" in the first valve of the Rossi circuit from reacting back on the Rossi preamplifier. This must not occur since it would interfere with the operation of the multiple event eliminating unit.

The Rossi circuit follows standard practice. The circuit is shown in Figure 4.4.2. Five channels are shown, but in the proportional counter experiment this was increased to six. V_{1A} B, C, D, and G are inverters. V_{2A}, B, C, D and G are the Rossi coincidence valves. The univibrator V_4 is triggered by coincidence pulses from the

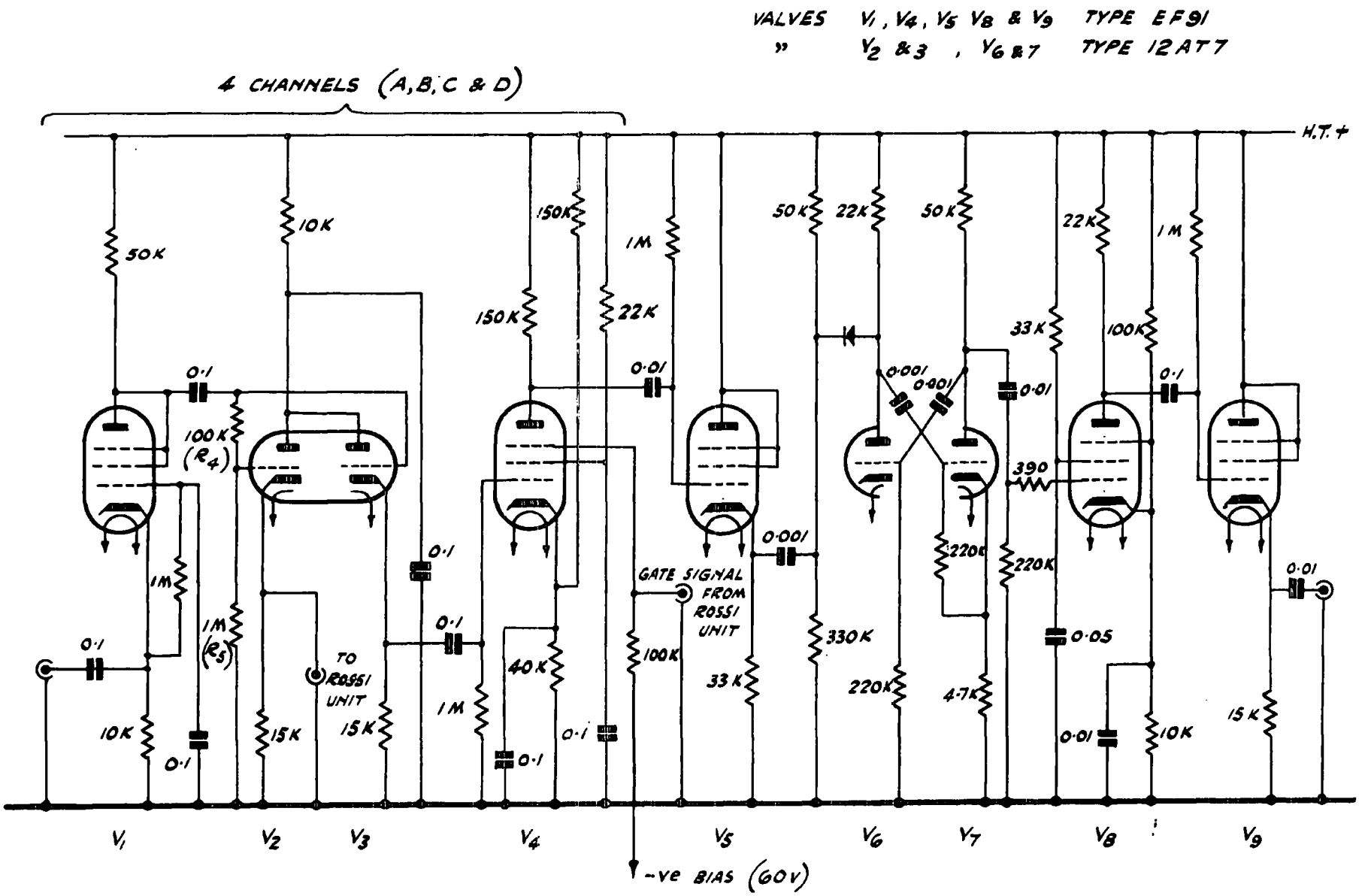

FIG. 4.4.1. THE ROSSI PREAMPLIFIER & MULTIPLE EVENT REJECTION UNIT

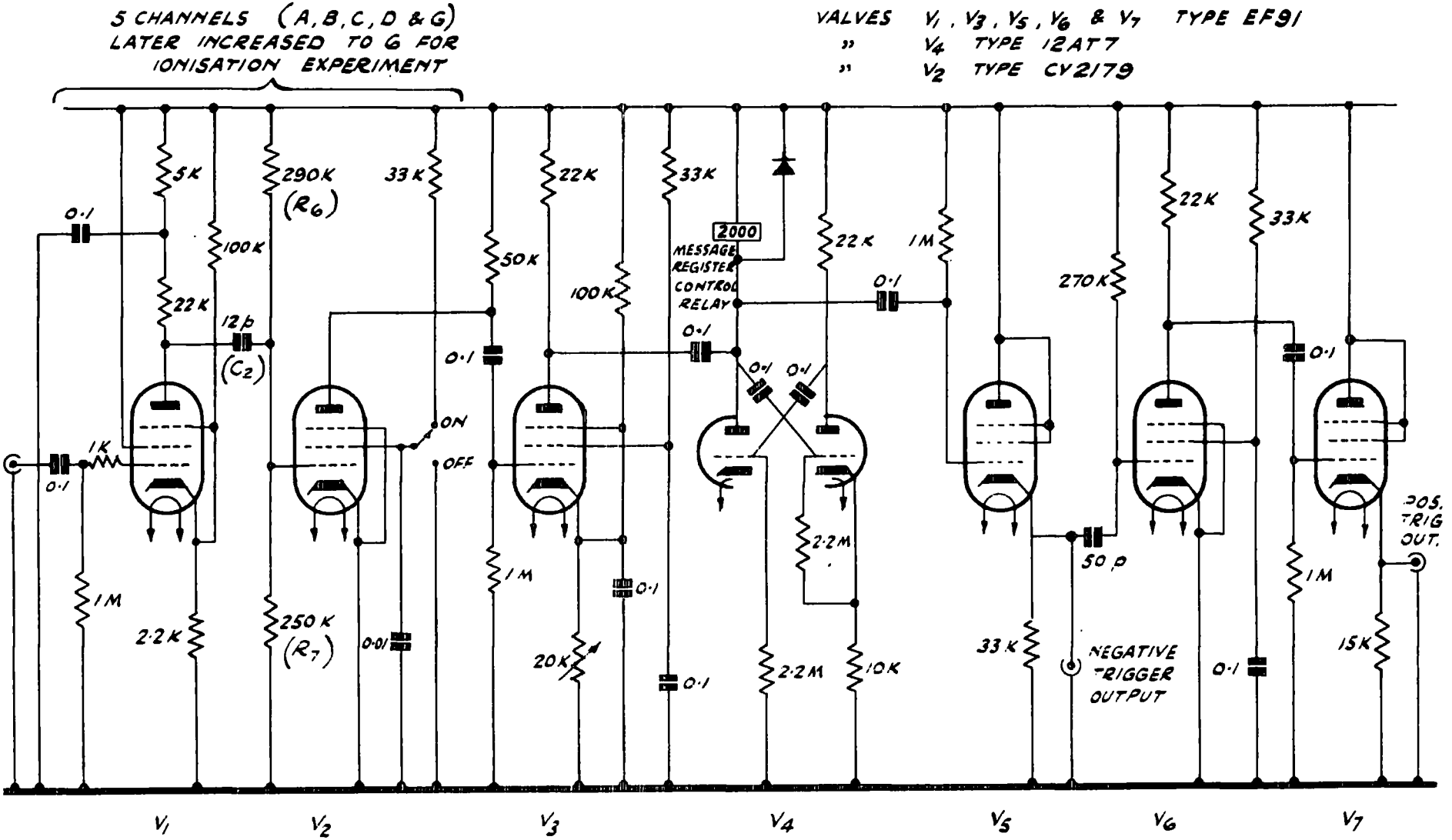

FIG. 4.4.2. THE ROSSI COINCIDENCE UNIT

discriminator valve V_3 and operates a message register recording the number of 5-fold coincidences. The unit gives negative and positive output trigger pulses. The negative one serves to trigger the time-base and the positive one is used to gate the circuit connected with the elimination of spurious records from multiple events and to gate the momentum selector circuit.

The resolving time of the coincidence circuit

The resolving time is controlled by either the length of the quenching unit pulses or by the time constant of the differentiating network which precedes the Rossi valve, depending on which factor limits the length of the pulse appearing at the Rossi valve anode. In this case the time constant of the differentiating network controls the resolving time, although the dependence is not linear, as it is also a function of the quiescent grid potential of V_2.

The choice of suitable values for the differentiating network components was a compromise between several opposing factors.

(a) The time constant should be as small as possible in order to reduce the number of spurious events.

(b) Instrumental limitations of the minimum value of the time constant.

In its original form the differentiating network did not include the resistor R_7 and the time constant was given by C_2R_6. The minimum value of R_6 was then limited by the grid dissipation of the

Rossi valve and further reduction is C_2R_6 could only be obtained by reducing C_2, but there was a limit here also. The grid resistor R_6 was in parallel with a capacity made up of the input capacity of the valve $g^Ck \sim 10pF$, and the stray capacity of the wiring, of the order of a few pf, and this, together with C_2 formed a potential divider across the source of the signal. Therefore if C_2 was reduced to only a few pF the signal reaching the grid would be insufficient to turn off the valve and would make discrimination difficult.

The purpose of the second resistor R_7 is to overcome this difficulty. R_7 is in parallel with R_6 as far as A.C. signals are concerned, and it is possible to reduce the time constant, without increasing the grid current or attenuating the signal. Short pulses $\sim 1\ \mu$sec. can be obtained, but unfortunately these short pulses are not rectangular in shape as the rise and decay times are also of the order of 1 μsec. This means that with short pulses the resolving time is a somewhat uncertain quantity and depends very much on the setting of the discriminator stage.

(c) <u>The Effect of Time Delays</u>

The signals from A, B, C, D and G do not arrive simultaneously. This will lead to a loss of 5 - fold coincidences if the resolving time is too short. The time delays are due to several causes.

1. Time delays in the Geiger counters ~few 0.1 μsec.
2. Variations in time delays between input and output pulse among quenching units due to the tolerance of components. A spread of up to 0.5 μsec. has been found.
3. The delay ~0.5 μsec. introduced into A, B, C and D, but not G counters by the Rossi preamplifiers and associated equipment.
4. Delays ~1μ sec. in the inverter stages of Rossi circuit as result of self biassing action and finite pulse rise times.

The distribution of the overall time delays was measured by triggering an oscilloscope from the G counters and examining the 5-fold coincidence pulses on the Rossi valve anode. The results shown in Fig. 4.4.3. are for the final circuit. From these results it is possible to determine:

(a) The mean time delay relative to the G counters. This was 2.5 μsec.

(b) An estimate of the number of 5-fold coincidences which were lost. This was less than 1%.

(c) A measure of the resolving time, since pulses arriving after this time are severely attenuated. The value obtained was 6.0 ± 1.0 μsec.

This value was checked by counting the number of 2-fold coincidences between two sets of counters and applying the formula:

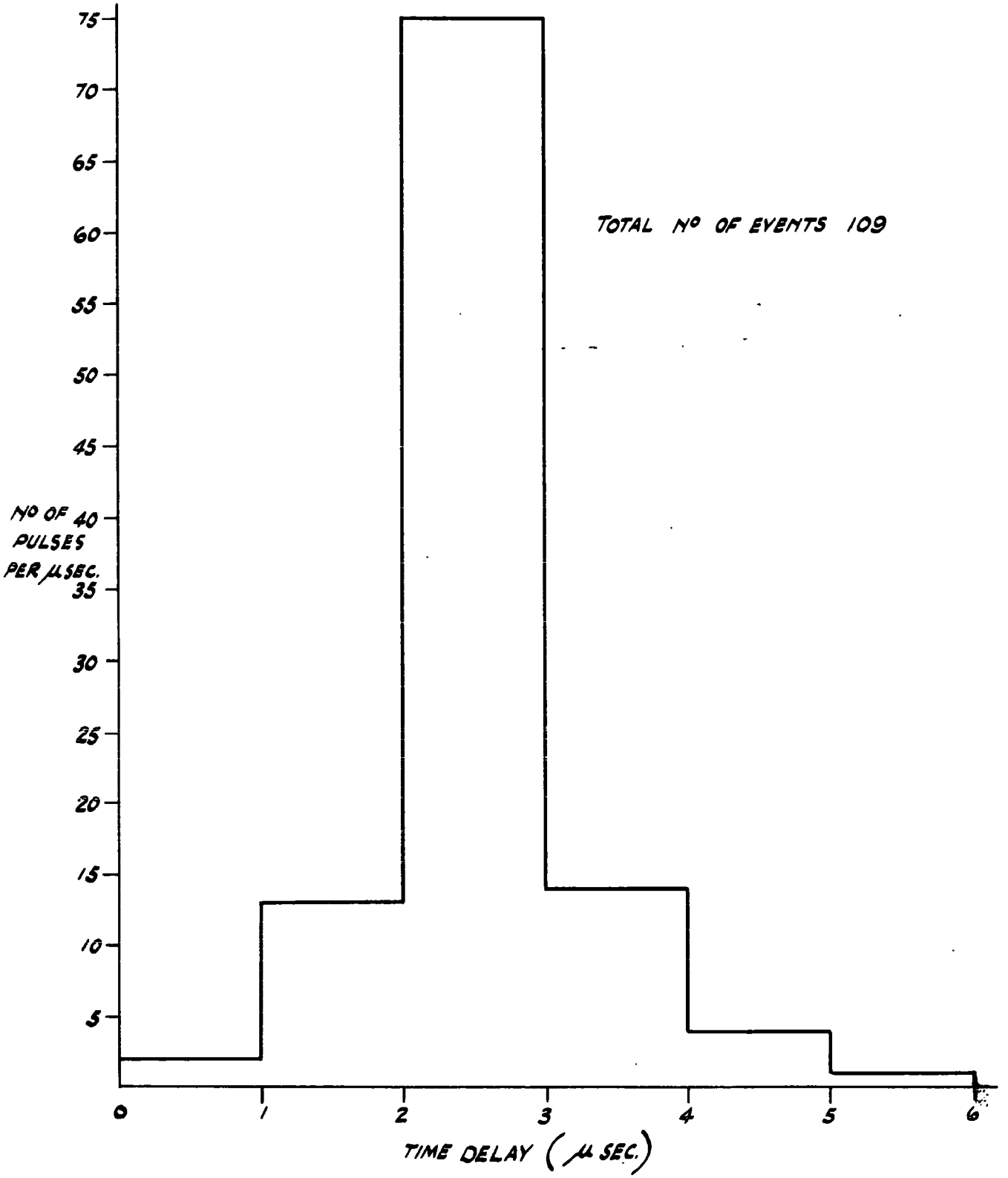

FIG. 4.4.3 DISTRIBUTION OF TIME DELAYS

$$n = 2N_1N_2\tau$$

where n = number of coincidences, N_1 and N_2 are the individual rates of two sets of counters and τ is the resolving time. After correction for the genuine 2-fold coincidence rate this gave $\tau = 6.2 \pm 0.6$ μsec. Using this value of τ the spurious 5-fold coincidence rate was found to be 0.3% of the total. (The calculation is given in Chapter 5).

The time delays also affect the amount of overlap of the pulses from the pulse forming units and it was found necessary to increase the original pulse length of the quenching units from 7 to 15 μsecs., in order to obtain a useful plateau region.

4.5. The time-base

The internal time-base of the oscilloscope (Furzehill) that was available was unsuitable and an appropriate one was constructed. The circuit used is shown in Fig. 4.5.1. The negative pulse from the Rossi circuit triggers V_1 a cathode coupled univibrator. The negative output pulse from this performs two functions.

(a) It cuts off V_2, producing an exponentially rising pulse at its anode. This pulse is then fed into the X-amplifier of the oscilloscope, and

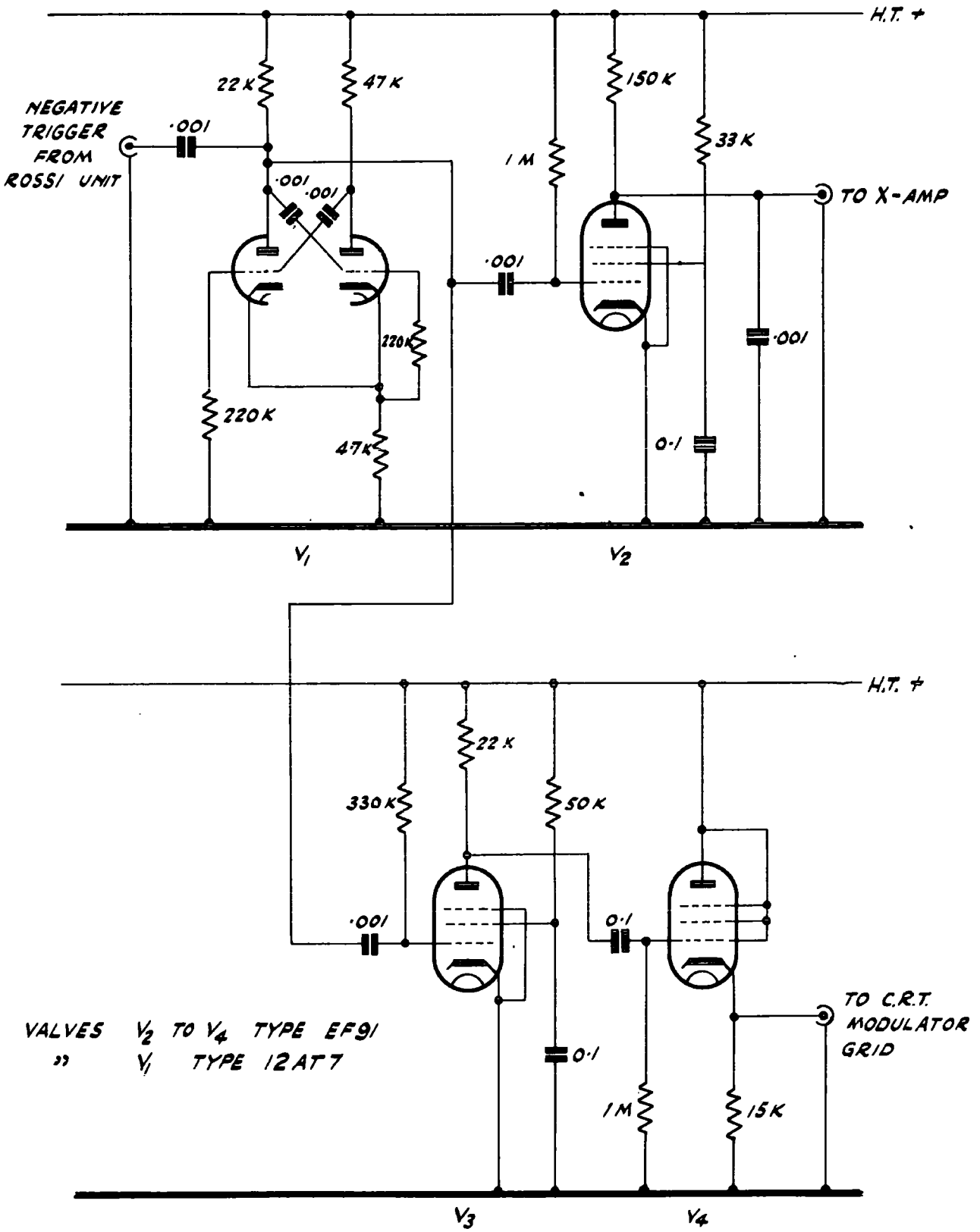

FIG. 4.5.1. THE TIME BASE

(b) It operates the automatic trace-brightening circuit V_3 and V_4. V_3 is an inverter and amplifier and V_4 is a cathode follower the positive output pulse from which is fed on to the modulator grid of the cathode ray tube.

4.6 The Elimination of Multiple Events

The purpose of the unit for the elimination of multiple events has already been explained. Its action is based on the fact that if m counters in one tray go off simultaneously the pulse on the common line is m times as large as that due to a single counter alone. A discriminator V_4 following the Rossi preamplifier (Figure 4.4.1.) discriminates between m = 1 and m >1 events, but as only those events which occur at the same time as a 5-fold coincidence are of importance the discriminator valve is normally biassed off at the suppressor grid. The valve is gated by a positive pulse from the Rossi circuit. The anodes of the four discriminators are joined, so that in event of a 2- or more-fold coincidence occurring in any tray at the same time as a 5-fold coincidence between A, B, C, D and G a pulse will appear across the common anode load and trigger the univibrator V_5. The univibrator and V_6 and V_7 then generate a negative pulse which is used to blank out the trace on the oscilloscope. The number of these events is recorded by a message register circuit.

4.7. The Oscilloscope and Pulse Recording Equipment

The screen of the oscilloscope, which is about three inches in diameter, is masked by a black disc with a vertical rectangular slot in the middle and a corresponding mask fitted inside the recording camera. Two bulbs are mounted inside the camera cone. One is used to illuminate the scale and the other to provide a time marker. The camera is motor driven, and has an f/1.9 lens which is used at full aperture. The film used is Ilford HPS.

4.8. Factors affecting the accuracy of the momentum analyser

1. Accuracy of measurement of R_3 and R_2

R_3 is of the order of one hundred times smaller than R_2 so that an accuracy of 1% in R_3 is quite sufficient.

R_2 can be measured to about 1 part of 10^4 at the low resistance end ($\sim$100K) and to about 1 part in 10^3 at the high resistance end ($\sim$520K). The limits are imposed by the sensitivity of the galvanometer used in conjunction with the Wheatstone Bridge. The accuracy of the latter is about 1 part in 10^5 at the rated temperature. The actual measurements were performed at a slightly higher temperature, but as relative values only were required this was not important.

It is important that high accuracy be maintained over an appreciable period of time. To this end high stability resistors were used. A small part of the carbon deposit on each was

carefully removed until their values were within 1% of the required calculated values. They were then coated with 'Aquatect', allowed to dry and soldered into position. A 'soak-test' in the form of the full H.T. voltage applied across them was performed and no changes in resistance were detected over some 24 hours. The resistors were then made up to the required values by adding small value carbon resistors in series or large values in parallel.

It had been hoped originally that temperature variations would have little effect on the resistors and that the 'cold' value of the resistors would be sufficiently accurate. Unfortunately this proved not to be the case. The temperature coefficient was found to be 10^{-2}% per ^{o}C and taking the ambient temperature of a resistor running at its rated value to be 70^{o}C (manufacturers' data) this gives an error of about 1%. If all the resistors operated at the same temperature the errors would tend to cancel out, but a considerable proportion of the resistors dissipate far less than their rated wattage. It was necessary therefore both to enclose the resistors in a thermostatically controlled cabinet and to measure their values at their maintained working temperatures under such conditions. This was achieved by measuring the resistance, with a bridge circuit, at various times after switching off the H.T., extrapolation back to zero time interval then gave the 'hot' value.

2. Variations of Diode Resistance

The diode resistance is a function of several variables, but nowhere does its resistance become greater than about 1/2% of the corresponding value of R_2. It is shown below that the maximum required accuracy for $R_2 + R_3 + R_{diode}$ is 1 part in 600, the accuracy required being directly proportional to pulse height. This means that R_{diode} must be known to about 10% to enable the value of $R_2 + R_3$ to be calculated and for reasonable allowances to be made for deviations of the experimental values from the required ones.

Method of Measurement

An identical copy of the practical circuit was set up. The voltage drops across both R_2 and the diode were measured with a high resistance voltmeter of high quality. The value of R_{diode} was found to be dependant on several parameters.

(a) Value of the anode current, i_a.

Theory shows that the potential drop across the valve should vary as $i_a^{2/3}$ (Child's Law). This was found not to be the case under the conditions in question. Reference to the manufacturer's data for the valve showed values of i_a and v_a which did agree with the 2/3 power law, but the values of i_a were all much larger than the ones being used here. Close examination of the assumptions made in derivation of the formula revealed that the initial kinetic energy of the electrons had been neglected. This contribution to the final energy of the electrons will become more important as v_a

decreases. Measurements showed that R_{diode} varied from about 500 ohm to 1K ohm over the range of i_a used in practice.

(b) Effect of age.

The effect of age on R_{diode} was found to be most noticeable under low current conditions where the initial kinetic energy of the electrons has most effect. The change in R_{diode} with time appeared to be most rapid in the first few hours after which it settled down.

(c) Heater Voltage, V_h.

A 10% variation in V_h gave a 10% change in R_{diode}.

A spread in the value of R_{diode} was also found for a group of valves operating under identical conditions. The spread amounted to $\pm$ 15% of the mean value.

The procedure eventually adopted to cope with these variations due both to heredity and environment was to divide the valves into groups according to their resistance. Valves from the numerically largest group were then used to fill the positions where R_{diode} is of greatest significance, i.e. where R_2 has its lowest values. The remainder were then filled with valves from groups of progressively lower resistance. In this way some compensation for the increase of R_{diode} with decrease of i_a could be made. This took care of the majority of the valves and the

values of R_{diode} in the few remaining positions was of such little importance that the remaining valves could be used in any order.

The value of R_{diode} used in the calculation is the measured value for R_{diode} for position 25, i.e. R_2 minimum.

Replacements for valves are obtained from a collection of aged valves.

3. The accuracy of the addition process

(a) Addition of pulses of the same polarity.

The equivalent circuit for this is shown in Fig. 4.8.1. From this it can be shown that the output (sum) pulse e_o is given by:

$$e_o = (e_{o1} + e_{o2})(1 - k)$$

where $e_{o1} = \frac{R_3 E}{R_{2,1} + R_3 + R_{diode}}$ & $e_{o2} = \frac{R_3 E}{R_{2,2} + R_3 + R_{diode}}$

and where $k = \frac{2R_3}{R_{2,1} + R_{2,2}}$

(b) Addition of pulses of opposite polarity.

The equivalent circuit is shown in Fig. 4.8.2. As in the above.

$$e_o = (e_{o1} + e_{o2})(1 - k)$$

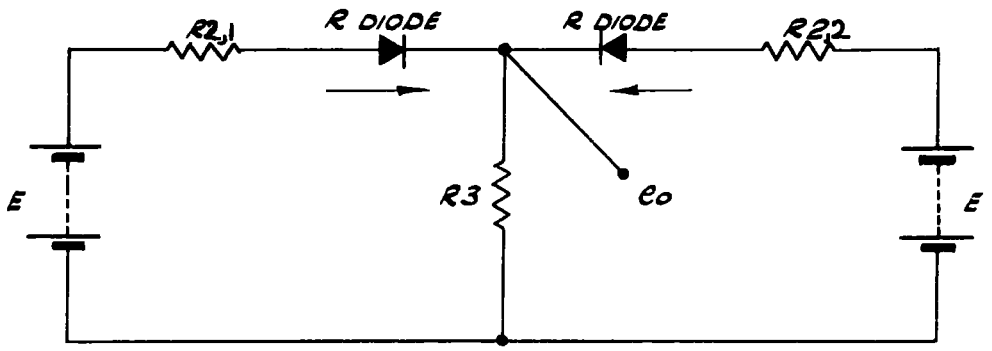

FIG. 4.8.1.

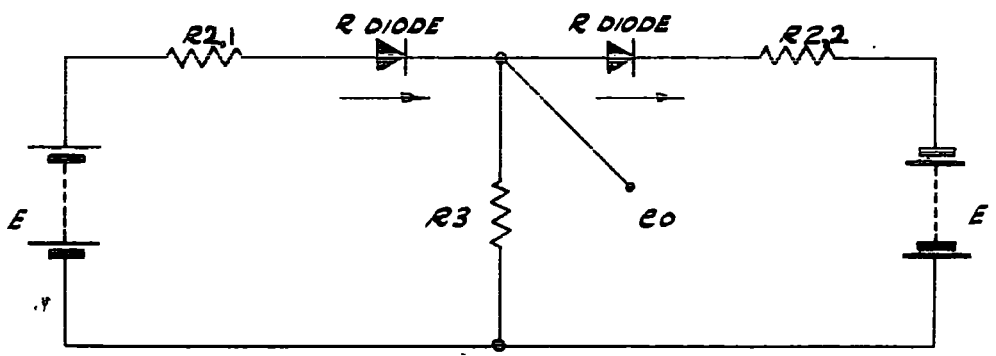

FIG. 4.8.2.

where $e_{o1} = \dfrac{R_3 E}{R_{2,1} + R_3 + R_{diode}}$ & $e_{o2} = \dfrac{R_3 E}{E_{2,2} + R_3 + R_{diode}}$

and in this case $k = \dfrac{R_3^2}{R_{2,1} \times R_{2,2}}$

For the values used here, i.e. $R_3 \sim 1k$ & $R_2 \sim 100K$ this expression is always very small and can be neglected.

The addition of the four pulses, one for each of the groups of pulse generators associated with trays A, B, C & D, can be considered in three steps.

(i) $e_A + e_D \longrightarrow e_f$ say

(ii) $e_B + e_C \longrightarrow e_g$

and finally (iii) $e_f + e_g \longrightarrow e_o$

Steps (i) and (ii) both involve the addition of pulses of the same polarity and are therefore subject to an appreciable error, but step (iii) is concerned with pulses of opposite polarity and introduce negligible error. In fact since the errors in e_f and e_g are oppositely directed they will tend to cancel out in step (iii).

The overall result of this is that because a given category number can arise in a variety of ways due to the several combinations of $e_A + e_B + e_C + e_D$ that give e_n, it will not be represented by a unique pulse height, but by a range of pulse heights. This spread in pulse height in a given category will depend on the category number. In category 0 it is clear from considerations

of symmetry that the errors in steps (i) and (ii) must always cancel, so that the overall error is nil. In other categories the spread increases with the category number.

Fig. 4.8.3. shows the calculated variation in the overall error as a function of category number.

The inaccuracy leads to a non-linear scale, but the actual spread of pulse heights corresponding to a given deflection is not serious.

Taking these facts into consideration it was decided to make the resistors (R_2) in the analogue pulse unit to an accuracy equivalent to 1/20 of a deflection category in the pulse height. This should ensure that the maximum spread of pulse height corresponding to a given category does not exceed $\pm$ 0.3 category.

4. Accuracy of the oscilloscope and associated equipment

There is a slight non-linearity in response of the oscilloscope to positive and negative signals. This has been corrected by using a non-linear scale.

5. The Stability of the Apparatus

The stability is mainly dependent on the constancy of the power supplies. The oscilloscope is fed from a constant voltage transformer. The pulse forming units have electronically stabilised H.T. supplies, also fed from a constant voltage transformer, and in practice it has been found that the drift in output pulse due to H.T. changes does not exceed 0.1 of a deflection category per day.

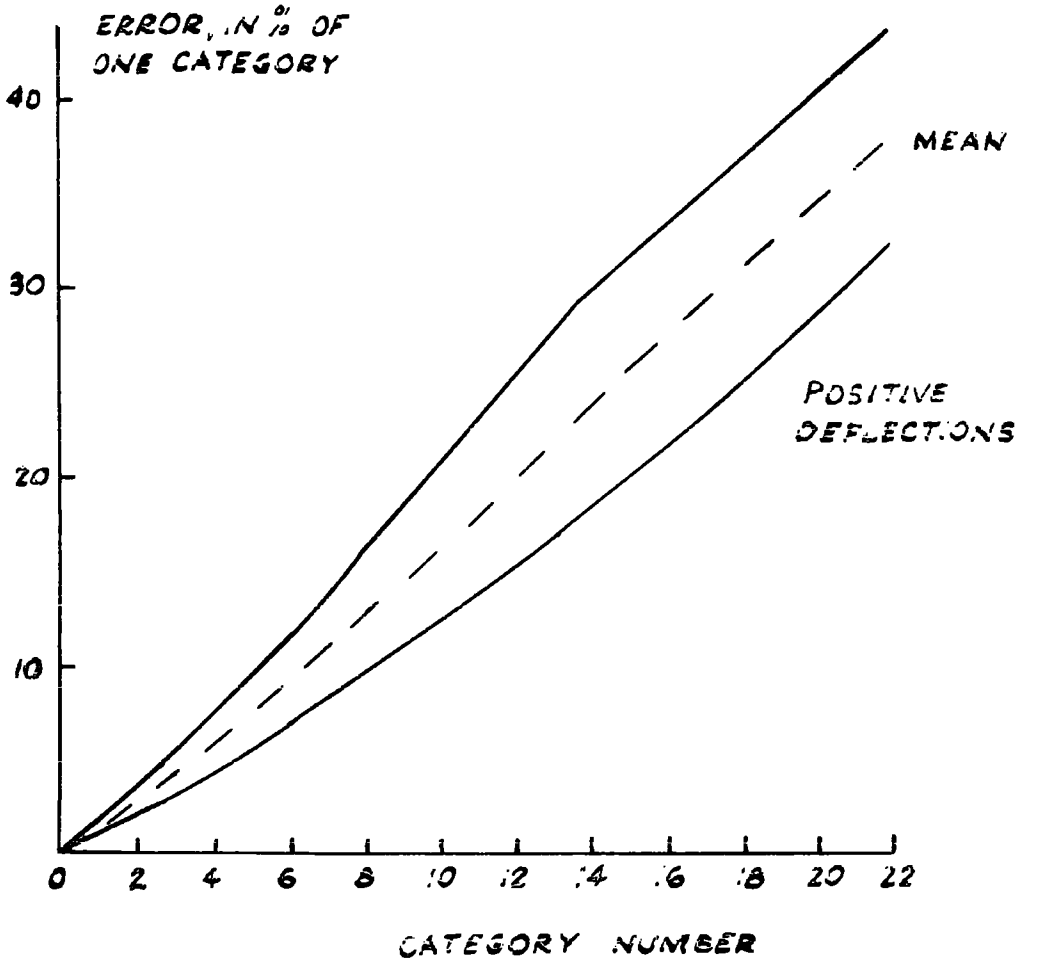

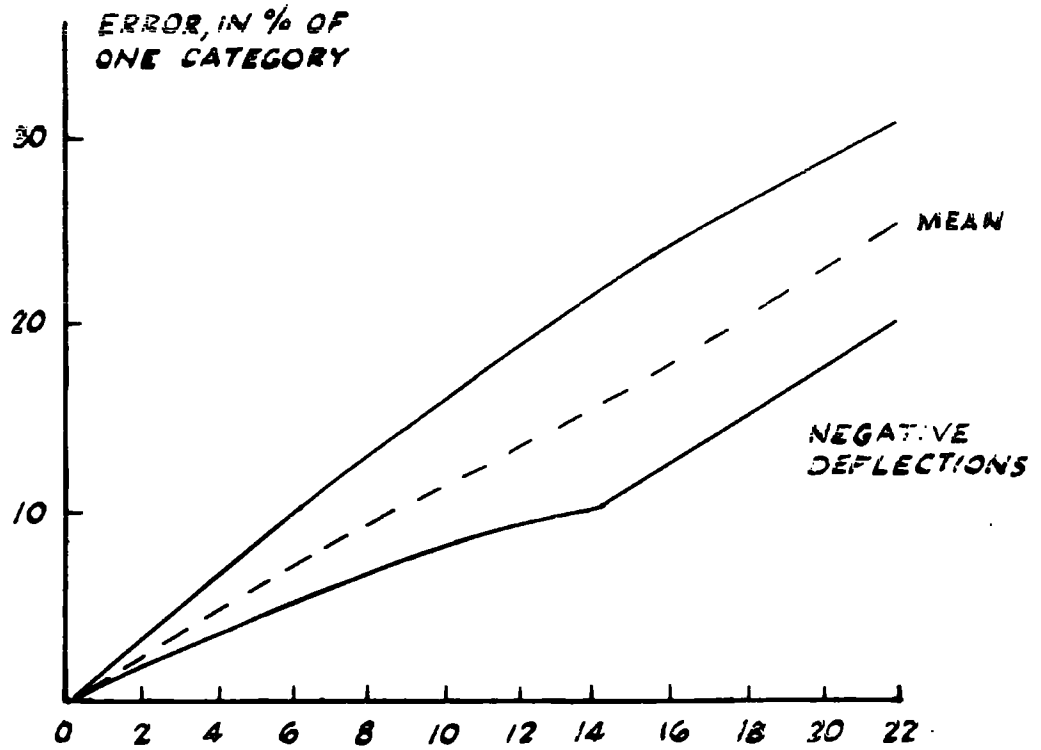

FIG 4.8.3. CATEGORY NUMBER

4.9. Operational Sequence for the Momentum Analyser

The sequence is, of course, governed by the actual experiment being performed. Much of the work, with the spectrograph has concerned the measurement of the spectrum and it is the operational sequence for this experiment that will be described.

Briefly, photographs are taken of the pulse heights corresponding to the cosmic rays passing through the spectrograph. Since the chance is small of successive particles having the same category number a number of pulses can be recorded on the same photograph. In practice it is sufficient to accumulate traces for a period of 2 minutes before moving on the film in the camera. Since the magnet current is not stabilised it is necessary to measure the current at frequent intervals; this measurement is performed photographically.

All timing operations are controlled by 1 second impulses from a standard clock. These operate a system of uniselectors which control

1. The oscilloscope camera motor. This is switched on for 1 sec. every 2 minutes.
2. The illumination of the oscilloscope scale. This is done every 2 minutes for 25 secs.
3. The flashing of a time marker bulb inside the camera cone. This occurs every 10 minutes, i.e. once in 5 frames.

4. The motor of the camera which records the time and the magnet current.

5. Illumination for the above camera.

Before the apparatus is allowed to operate automatically a number of checks are performed manually. These are as follows:-

1. Adjustment of stabilised H.T. voltages to give equality between positive and negative pulses. This is done by triggering all the pulse forming units corresponding to the central counters, i.e. to number 13, from a common line. The positive H.T. supply is then altered until zero output is obtained when the coincidence circuit is set to 4-fold operation.

2. Adjustment of CRO amplifier. This time the pulse forming units corresponding to A25, B13, C13 and D13 (i.e. corresponding to category 12) are triggered from the same counter and the gain control adjusted until the pulse height coincides with the + 12 mark on the scale. The adjustment is then checked by substituting A1 for A25. This should give a pulse height of - 12 units.

3. Photographic calibration of the scale to correct for non-linearity. The brilliance of the spot is reduced and the camera replaced. The Rossi circuit is then switched to 2-fold A-B operation and the traces recorded photographically for about 2 minutes after

which the scale is illuminated. The 2-fold coincidence rate is high enough to ensure that in general all possible pulse heights are recorded in the 2 minutes and this calibration is used when the film is projected for analysis.

4. The actual run. All the important parameters are noted, e.g. H.T. plus and minus, Rossi circuit message register, multiple event message register; and the total counting rates for all 5 trays measured. The 'run' is then started using 5-fold coincidences at some noted time, by switching on the uniselector system and the E.H.T. supply for the Geiger counters.

CHAPTER 5

THE PERFORMANCE OF THE SPECTROGRAPH

5.1. Consistency of pulse heights

Some idea of the consistency of the pulse height for a given category number derived from different combinations of counters can be seen from Plate 5.1. The first photograph (A) shows about 200 pulses derived from AB coincidences and (B) a similar number from CD coincidences. The strong peaking of the distribution of pulse heights about the category numbers is very marked.

A set of typical records for 5-fold coincidences is shown in photograph (C). Each frame corresponds to a 2 minute exposure and the average number of pulses per frame is ~ 7 (at maximum field). As already mentioned, this exposure was chosen as a compromise between excessive use of film for short exposures and large numbers of unresolved superimposed pulses for long exposures.

In Fig. 5.1.1. is shown the distribution of nominal category 0 pulses about zero. The observed spread in value is due entirely to inaccuracies in the individual pulse heights, since the analysis in Chapter 4 has shown that the error in the addition process is zero for category 0 irrespective of which combination of pulse heights from A, B, C & D yields this value.

The distribution curve is not absolutely symmetrical about the origin, but this is almost certainly due to an error in determining the position of the origin. The mean spread (standard deviation)

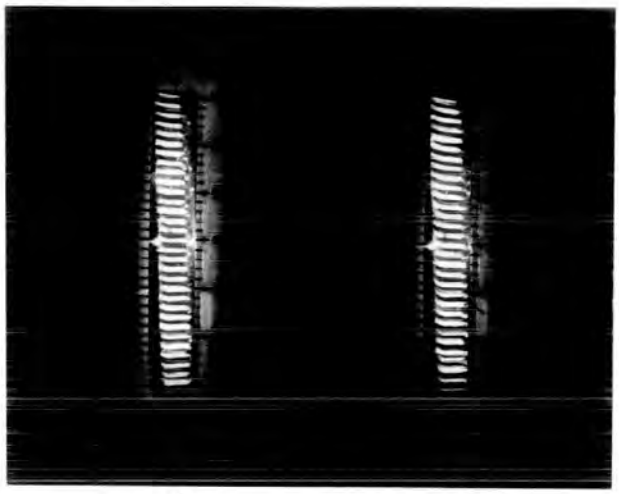

A B

2 - FOLD COINCIDENCES

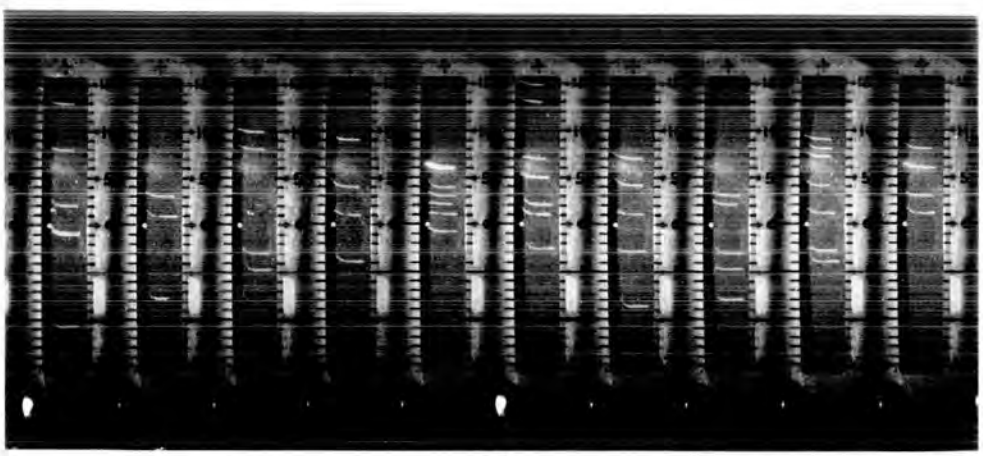

C

5 - FOLD COINCIDENCES

PLATE 5.1.

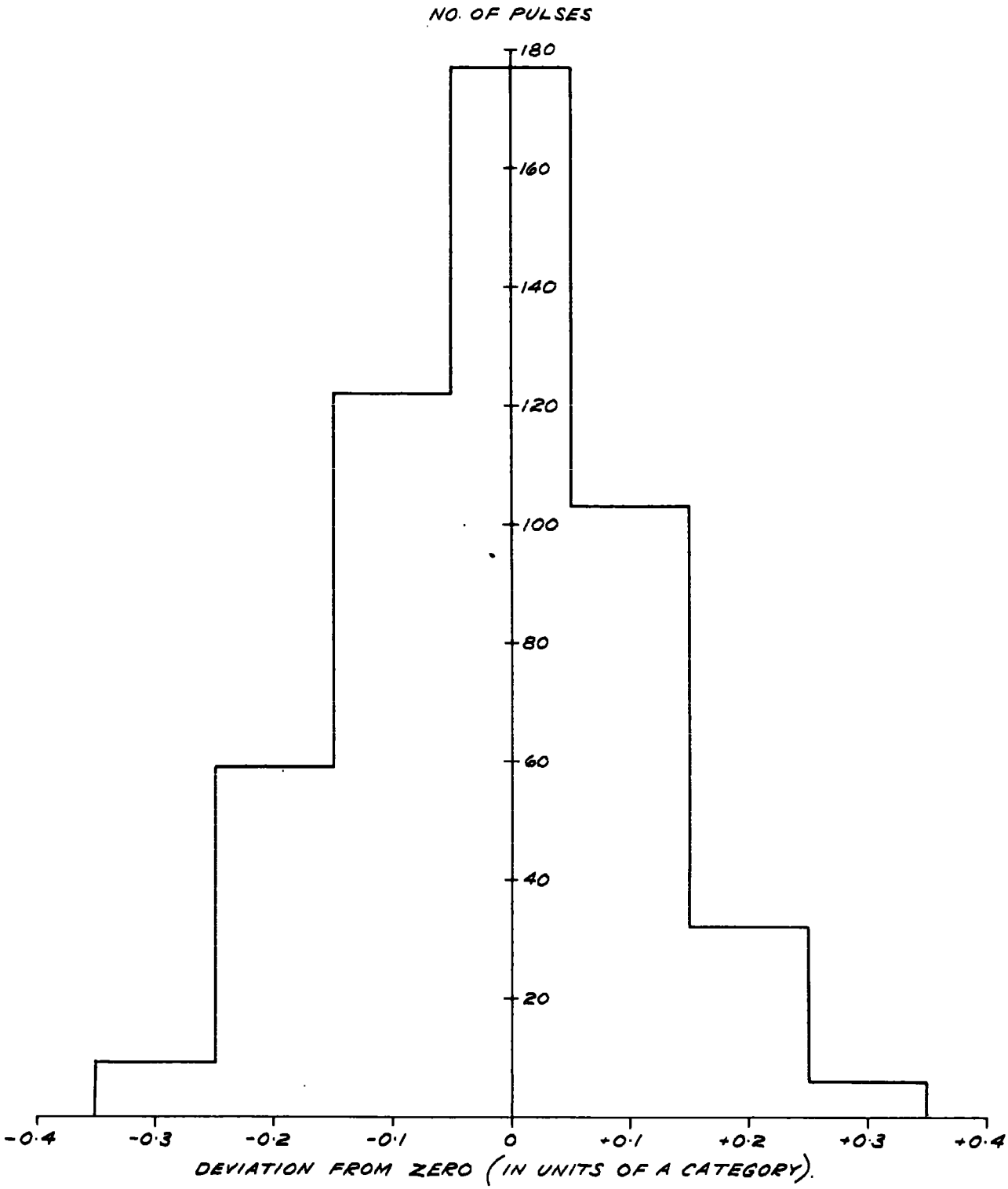

FIG. 5. 1. 1. DISTRIBUTION OF CATEGORY 0 PULSES

is approximately 0.1 category and the maximum observed spread is 0.35 category.

It can reasonably be assumed that the spread about the nominal value in categories other than zero will be similar except for an additional spread due to the addition process. By reason of this the possibility of overlap between adjacent categories will be greatest at the highest category numbers. In category 15 for example which is the highest category number that is measured, the maximum deviation from the centre of the distribution corresponding to this category is 0.06 category.

From this it is concluded that the probability of a particle being allocated to the wrong category is negligible.

5.2. The Frequency of Accidental Coincidences

The measured 5-fold rate includes these events in which more than one particle has traversed the spectrograph within the resolving time (6 μsec.) of the electronic circuits. In this group are included not only those events in which a particle traverses the whole of the spectrograph accompanied by another particle which discharges counters in one or more trays, but also those events in which the 5-fold coincidence is the net result of two particles, for example, one discharging counters in A and B and the other discharging counters in G, C and D. All such events lead to spurious momentum measurements and it is important to estimate their expected frequency.

The estimate is made by considering the way in which chance 2-fold and 3-fold etc. coincidences between sets of counter trays could give rise to spurious 5-fold coincidences. (this includes both the above cases). The counting rates for these particular sets of counter trays are then determined and the values substituted in the appropriate equations i.e.

$$n_2 = 2N_1N_2\tau \quad \text{for chance 2-fold coincidences}$$

$$\& \quad n_3 = 3N_1N_2N_3\tau^2 \quad \text{for chance 3-fold coincidences}$$

where N_1, N_2 and N_3 are the rates of the three independent events and τ is the resolving time of the circuit in question. It was found that the contribution from chance 3-fold coincidences could be neglected, as also could that from 2-fold combinations of the type AB + GCD whose total contribution amounted to a few percent only of the whole. The important contribution was that due to chance 2-fold coincidences between the counters of a single tray and the 4-fold coincidences of the other four. The results are listed in table 5.2.1. from which it can be seen that about 80% is due to A + BCDG & D + ABCG. The overall spurious rate at this stage is 1.19%.

A large proportion of these spurious 5-fold events are eliminated by the device which detects these events in which 2 or more counters are discharged simulataneously in any one of the four trays A, B, C & D. This device has been described in Chapter 4. The remaining spurious 5-fold rate may then be estimated as follows. Consider, as before, the various possibilitiesl

1. Combinations such as B + AGCD. The required AGCD rate will be that corresponding to particles that have traversed counter tray B without discharging any of its counters since from geometrical consideration the particles must go through B. This rate is found by subtracting the 5-fold ABGCD rate from the measured 4-fold AGCD rate. From this resultant rate and the measured B rate an upper limit for this contribution to the spurious 5-fold rate can be obtained. This is an upper limit since the corrected AGCD rate contains chance 4-folds which are not detected in these simple rate measurements, and the B rate includes particles which discharge counters in the other trays, but also go undetected. Similar considerations apply to the other four combinations.

2. Combinations such as AB + GCD. From geometrical considerations, with one exception, one or both the particles concerned in any one such event must traverse at least one counter tray without discharging a counter. The probability of this occurring is $\sim 13\%$ for each traversal so that this already small contribution becomes negligible. The exception is the combination AD + BGC where there exist possible trajectories which do not give to multiple discharges in any of the trays, but even in this case the contribution is $\lesssim 10^{-4}$ c/min. and can be neglected.

The values are listed in table 5.2.2. The upper limit of the spurious rate becomes 0.33% and it is again seen that A + BCDG and D + ABCG making up $\sim 80\%$ of this rate.

Table 5.2.1. (a)

Counter Tray	Rate (c/min)
A	17,019 ± 131
B	3,162 ± 56
C	2,541 ± 50
D	18,258 ± 135
G	638 ± 25
ABCDG	4.01 ± 0.08
BCDG	5.68 ± 0.10
ACDG	4.55 ± 0.35
ABDG	6.14 ± 0.40
ABCG	5.43 ± 0.11
ABCD	6.35 ± 0.47

Table 5.2.1. (b)

Combination	Chance 5-fold rate (c/min)
A + BCDG	$2.00 \pm 0.20 \times 10^{-2}$
B + ACDG	$3.0 \pm 0.37 \times 10^{-3}$
C + ABDG	$3.2 \pm 0.4 \times 10^{-3}$
D + ABCG	$2.05 \pm 0.20 \times 10^{-2}$
G + ABCD	$8.4 \pm 1.07 \times 10^{-4}$

$\tau = 6.2 \pm 0.6$ μsec.

Total Spurious rate = 1.19 ± .07%

Table 5.2.2. (a)

Combination	Rate (4-fold 5-fold) (c/min)
BCDG	1.67 ± 0.13
ACDG	0.54 ± 0.36
ABDG	2.13 ± 0.41
ABCG	1.42 ± 0.14
ABCD	2.34 ± 0.48

Table 5.2.2. (b)

Combination	Chance 5-fold rate (c/min)
A + BCDG	$5.89 \pm 0.74 \times 10^{-3}$
B + ACDG	$3.6 \pm 2.4 \times 10^{-4}$
C + ABDG	$1.12 \pm 0.24 \times 10^{-3}$
D + ABCG	$5.39 \pm 0.75 \times 10^{-3}$
G + ABCD	$3.1 \pm 0.7 \times 10^{-4}$

Total Spurious Rate = 0.33 ± 0.03%

It is concluded that the spurious rate arising from accidental coincidences is sufficiently low for almost all envisaged applications of the spectrograph.

5.3 Operation With Zero Magnetic Field

By analogy with the "no-field operation" of a magnet-cloud chamber the magnitude of spurious effects can be estimated from the results found with the spectrograph operated without magnetic field.

For example, inaccuracy in the alignment of the counter trays and certain types of electronic faults will result in the ratio $(+/-)$ being significantly different from unity. Other inaccuracies etc., can be inferred from the absolute magnitudes of numbers of particles having high category numbers.

When operated with zero magnetic field, particles are recorded having category numbers other than zero due to the following:-

1. Tracks of zero deflection contribute to categories - 1, 0, + 1. This is an instrument characteristic.
2. The scattering of low energy particles in the various layers of the instrument.
3. Accidental coincidences of different particles passing through the layers but satisfying the condition that only one counter be discharged in the layers A, B, C and D.
4. Malfunctioning of the apparatus.

The instrument was operated for an extended period in which 48,900 particles were recorded. The results were analysed by a

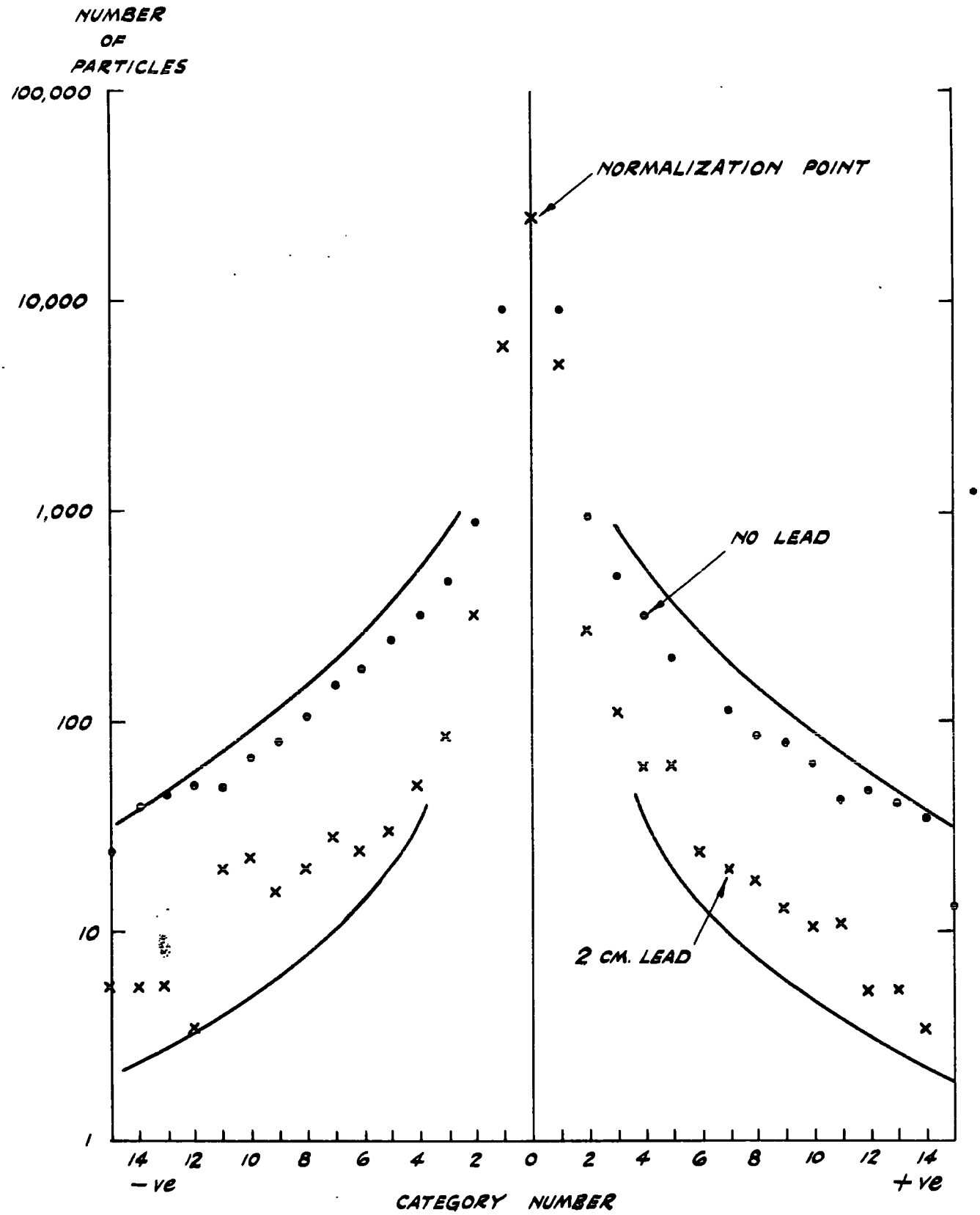

FIG. 5.3.1. ZERO FIELD RESULTS

colleague Mr. M. Gardner and the distribution that he obtained is shown in Figure 5.3.1. Also shown is the expected distribution considering Item 2 above. Almost the whole contribution arises from the scattering of electrons. The expected distribution was calculated using the data summarised by Puppi (1956). Complete agreement between the two was not to be expected as Puppi's spectrum includes electrons which are produced accompanied by another particle and which are rejected by this instrument if the two pass through any of the detecting levels.

In order to investigate Items 3 and 4, a 2 cm lead absorber was placed some distance above the spectrograph. This had the effect of attenuating the electron flux considerably: slow electrons were absorbed and many fast electrons produced showers which discharged more than one counter and were rejected. The distribution of category numbers for 20,900 particles normalised to the same number of particles in category zero as for the previous experiment is also shown in Figure 5.3.1, together with the expected distribution based on Wilson's data (1952) on the probability of electron penetration. The excess of observed frequency over expected frequency is not inconsistent with a spurious rate of a few per 1,000, as expected from the analysis of the resolving time of the circuits and the known particle rates given in 5.2.

5.4 Operation With Magnetic Field

In an extended experiment at the maximum field 102,874 particles were recorded. The direction of the field was reversed periodically and roughly half of the particles were recorded for each field

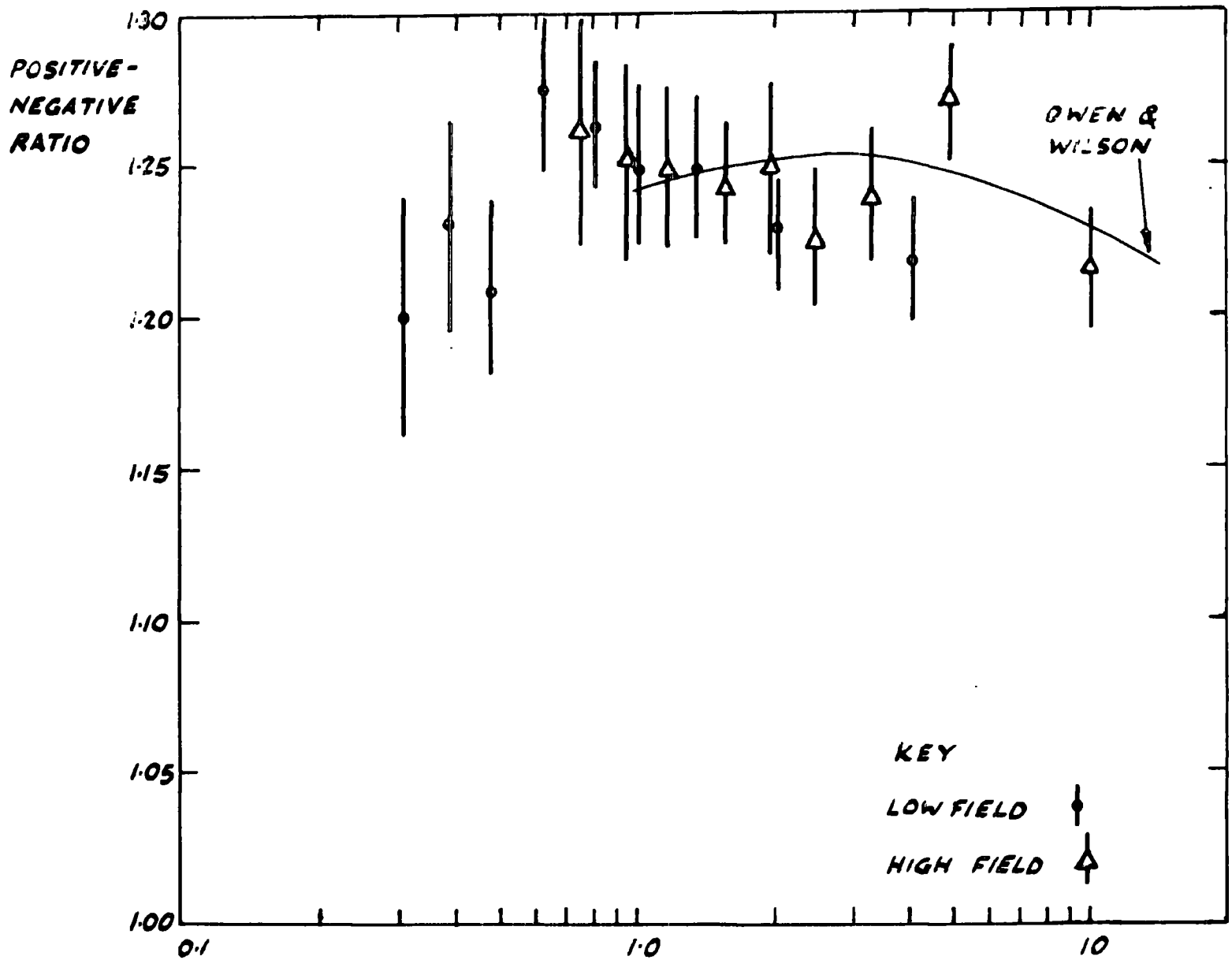

FIG.5.4.1. MEAN MOMENTUM, IN GeV/C

direction. The positive-negative ratio has been determined from the data by Mr. M. Gardner and Figure 5.4.1. shows his results for the variation of this quantity with momentum. A difference between the values for the ratio found with opposite fields was accounted for by a small displacement in G. The error in the mean ratio due to this displacement is second order and estimated to be $<1\%$.

The variation of the positive-negative ratio with momentum is compared in Figure 5.4.1., with the previous most accurate result found by Owen and Wilson (1951) for the total flux (i.e. mesons and protons) at sea level. It is apparent that there is no significant difference between the results of the two experiments.

Also shown in Figure 5.4.1. are the results of an extended experiment with reduced magnetic field $\int Hdl = 2.67 \times 10^5$ gauss-cm. The results are seen to be consistent with those at higher field.

CHAPTER 6

THE MOMENTUM SELECTOR

6.1 The Basic Principle

It has been mentioned already (Chapter 3) that the speed of analysis of high momentum particles is considerably increased if the flash-tube part of the spectrograph is triggered only for the high momentum particles. In practice this means the selection of categories 0 and 1. The method used is to measure the height, regardless of sign, of the pulses from the momentum analyser, and to mix any pulse greater than that corresponding to category 1 in anticoincidence with the 5-fold pulse from the Rossi circuit.

6.2 The Electronic Circuits.Difficulties of Design

In the design of the circuit there were three main difficulties to contend with.

1. Differing time delays between a particle passing through the spectrograph and the start of the four momentum analyser pulses corresponding to levels A, B, C and D produce output pulses with large peaks at the beginning and end. This is overcome by applying a delayed gating pulse to the amplitude discriminator.
2. The amplitude of a category 1 pulse is roughly 80mV and in order to discriminate satisfactorily against pulses greater than this prior amplification is necessary. The degree of amplification must be such as to make the division between category 1 and 2 pulses quite distinct despite the spread in pulse amplitude associated with each category. An amplification factor of 100 is suitable,

since if the minimum separation is 0.3 category (See Chapter 5) this will give a difference of at least 2.4 volts which makes the design of the discriminator a relatively straightforward task. Unfortunately the amplifier has a wide range of input pulses to deal with varying from a possible -3.7 volts corresponding to B18 - C18 to + 4.8 volts corresponding to A25 + D25. A normal amplifier would overload on many of these pulses and even if the rate of input pulses was low enough to allow the amplifier to recover between successive pulses trouble would still be experienced from the large positive peak that precedes tha plateau region of the pulse. If this initial positive voltage excursion is sufficient to overload the amplifier, then the amplifier will be blocked to normal operation throughout the operative period of the discriminator.

2. The circuit must be capable of dealing with the high rate of input pulses ~50,000/min, the main problem being to avoid the pile-up of pulses anywhere in the circuit. This is most likely to arise as the result of overloading in the amplifier which will cause grid current to flow and charge up the coupling condensers through the relatively low grid to cathode resistance. Discharge at the end of the pulse can then only take place through the grid resistor, so that the overloading pulse will give rise to a long exponentially decaying tail which at worse will block the amplifier to normal operation and at best introduce an uncertain amount of jitter in the zero level.

The Amplifier

A conventional amplifier could be made to operate satisfactorily

under these conditions, but it would be necessary to use a high voltage h.t. line and valves which would handle the power involved and yet remain capable of operating in the Mc/s region. An alternative solution is to use the amplifier designed by Chase and Higinbotham (1952). This is so designed that it never blocks on negative input pulses and will handle positive input pulses u p to an appreciable fraction of the h.t. line voltage.

The basic circuit is shown in Figure 6.2.1. V_1 and V_2 are long tailed pairs. The resistance condenser network R_1 R_2 and C forms the negative feedback loop. The amplifier operates normally for small pulses, say c/volt, but a large negative input pulse causes V_{1a} to be cut off and the current through V_{1b} to approximately double. The resultant negative pulse at the anode of V_{1b} is then treated in a similar manner by V_2. Thus with the proviso that V_{1b} can carry twice its quiescent current without being driven into the grid current region there is no limit to the size of a negative input pulse than can be handled without "blocking".

The conditions for a positive input pulse are more critical. A large positive input pulse raises the potential of V_1 cathode eventually causing V_{1b} to be cut off and allowing V_{1a} to function as a cathode follower. The maximum allowable input pulse is then that which just does not draw grid current and can be an appreciable fraction of the h.t. voltage. V_2 must of course be capable of dealing in similar manner with the positive pulse produced when V_{1b} is cut off.

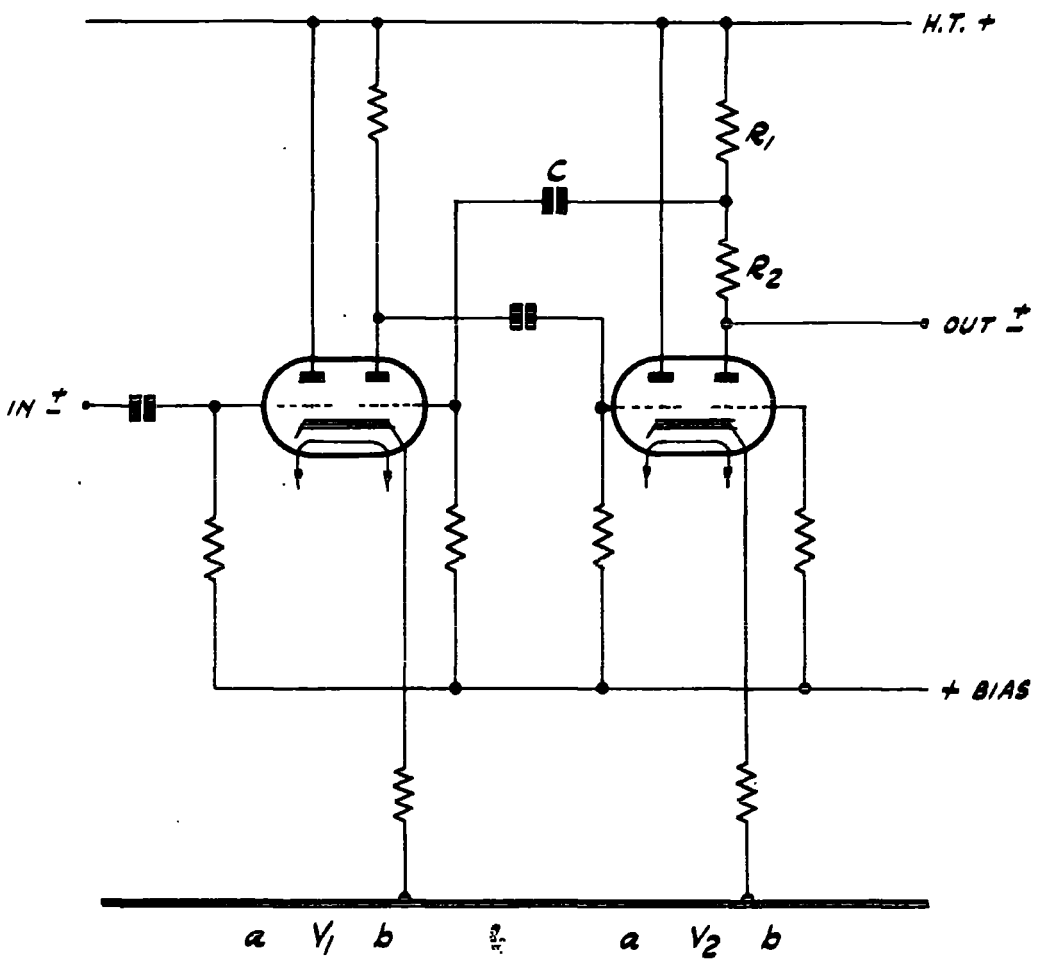

FIG. 6.2.1. THE BASIC CHASE - HIGINBOTHAM AMPLIFIER

The Complete Circuit

A block diagram of the final circuit is shown in Figure 6.2.2. and the complete circuit in Figure 6.2.3.

The mode of operation is as follows: The input pulses from the momentum analyser are amplified 100 times and fed via a phase splitter to two identical discriminators whose outputs are connected in parallel. One of the discriminators operates on positive pulses produced by negative input pulses and the other on positive pulses produced by positive input pulses. Separate controls for their bias levels enable any differences in amplification of positive and negative signals to be corrected. The discriminators are normally off in operation, being biased off by their suppressor grids, and are gated by a 4 μs pulse from a pulse generator which is triggered by a delayed pulse ($\sim 2\mu$s) from the Rossi circuit, so that the height of the plateau region of the desired pulse is measured. If this pulse is sufficient to operate either discriminator an output pulse is produced triggering a univibrator. This generates a negative anticoincidence pulse which serves to cut off a valve through which a further delayed pulse from the Rossi would normally pass. If the pulse is insufficient to operate the discriminator the delayed Rossi output pulse passes through this anticoincidence valve, is inverted and is fed to the flash tube high voltage pulse generator via a cathode follower.

In the main circuit diagram Figure 6.2.3. V_1 V_2 and V_3 form the amplifier and V_4 the phase splitter. V_{12} V_{13} and V_{14} generate the 4 μs pulse which gates the discriminators, V_5 and V_6. The usual

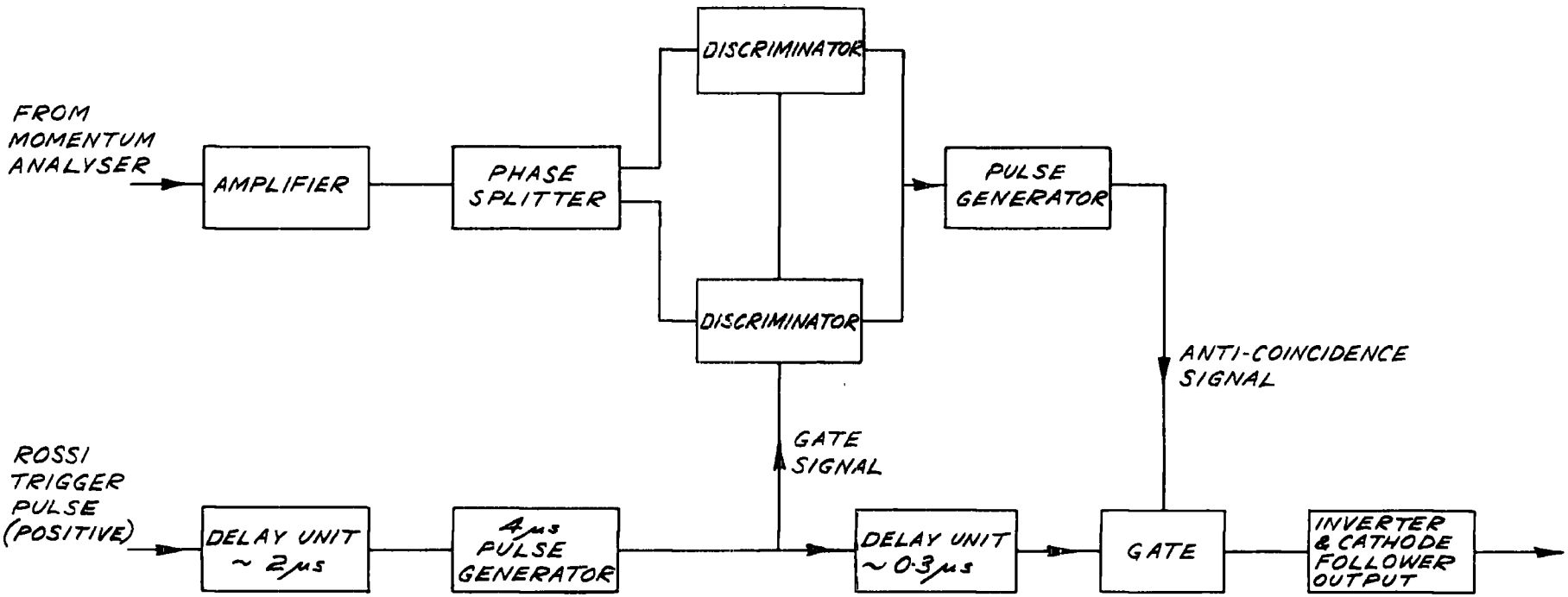

FIG. 6.2.2. BLOCK DIAGRAM OF MOMENTUM SELECTOR

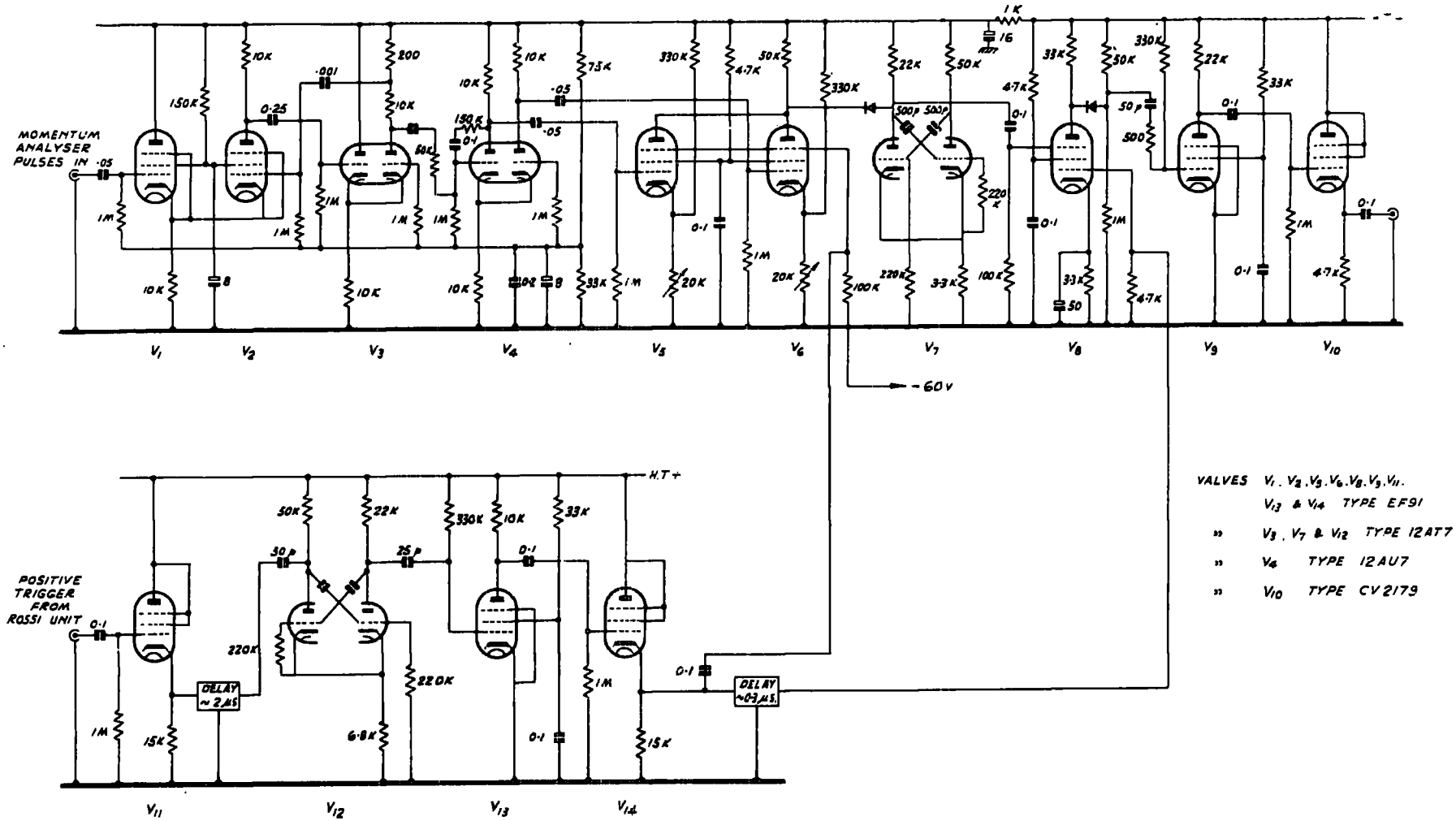

FIG. 6.2.3 THE MOMENTUM SELECTOR

cathode decoupling condensers are omitted from these valves so that they always present a high input impedance to the limited range of output pulses from the amplifier. V_7 is the univibrator which controls the anitcoincidence valve V_8. The period of this univibrator is designed to be shorter than that of the univibrator in the 4 μsec. pulse generator so that there is no confusion if the pulses arrive within a short time of each other. V_9 and V_{10} form the inverter and output cathode follower respectively.

The circuit was tested by the author and shown to discriminate between pulses from adjacent categories. A short period test using attenuated input pulses showed discrimination to within 1/5 category.

The instrument has since between operated by a colleague Mr. F.E. Taylor in the measurements on the cosmic ray spectrum referred to in the next section.

6.3 Performance of the Spectrograph When Operated With the Momentum Selector

The spectrum of fast μ-mesons has been determined by the author's colleagues and the main result is given here for the sake of completeness. The differential spectrum is shown in figure 6.3.1. The 5-fold counter measurements refer to the results in which the momentum analyser was used to determine the particle momenta. At higher momenta the flash tubes were used to give the necessary higher spatial resolution. For points marked "5-fold" all 5-fold coincidences operated the flash tubes. "Selector" refers to the use of the momentum selector; analysis in this range was by measurements of the track

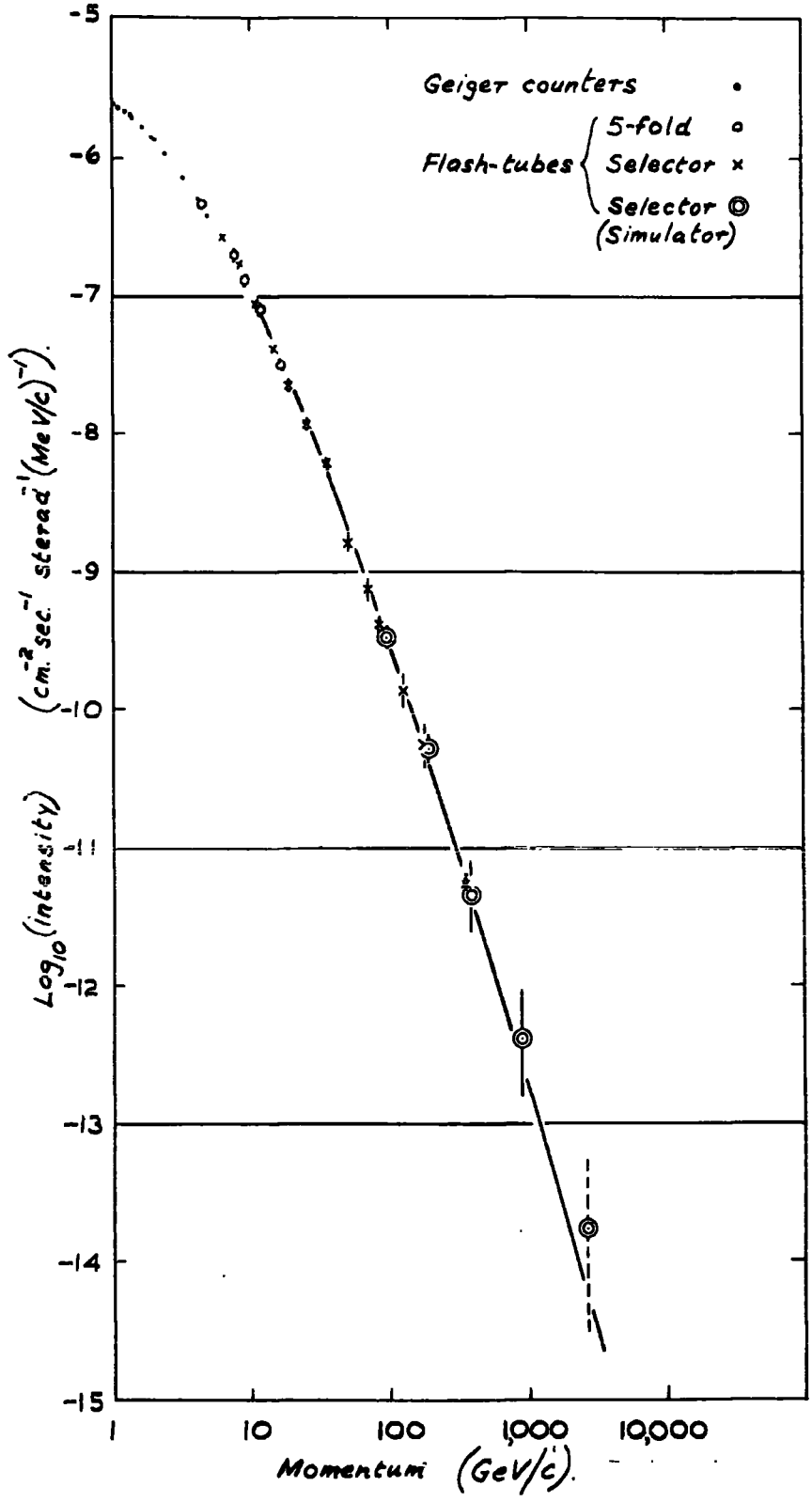

FIG. G.3.1. THE DIFERENTIAL COSMIC RAY SPECTRUM AT SEA LEVEL

positions on the photographs the accuracy being $\sim$1 mm at each level. For the "Selector - Simulator" points measurements of the highest accuracy were made.

An approximate analysis has been made to determine the form of the π^- mesons production spectrum which gives rise to a predicted sea level μ-meson spectrum which fits the observed spectrum. It is found that the π^--meson production spectrum can be written in the form

$$N(p)\,dp = Kp^{-\gamma}\,dp$$

where γ is roughly constant over the momentum range 1 - 1000 GeV/$_c$ and equal to 2.6.

The fact that there is no inconsistency apparent in the overlap regions of momentum where differing techniques give concordant results is of considerable relevance to the present study of the technical aspects of the instrument.

CHAPTER 7

THE IONISATION LOSS PROCESS

7.1 General Features

Charged particles traversing matter lose energy in a variety of ways, one of the most important, the so-called ionisation loss process, is the subject of the present study. This energy loss arises from collisions between the incident particle and atomic electrons. The most probable value of this energy loss for a particle traversing a section of a given medium is independant of the mass of the particle and is a function only of its charge and velocity. It is proportional to the square of the charge and varies with velocity v and energy (expressed in terms of the rest mass) in the manner shown in Figure 7.1.1. From this figure it can be seen that initially the energy loss decreases with increasing velocity as $\frac{1}{v^2}$, reaching a minimum at about $v = 0.96C$, and thereafter rises logarithmically with energy reaching a steady value at an energy (and velocity) dependent on the nature of the medium traversed.

The initial $1/v^2$ dependence results from the decrease in collision time with increase in velocity, tending to a limiting value as $v \rightarrow c$ and can be explained on simple classical grounds. The logarithmic rise after the minimum position, on the other hand, is a relativistic effect, and is due to the Lorentz elongation of the electric field of the incident particle in the direction at right angles to its path. This extends the region

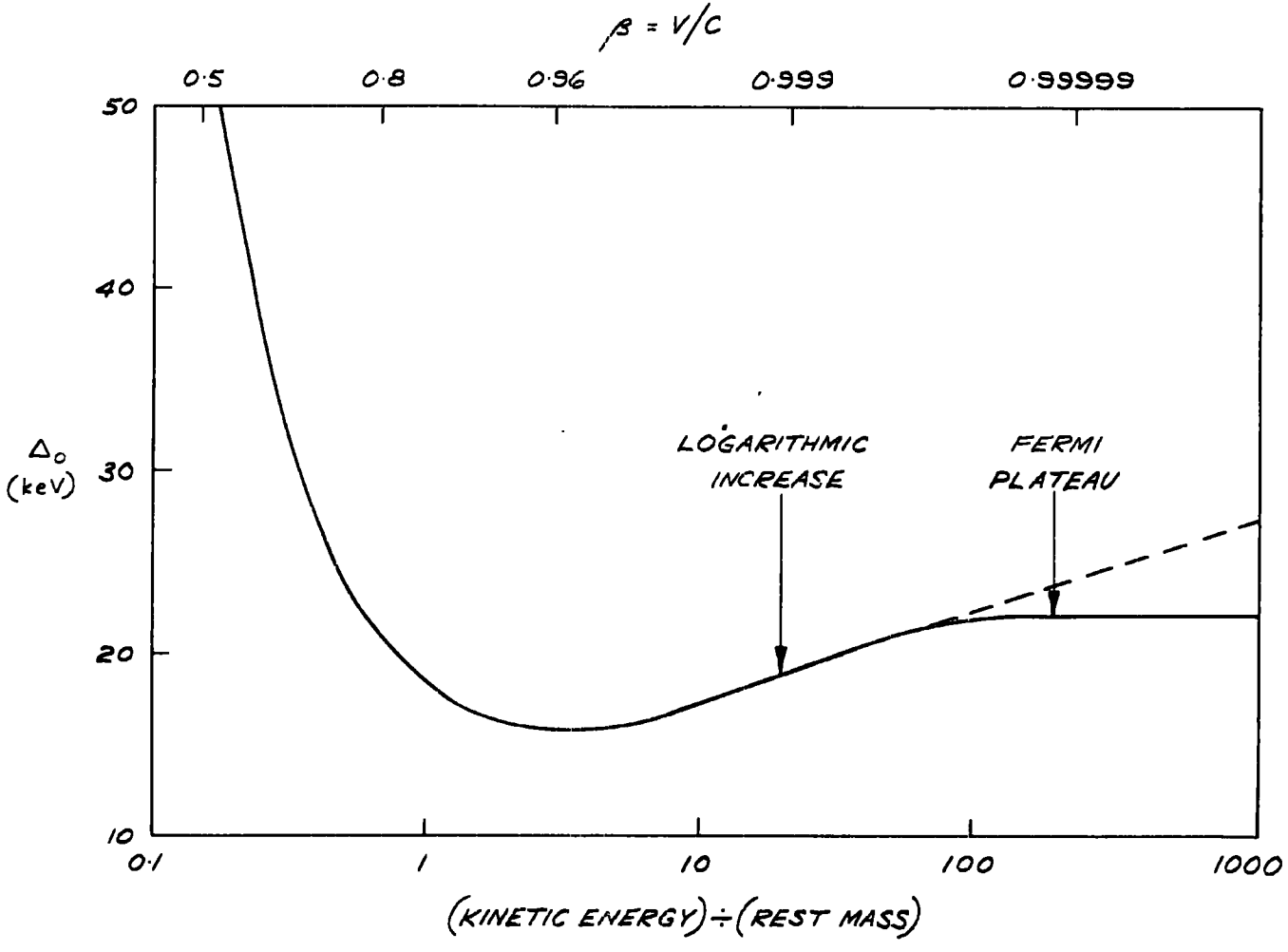
β = V/C
0·5
0·8
0·96
0·999
0·99999
50
40
30
20
10
Δ₀
(keV)
LOGARITHMIC
INCREASE
FERMI
PLATEAU
0·1
1
10
100
1000
(KINETIC ENERGY) ÷ (REST MASS)

FIG. 7.1.1.

of influence of the particle and increases the number of inelastic collisions. The increase with velocity does not continue indefinitely however, as the polarisation induced in the medium by the field reduces the field at large distances from the particle trajectory and screens electrons which would otherwise be affected. This saturation effect is known variously as the Polarisation or Density Effect.

7.2. Specific Features of the Process

The total energy loss, by collision, of a particle traversing a given thickness of a medium is governed by random processes and therefore does not lead to a unique value for the energy loss; thus in order to interpret the mechanism quantitatively a mean value has to be chosen. Two mean values are in common usage. The first is the average value of the energy distribution, defined by $\bar{E} = \int_0^\infty f(E)\, E\,dE$ where $f(E)dE$ is the probability of an energy loss $E \rightarrow E + dE$, and secondly there is the mode, or most probable value, of the energy distribution.

The most important difference between them is that the average value depends on both high and low energy collisions and is much affected by the relatively few high energy ones, which, because of the small impact parameters involved, depend on the nature of the particles involved in the collision, i.e. on their masses and spins etc. The most probable value on the contrary is determined mainly by the more frequent low energy collisions, and the nature of the particle (other than the charge) is not important. The two mean values can therefore be expected to differ in their

variation with velocity and on their dependance on the particles involved. It must be pointed out, however, that the average value measured in some experiments is not the average of all the results, but is an average value based only on those results in which the particle does not lose more than a certain amount of energy in a single collision. The extent of the difference between the behaviour of the two means will therefore be determined by the choice of the upper limit imposed on the energy loss in a single collision and it is clear from this that measurements of the average energy loss defined in this way are confined to experiments in which the individual collisions can be examined.

7.3 The Average Energy Loss

A theory of the collision loss process was worked out by Bohr as early as 1915 by using purely classical methods. Bohr obtained for the average rate of energy loss for a particle, charge ze and velocity V traversing an absorber the expression:

$$-\frac{dE}{dx} = \frac{4\pi z^2 e^4 n}{mv^2} \ln \frac{b_{max}}{b_{min}}$$

Where n is the number of electrons/gm, m is the mass of an electron, the thickness is measured in gm/cm^2 and $b_{max.}$ and $b_{min.}$ are the limits of the impact parameter that results in an inelastic collision. $b_{min.}$ corresponds to the maximum energy transfer, and can be determined from the amount of energy lost in a "head on" collision. $b_{max.}$ can be found from the fact that if the collision time, $\sim \frac{b}{v}$ is greater than the period of oscillation of the atomic electron no energy is transferred (When Bohr's original paper

appeared this referred to oscillation about an equilibrium position not to revolution about an atomic nucleus).

At a later date quantum mechanics was introduced into the theory to the extent of modifying one of the limits. $b_{min.}$ was then determined by the fact that impact parameters smaller than the dimensions of the wave packets representing the electron and incident particles have no meaning.

This method of introducing quantum mechanical considerations was not very satisfactory and in any case the theory did not give the correct frequency distribution of energy transfers. A more direct approach to the problem was made by Bethe (1932, 1933). He considered the case of energy loss resulting from distant collisions where it is necessary to consider the shell structure of the atom. Using Born's approximation for the atom he obtained for a singly charged particle

$$-\frac{dE}{dx} = \frac{2\pi e^4}{mv^2}\,\frac{NZ}{A}\left[\ln.\frac{2mc^2\beta^2\eta}{(1-\beta^2)I^2(Z)} - \beta^2\right]$$

η is the maximum energy transfer for which this model is appropriate $\eta \sim 10^4 - 10^5$ ev. $I(Z)$ is the minimum energy transfer leading to excitation or ionisation. Empirically it is found that $I(Z) = I_H Z$ where $I_H = 13.5$ ev (Bloch 1933). (Rather higher values have been taken in very recent work, e.g. $I_H = 14.6$ eV (argon) & $I_H = 24.7$ eV (helium) ref. Kepler et al (1958)

The total energy loss is the sum of this energy loss and that due to close collisions. In a close collision the electrons can be considered to be free. The lower energy limit in any collision

for which this is a reasonable assumption is of the same order as η

$$-\frac{dE}{dx}(>\eta) = \int_{\eta}^{E'_{max}} E' \Phi_{col}(E,E')\, dE'$$

where is the energy loss in a given energy transfer and $\Phi_{col}(E,E')dE'$ is the probability per unit path length $(gm\,cm^{-2})$ of absorber that a particle of energy E will lose an amount of energy $E' \rightarrow E'+dE'$ in a collision. Theoretical expressions for $\Phi_{col}(E,E')dE'$ for various particles are listed by Rossi (1952). For single charged particles heavier than electrons:

$$\Phi_{col}(E,E')dE' = \frac{2\pi N Z}{A}\frac{e^4}{mv^2}\frac{dE'}{(E')^2}\left[1-\beta^2\frac{E'}{E'_{max}}\right]$$

Then:

$$\int_{\eta}^{E'_{max}} E' \Phi_{col}(E,E')\, dE' = \frac{2\pi N Z}{A}\frac{e^4}{mv^2}\left[\ln\frac{E'_{max}}{\eta} - \beta^2\right]$$

for $E'_{max} \gg \eta$.

The total energy loss from both close and distant collisions then becomes:

$$-\frac{dE}{dx} = \frac{2\pi e^4}{mv^2}\frac{NZ}{A}\left[\ln\frac{2mc^2\beta^2}{(1-\beta^2)I^2(Z)}E'_{max} - 2\beta^2\right]$$

where E'_{max} is given from dynamical considerations by

$$E'_{max} = \frac{E_0^2 - \mu^2c^4}{\mu c^2(\mu/2m + m/2\mu + E_0/\mu c^2)}$$

where E_0 is the total energy of the incident particle and μ is its rest mass.

If $\mu \gg m$ and in addition $\frac{E_0}{Mc^2} \ll \frac{\mu}{m}$.

$$E'_{max} \simeq \frac{2mc^2\beta^2}{1-\beta^2}$$

$$\text{and } -\frac{dE}{dx} = 4\pi \frac{e^4}{mv^2} \frac{NZ}{A}\left[\ln \frac{2mc^2\beta^2}{(1-\beta^2)I(Z)} - \beta^2\right]$$

7.4 The Primary and Secondary Ionisation

The above equation describes the variation with velocity of the total average energy loss by collision of a charged particle, that is, energy loss both by ionisation and excitation processes, whereas in prectice it is the ionisation alone that is measured. This ionisation is made up of the primary ionisation produced directly by the incident particle and the secondary ionisation produced by the more energetic products of the primary ionisation. The primary specific ionisation, defined as the average number of ionising collisions per cm. at N.T.P., is given according to Bethe (1933) by

$$J_{pc} = 2\pi r_0^2 mc^2 n_0 z^2 \frac{Z}{I\beta^2}\left[\ln \frac{2mc^2\beta^2}{(1-\beta^2)I_0 z} + b - \beta^2\right]$$

Where $r_0 = \frac{e^2}{mc^2}$ is the classical radius, n_0 the number of atoms per c.c. of gas and a and b are constant for the given gas. a and b have been calculated for atomic hydrogen, but for other gases have only been determined by adjusting their values to fit experimental results.

The secondary specific ionisation has until fairly recently not been similarly evaluated as it is a complex problem involving many factors. Experimentally it is found to contribute about the same amount of ionisation to the total as the primary ionisation. Because of this uncertainty, therefore, it was not possible to obtain an expression for the total specific ionisation, which is the quantity that is most easily measured, but experiments have shown that there is a relationship between the total specific ionisation and the total energy lost by collision over the same path. This relationship is that the average energy required to form an ion pair in a given gas is to a good approximation a function only of the gas and is independent of the velocity or nature of the incident particle, so that the total energy loss by collision can be measured simply by measuring the amount of ionisation formed.

The degree of accuracy with which the relationship holds varies from gas to gas. Argon is particularly good in this respect. Most of the gases commonly used in ionisation experiments have been investigated and a review of much of this work has been given by Valentine and Curran (1958). Measurements of the amount of energy required to form an ion pair have been performed with electrons up to a few MeV and with protons up to 340 MeV. In the former case the range was fairly extensively covered, but in the case of the protons the high energy measurements were made at energies of 7.65 MeV (Gray, 1944) and at 340 MeV (Bakker and Segrè, 1951). From the measurements that have been made it is believed that for fast particles the average energy per ion pair is constant to within

a few percent.

Later work by Budini and Taffara (1956) has resulted in a sounder theoretical expression for the primary specific ionisation. This theory takes into account the detailed nature of the effect of collisions at large inpact parameters, considering the effect of energy loss by Cerenkov radiation and its possible re-absorption close to the particle trajectory. This it does by considering a multi-frequency model of the gas traversed. The theory predicts the relativistic logarithmic rise and the saturation effect at higher particle momenta. It allows the calculation of the primary specific ionisation for a given gas provided that the relevant energy transfers, oscillator strengths etc., are known.

More recently Budini et al (1960) have extended their previous work to cover secondary and tertiary specific ionisation. They have shown that the behaviour of the primary ionisation, the total ionisation and the total energy loss are different in the relativistic region. For instance, the value of the maximum energy transfer in a single collision that is appropriate to a given experiment determines both the total ionisation and the total energy less to a great extent, whereas the primary ionisation is little affected by the choice. Also, the fact that the secondary and further generations of ionisation are in general produced by non-relativistic electrons means that the relativistic increase of the primary ionisation will be greater than that of the total ionisation.

Their expressions for the mean primary, secondary and tertiary

specific ionisation are rather laborious to apply to actual gases, and so far only hydrogen and helium have been considered. The agreement between their theory and actual results is considered in the next chapter.

7.5 Fluctuations

As a result of the statistical nature of the collision processes there are considerable fluctuations in the values of the energy loss obtained when particles of equal velocity pass through a thin absorber. This spread in value is due to both the Poisson distribution of the number of collisions and to the variation in energy loss that can occur in any given collision.

Landau (1944) calculated the expected frequency distribution of energy loss for such a case. The result that he obtained is shown graphically in Figure 7.5.1. There it is plotted in the form of a universal relationship in terms of Δ_o, the most probable energy loss, and ξ defined by:

$$\Delta_o = \xi \left[\ln \frac{3000\,\beta^2 \xi}{z^2 (1-\beta^2)} + 1 - \beta^2 \right] \text{eV}$$

$$\text{and } \xi = \frac{2\pi N e^4}{mv^2} \rho \frac{Z}{A} x = \frac{1.54 \times 10^5}{\beta^2} \rho x \frac{Z}{A} \text{ eV.}$$

(x in cm)

The curve of the frequency distribution is seen to be roughly Gaussian in shape with a long tail on the high energy side. The peak at low energies is due to the many collisions with large impact parameters.

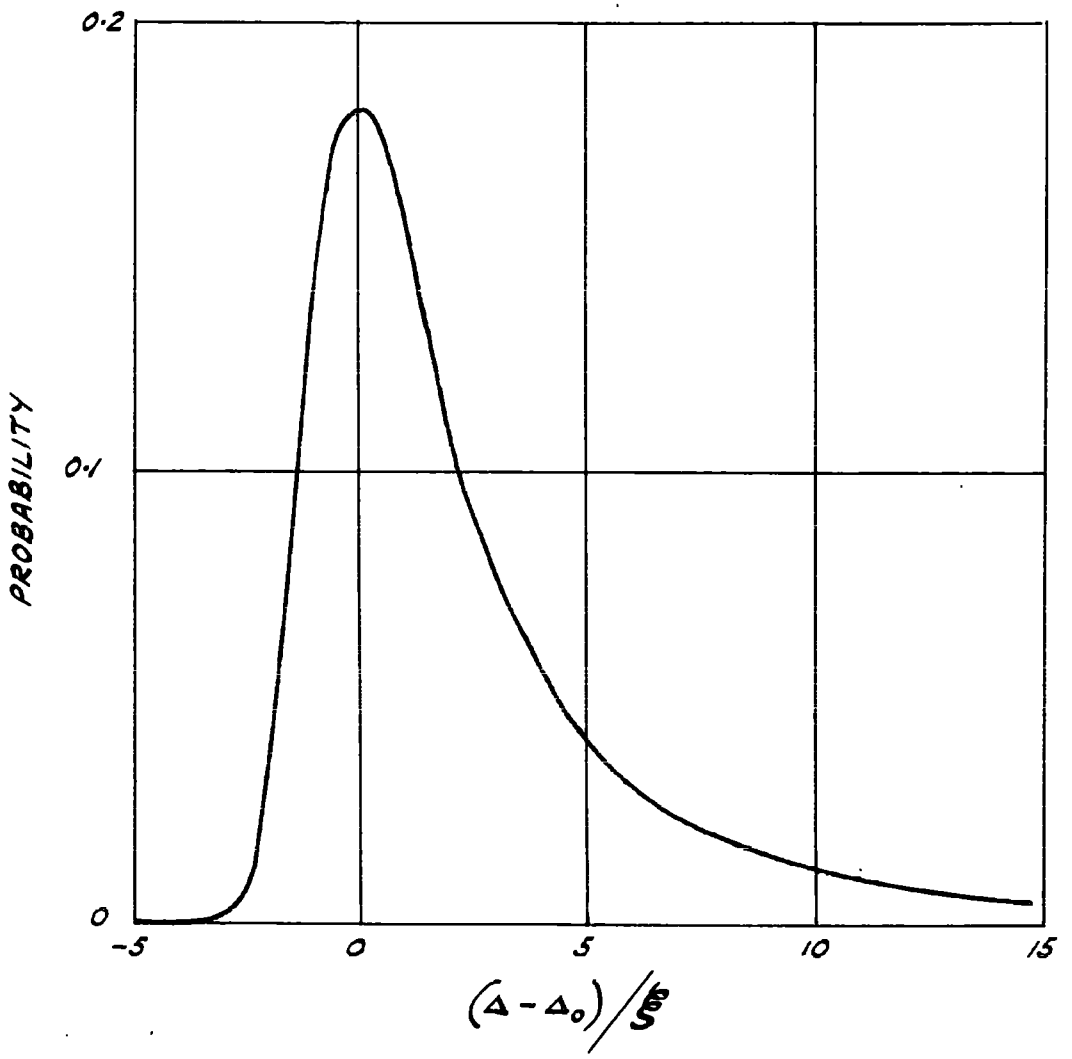

FIG. 7.5.1. LANDAU DISTRIBUTION

Experimentally it has been found that the width of the distribution defined as the width at half height, is wider than that predicted by Landau's theory even after correction has been applied for the uncertainty introduced by the measurements. For example, in measurements with a proportional counter a monoenergetic source of ionisation would give an approximately Gaussian distribution of width $\sim$ 8%. Two reasons have been advanced to account for this discrepancy. Fano (1953) and Hines (1955) have cast doubt on Landau's theory, pointing out that some of the approximations that he adopted were not strictly justifiable. On the other hand, Price (1955) has shown that Landau's theory should not be applied to many of the experiments performed with proportional counters, as these are much thinner absorbers than those envisaged by Landau in his treatment. In fact, for a gas, the product of the pressure in atmospheres and the depth in cm should be much greater than two for Landau's treatment to be applicable. Experiments by Bradley (1955) suggest that the product should be as high as $\sim$ 70.

The exact shape of the high energy tail of the distribution is difficult to determine experimentally. There is often an instrumental cut off at high levels of ionisation which eliminates some of the higher energy events. In the case of the proportional counter this can arise because of non linearity or even saturation of the counter or its associated amplifier. In addition this type of measurement would also be affected by rare events such as electrons knocked on from the walls of the counter or the undetected simultaneous passage of two particles through the counter. There is little

prospect therefore of making measurements of the average value of the distribution, affected as it is by the few higher energy events in the tail, and only the most probable value can be determined.

In cloud chamber measurements this difficulty can be avoided by measuring a restricted average value as mentioned above. $E_{max.}$ is then determined by the condition of the experiment and is not the maximum possible energy transfer in a single collision.

The average value defined in this way is a much easier quantity to determine than the most probable value, as the latter involves fitting a best curve to the results. In this respect therefore the cloud chamber possesses an undoubted advantage over the proportional counter.

7.6. The Density Effect

The effect due to the polarisation of the medium tends to nullify the increasing lateral extension of the incident particle's electric field as its velocity approaches that of light. The existence of this effect was suggested by Swan in 1938, but it was left to Fermi (1939, 1940) to make the first estimate of the magnitude. To do this he divided the medium surrounding the trajectory into two regions. Energy loss in the inner region was treated by using the Bethe-Bloch equation, and energy losses in the outer region by assuming this to be governed by purely classical electromagnetic interactions. The medium in this outer region was considered to act as homogeneous dielectric, composed of linear oscillators of one single frequency and the Poynting flux

across the boundary between the two regions was equated to the energy loss in the outer region. On comparing this result with that obtained when the Bethe-Bloch equation was applied to the whole medium Fermi obtained the following corrections.

$$\Delta = 2\pi \frac{NZ}{A} \frac{e^4}{mv^2} \ln \epsilon \quad eV/gm\,cm^{-2} \quad \text{for } v < c/\sqrt{\epsilon}$$

$$\Delta = 2\pi \frac{NZ}{A} \frac{e^4}{mv^2} \left[\ln \frac{\epsilon - 1}{1-\beta^2} + \frac{1-\epsilon\beta^2}{\epsilon - 1} \right] eV/gm\,cm^{-2} \quad \text{for } v > c/\sqrt{\epsilon}$$

Where ϵ is the dielectric constant.

If the correction for the case of $v \to c$ is applied to the expression for the most probable value of the ionisation loss given by Landau it is seen to lead to a constant value of the ionisation loss at these velocities. This is to be expected since the most probable value is determined almost entirely by the large impact parameter collisions which are effected by the Density Effect. If, however, the correction is applied to the average value given by the Bethe-Bloch equation no such saturation is indicated since the increase with velocity of the average value of the ionisation loss in the relativistic region depends both on the lateral extension of the field and on the reduction in the size of the smallest impact parameter in an inelastic collision. The correction will therefore not lead to a constant value, but merely a change in the rate of increase.

Halpern and Hall (1940, 1948) and Wick (1941, 1943) have extended

Fermi's theory taking into account the shell structure of the atoms using a multi-frequency dispersion model. Halpern and Hall's theory agrees with that of Fermi at very high and very low energies, but differs in the intermediate region.

The expression for the energy loss predicted for the outer region of Fermi's theory does not drop to zero as the dimensions of the inner region tend to infinity, but instead approaches a constant value. Fermi attributed this to energy emitted in the form of Cerenkov radiation, which is a form of electromagnetic disturbance emitted by a charged particle when its velocity through a medium exceeds that of the velocity of electromagnetic propagation in the same medium. It was pointed out later by Bohr (1948) and Messel and Ritson (1950) that the magnitude of this energy loss alone was equal to the entire increase in energy loss beyond the minimum value, and that if Fermi's model was correct it was difficult to see how the Cerenkov radiation could be trapped in the immediate neightbourhood of the particle trajectory and thereby produce the increase in ionisation loss that had been found experimentally. This criticism was equally true for Halpern and Hall's theory.

Later work by Huybrechts and Schonberg (1953), Fowler and Jones (1953) and Budini (1953) has shown that the amount of energy going into Cerenkov radiation is much smaller than that predicted by Fermi's theory. Budini has shown that the determining factor which also controls the form of the onset of the plateau region is the ratio of the breadth of the spectroscopic lines to the density

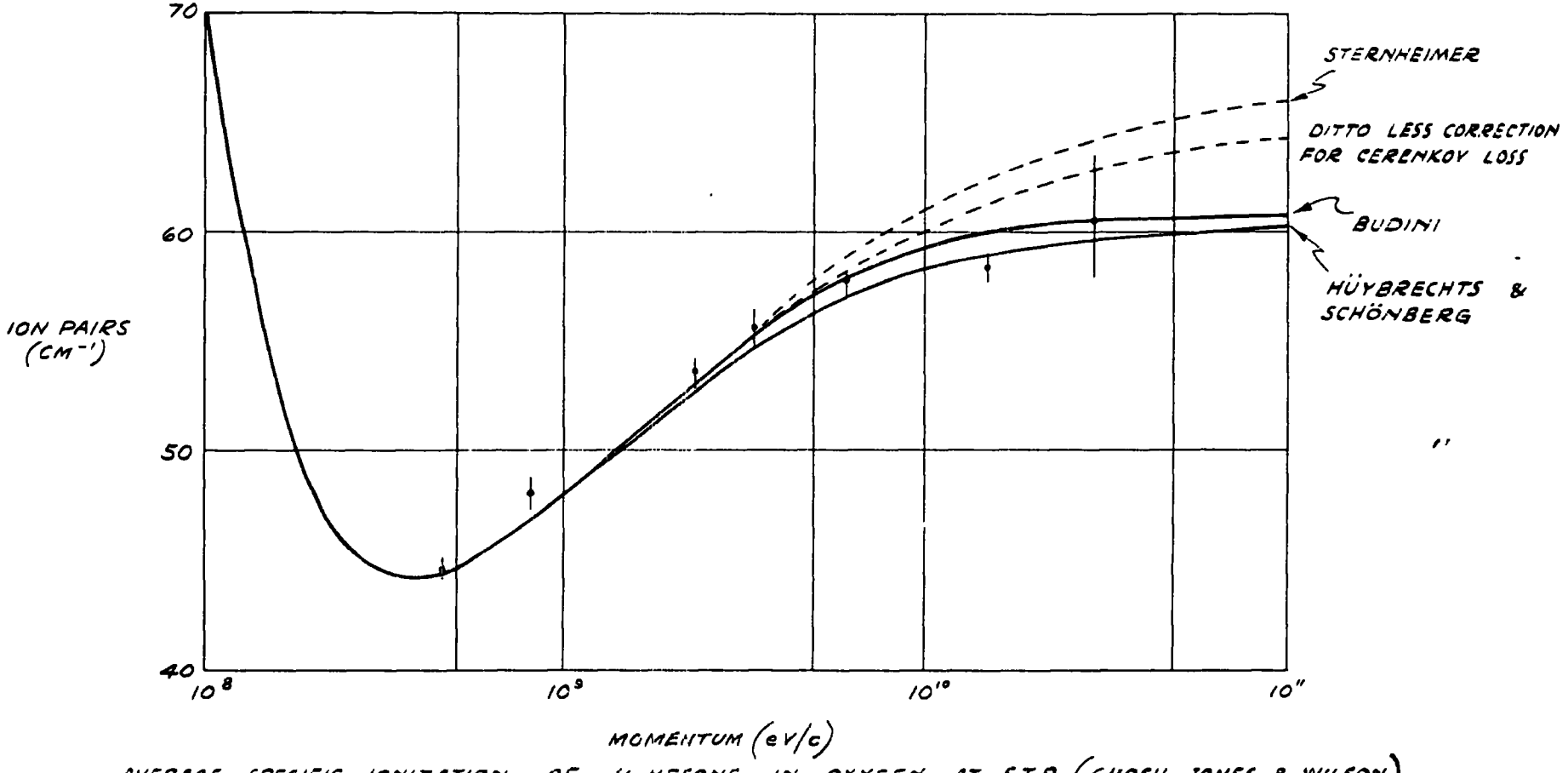

AVERAGE SPECIFIC IONIZATION OF μ MESONS IN OXYGEN AT S.T.P (GHOSH, JONES & WILSON)

FIG. 7.6.1.

of the medium.

Sternheimer (1952, 1953) has further developed the multi-frequency model and in a series of papers (1952, 1953, 1954, 1956) has applied his theory to a variety of different media. At present general agreement exists with regard to the overall features of the ionisation loss process, but there is disagreement on the exact form of the changeover from the log rise to plateau region.

The object of recent experiments on ionisation loss has been to investigate the nature of this transition region and to attempt to decide which of the various theories gives the best fit to the experimental data. The degree of agreement that exists between theory and experiment is illustrated by some results of Ghosh et al (1954) shown in Fig. 7.6.1. These are compared with the theoretical predictions of Budini (1953), Sternheimer (1953) and Huybrechts and Schonberg (1952). From this it can be seen that it is not possible to decide which theory represents the results better. This is so partly because of the low statistical accuracy of the results in the important transition region and partly because of the low upper momentum limit of the experiment. Work by other groups will be discussed in the next chapter, but the overall conclusions remain unchanged.

The majority of the theoretical work has been concerned with formulating expressions for the average energy loss. This, of course, can only be measured in a cloud chamber so that some of the theories, for example those of Budini and Huybrechts and Schonberg can, strictly speaking, only be compared with measurements made in

this way. Only Sternheimer's work is really applicable to measurements of the most probable energy loss, although for example Budini's theory will be approximately correct if a suitable value is chosen for the maximum energy transfer in a single collision. Since if this is about 1 Kev the average value will differ little from the most probable value in its variation with velocity.

Sternheimer's theory applied to the most probable value of the ionisation loss consists in essence of Landau's expression for the most probable energy loss together with a density effect correction based on a multi-frequency model. The validity of Landau's theory as applied to proportional counters has already been questioned, so that comparison of theory and data from proportional counter measurements is not very satisfactory. With this in mind the present study of the most probable value of the ionisation loss in neon was formulated, not only in order to obtain a statistically more accurate description of the transition and plateau regions, but also in the hope that statistically significant differences between theory and experiments might be found which would prompt and justify further theoretical investigations.

CHAPTER 8

PREVIOUS EXPERIMENTS ON IONISATION LOSS OF FAST μ-MESONS

8.1. Introduction

A variety of techniques have been used to study the ionisation loss of fast μ-mesons, but only two, drop counting in a cloud chamber and the proportional counter method, have proved really suitable for extensive and accurate measurements on the ionisation loss in gases.

8.2. The Cloud Chamber

In Cosmic Ray work the cloud chambers are usually counter controlled. The time sequence of events following the detection of a particle depends on the type of measurement to be performed. If the primary specific ionisation is to be measured, the cloud chamber is expanded immediately the particle has been detected. The ions then have little time to diffuse away from their points of origin and the droplets formed on the primary ions and their secondaries are so close together that they are either not resolved or they form a single blob. If instead the most probable value of the ionisation loss or the average value is to be measured then the ions are given time to separate before the expansion takes place. In a typical chamber measuring the latter the time sequence would be:-

Time 0 Particle detected and expansion started.

\+ 20 msec. Supersaturation achieved.

\+ 250 msec. Chamber illuminated and track photographed.

The chamber is then given a series of slow partial expansions to remove the droplets. The period of waiting time before it is ready for use again is ~10 min.

Two examples of the use of the Cloud Chamber technique are afforded by the work of Kepler et al (1958) and the work of Ghosh et al (1952). Kepler investigated the ionisation loss process using one cloud chamber operated in a magnetic field, so that momentum and ionisation measurements could be performed simultaneously. The maximum detectable momentum therefore varied with the gas under investigation and the method suffered from the disadvantage that the condition for maximum drop resolution did not coincide with that giving maximum location accuracy. Although by the use of improved techniques and helium and helium mixtures the conflicting requirements could be more nearly reconciled than heretofore. Kepler's results on the ionisation loss of μ-mesons covered the range of $\beta\gamma = 3$ to $\beta\gamma = 80$ (ie: p from ~300 MeV/c to 8 GeV/c) and in order to extend these measurements to higher values of $\beta\gamma$ a further series of measurements were made on electrons also from cosmic rays. In this way results were obtained up to $\beta\gamma = 1000$.

The values obtained for helium and helium + argon by Kepler et al are shown in Figs. 8.2.1. and 8.2.2. together with the predicted curves based on the theoretical work of Sternheimer and Budini. In the case of helium, agreement between theory and experiment is very good, but as the differences between the curves based on the alternative models are comparable with the errors involved in the measurements it is not possible to distinguish between them.

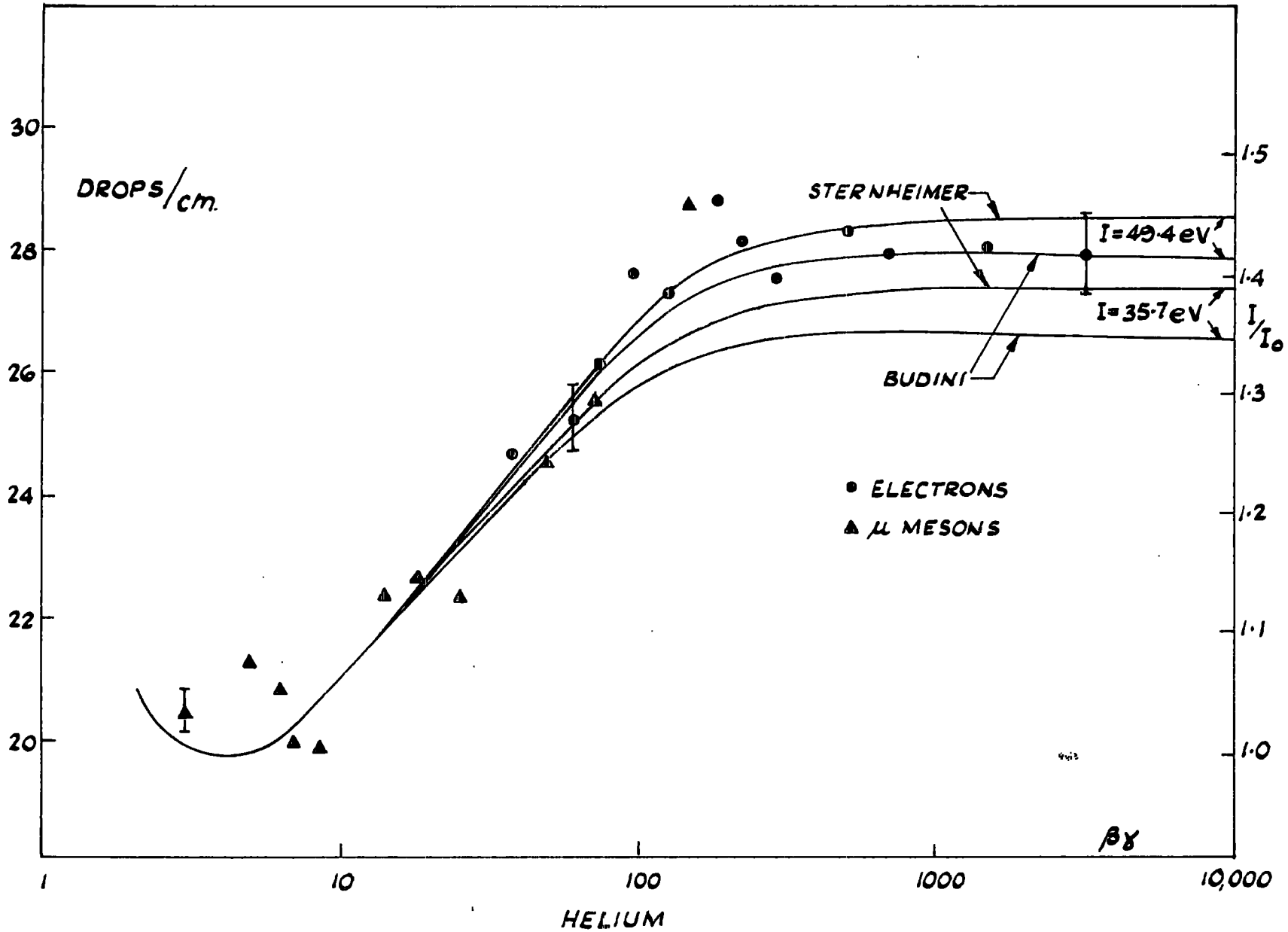
DROPS/cm.
30
28
26
24
22
20
STERNHEIMER
I=49·4eV
I=35·7eV
BUDINI
1·5
1·4
1·3
1·2
1·1
1·0
I/I₀
● ELECTRONS
▲ μ MESONS
βγ
1
10
100
1000
10,000
HELIUM

FIG. 8.2.1.

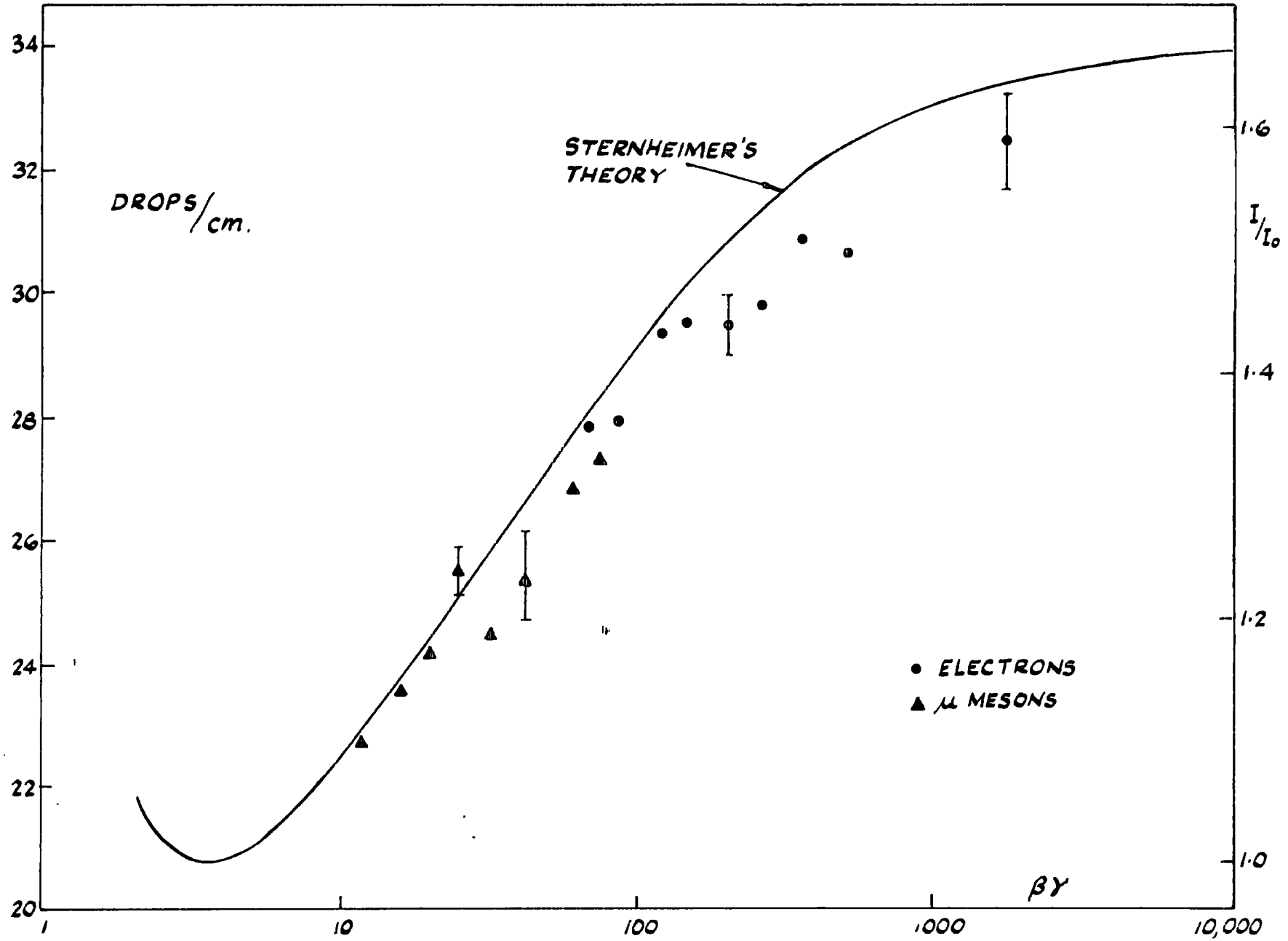
34
32
30
28
26
24
22
20
DROPS/cm.
STERNHEIMER'S THEORY
1·6
1·4
1·2
1·0
I/I₀
● ELECTRONS
▲ μ MESONS
βγ
1
10
100
1,000
10,000
ARGON & HELIUM

FIG. 8·2·2

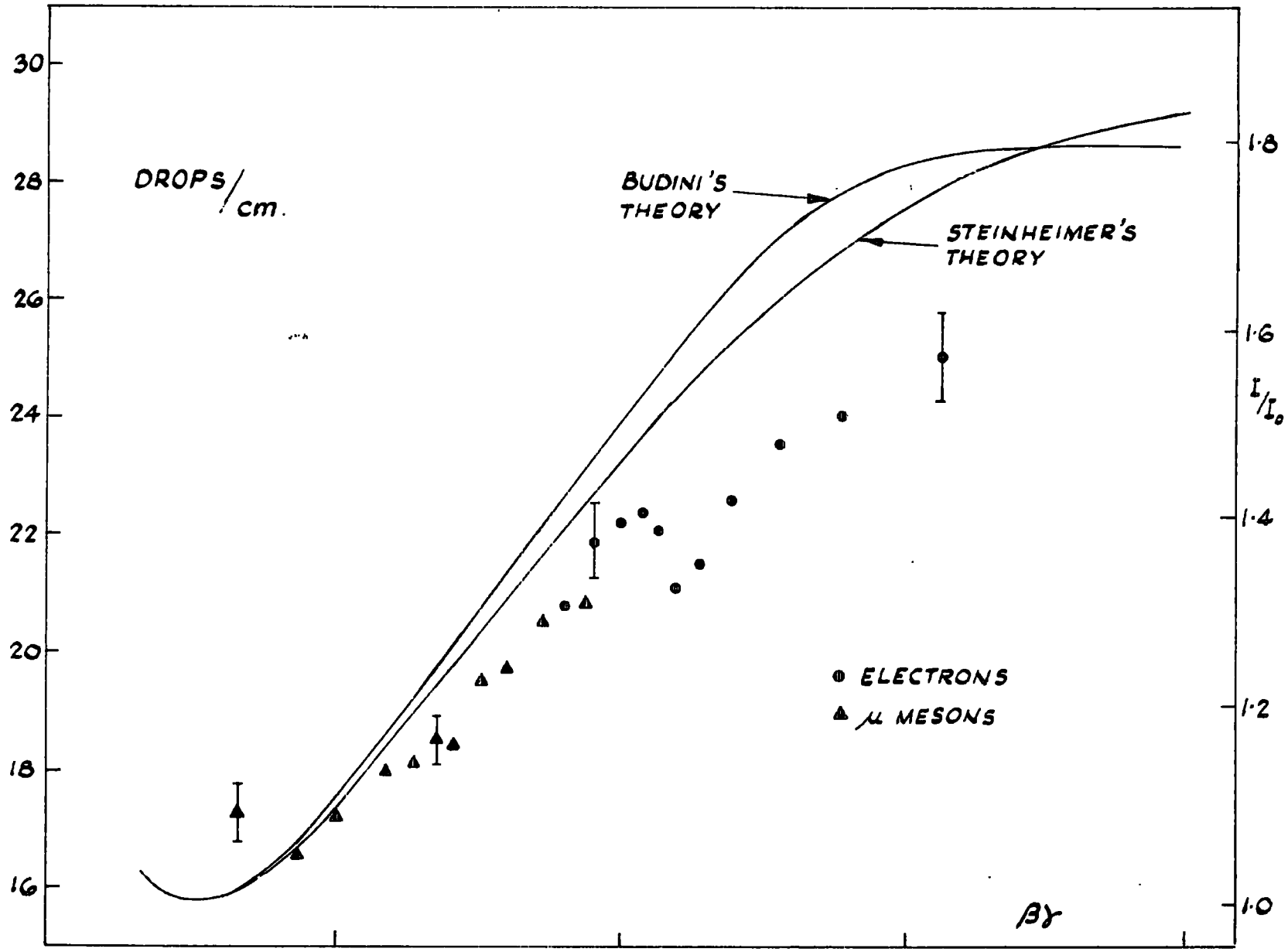
30
28
26
24
22
20
18
16
DROPS / cm.
BUDINI'S THEORY
STEINHEIMER'S THEORY
1·8
1·6
1·4
1·2
1·0
I/I₀
ELECTRONS
μ MESONS
βγ
10
100
1000
10,000
XENON + HELIUM

FIG. 8.2.3.

Agreement in the case of the helium + argon mixture is reasonable. The individual points are not significantly different from the predicted curve (Sternheimer's), but taken as a whole they yield a best fit curve that lies below the predicted one. This is even more evident in the heavier gases such as xenon (See Fig. 8.2.3.)

Kepler et al have suggested that these differences may be accounted for by an over simplification in the calculation of the maximum energy transfer involved in a single collision. Alternatively the screening of the inner electron shells in the case of the heavier gases may be important in the relativistic region where the impact parameters leading to ionisation are so much larger than at minimum ionisation. As this and other effects may operate much theoretical work needs to be done in order to disentangle the possible causes.

Returning to the work of Ghosh et al (1952), these workers measured the ionisation loss of μ-mesons in oxygen using a cloud chamber placed in the beam of the Manchester Spectrograph. In this way they were able to extend their measurements up to a momentum of $\sim$ 30 GeV/c, corresponding to $\beta\gamma$ = 300, and were able to establish the general form of the onset and shape of the plateau, but as pointed out previously, the accuracy of their points in this region was too low to distinguish between the models of the ionisation loss process proposed by Budini, Huybrechts and Schonberg and Sternheimer (See Figure 7.6.1.) Technically their method is potentially superior to that employed by Kepler et al, since the cloud chamber is used solely for ionisation measurements and the

counter spectrograph is in any case a more efficient instrument for measuring momentum for reasons that have been discussed before. Providing the time and effort were available there seems no reason why this method should not enable a decision on the correct model to be reached.

In connection with Kepler's work on electrons it is interesting to note that Barber (1956) has used the intense sources of electrons from an accelerator to investigate the ionisation loss. In this way he was able to use an ionisation chamber to perform his measurement. The gases investigated were hydrogen and helium at both 1 and 10 atmospheres and his electrons had energies varying from 2 to 35 MeV ($\beta\gamma$ from 4 to 70). His results agreed with Sternheimer's predictions to within the experimental error involved. This was $\sim 1\%$.

The results of Barber's work have also been applied to test the calculations of Budini et al (1960). They found good agreement between the experimental results for the total specific ionisation and their theoretical prediction in the case of helium and slightly less good agreement in the case of hydrogen. The experimental values in the latter case are 5 - 8% greater than the theoretical ones. This lack of agreement may be the result of the greater uncertainty in the theoretical data applicable to molecular hydrogen as opposed to the atomic helium.

8.3. Proportional Counter Measurements

The principle of operation of the proportional counter is

discussed in some detail in the next chapter. Essentially it consists of a vessel filled with gas and containing two electrodes. The cathode takes the form of a cylindrical or rectangular box and the anode is a fine wire stretched down the centre. Ion pairs formed in the gas are accelerated in the electric field between the electrodes and in the neighbourhood of the wire the electrons gain sufficient energy between collisions with the molecules of the gas to produce further ionisation. Under certain conditions the resultant overall charge multiplication factor is independent of the initial ionisation and the instrument is then known as a proportional counter. By exploiting this linear gas multiplication it becomes possible to measure amounts of ionisation that would otherwise pass undetected. The amount of ionisation produced by a relativistic μ-meson (~ 2 MeV/gm cm^{-2}) falls into this category.

As in the cloud chamber experiments the momentum of the ionising particle is measured by the same techniques as used in spectrum measurements. The proportional counter or counters are placed in the beam of the spectrograph together with a set of geiger counters, which act either as a simple telescope, or as guard counters, and ensure that the particle whose ionisation is measured actually passes through the uniformly sensitive region of the proportional counter.

Several workers have used this technique, e.g. Becker et al (1952) who measured the momentum with a cloud chamber in a magnetic field, Parry et al (1953) who used the Sydney Spectrograph, but

the group that have made the most extensive measurements on the one gas, neon, are the Manchester group, Eyeions et al (1955). Using the Manchester spectrograph in its modified form to determine the particle momenta they were able to make ionisation measurements on μ-mesons with momenta up to $\sim$100 GeV/C, i.e. $\beta\gamma$ = 1000. Four proportional counters were used stacked one upon another, so that four ionisation measurements could be made on each particle. Each of the counters was 25 cm. long, 9 cm. wide and 7.0 cm. deep and was filled with a mixture of neon and methane at partial pressures of 40 cm Hg and 4.4 cm Hg respectively at a temperature of 15^{o}C.

The relationship between output pulse height and the amount of initial ionisation produced in the counter was obtained by calibrating with the x-rays from Cr 51 and the linearity of response checked by using a series of such sources. Their results were based on some 5000 particles and covered a range from $\sim$1 GeV/c to $\sim$100 GeV/c. These results were split up into momentum bands balancing increasing statistical accuracy against the increasing uncertainty in the momentum to be ascribed to a given band as the number of the bands was decreased and the width increased. The most probable value of the ionisation loss for each group was then calculated, using the method of linear unbiased estimators of minimum variance devised for this problem by Hammersley and Morton (1955).

Their results are shown in Fig. 8.3.1. together with a theoretical curve based on Sternheimer's theory (1952, 53).

• EXPERIMENTAL RESULTS

⊘ " " PLUS 2%

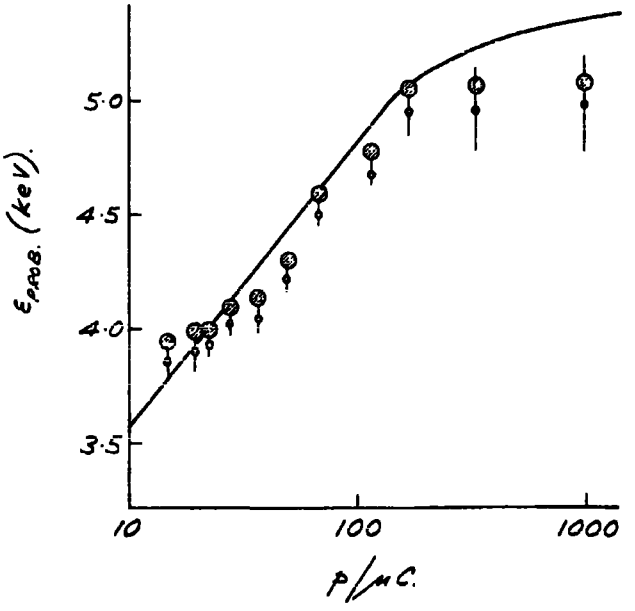

FIG. 8.3.1. IONIZATION LOSS OF RELATIVISTIC μ-MESONS IN NEON.

(EYEIONS, 1955)

The results suggest that the variation in ionisation with momentum falls off more rapidly than that predicted by theory, although the statistical accuracy is such that these results cannot be considered conculsive evidence for such an effect.

Greater statistical accuracy is required and possible an extension of the results to higher momentum regions, but whether the latter is a profitable policy taking into account the shape of the incident cosmic ray spectrum at these energies will depend largely on the size of the spectrograph. In any case the region already covered must be investigated again and to much greater statistical accuracy, and to do this a spectrograph with a greater collecting area than the Manchester one will be required, so as to accomplish the task in a reasonable time. It is expected that the Durham Spectrograph will enable this to be done.

8.4. Advantages and Disadvantages of the two methods

It is easiest if the various points are summarised.

1. Cloud Chambers

(a) Advantages: Long track length enables a series of measurements to be performed on the one track giving good statistical accuracy for one particle measurement. Rare high energy events can be excluded without losing more than a small fraction of the track length. It can be used to investigate gases with a high electron attachment coefficient. It is completely insensitive to all normal forms of electrical noise. Can distinguish between two

simultaneous events.

(b) Disadvantages: Bulky not easily adaptable. Slow, requires a long time to recycle. Difficult to maintain constant condensation efficiency, both with respect to time and position in chamber. Track measurements very tedious.

2. Proportional Counters

(a) Advantages: Capable of dealing with high particle rates. Operation can be made very stable. Easily calibrated. Easily adaptable. Easy to make measurements.

(b) Disadvantages: Very sensitive to electrical interference and so careful screening required. Difficult to construct counter of dimensions comparable with those of cloud chamber. Cannot distinguish between two simultaneous events. Only one ionisation measurement per particle. Only the most probable energy loss can be measured. Cannot use gases with high electron attachment coefficients.

Conclusions

It was decided to use the proportional counter technique to carry out the ionisation loss measurements. This decision was based on the following requirements and facts.

1. At low mementa the particle rate through the spectrograph is $\sim$ 2/min. and too high for a cloud chamber.

2. Time and resources for construction, operation and data analysis were limited.

On all these counts the proportional counter was the obvious choice. Its mode of operation and the factors affecting the accuracy of the ionisation measurements will be considered in some detail in the next chapter.

CHAPTER 9

THE PROPORTIONAL COUNTER

9.1 The Mechanism of the Proportional Counter

9.1.1. The Basic Processes: The ionisation chamber.

The degree of ionisation of a gas can be determined by applying an electric field between two electrodes immersed in the gas and measuring the charge collected. At low fields the separation and collection of the ions is considerably hampered by the reverse process of recombination and the opposing forces due to diffusion, but as the field strength is increased more and more of the ions are collected until eventually "saturation" sets in and all the ions reach the electrodes. An instrument operating under these conditions is known as an ionisation chamber.

The method of measuring the collected charge depends on whether the gas is subject to continuous ionisation, for example from a nearby radiation source, or whether the ionisation is produced "instantaneously" by the passage of a charged particle through the gas. In the former case the continuous current passing between the electrodes may be measured either directly with a galvanometer system or indirectly by allowing the charge to collect for a given period and then measuring the resultant voltage change. The ionisation produced by a single particle is more difficult to measure, for two reasons. In the first place the response time of the ionisation chamber and its associated measuring apparatus limits the maximum rate at which particles can traverse the instrument and still be recorded separately, and secondly, if the effects

of individual particles are to be studied then methods which depend on the integrated effects of many particles cannot be used to raise the signal level.

The response time of an ionisation chamber is limited by the transit time of the positive and negative ions from their point of origin to the appropriate electrodes. In an ordinary air filled chamber this will be of the order of milliseconds so that the maximum particle rate cannot be higher than a few tens, or possibly a few hundreds, per second, but by using certain other gases this rate can be increased considerably.

In some gases e.g. O_2 it is found that the mobilities of the positive and negative ions are roughly the same while in other e.g. N_2 and A, they differ by a considerable factor. This is because in the latter case the negative charge is carried by free electrons. In all gases the negative charge carrier starts as an electron, but in these gases, such as oxygen, which have a high probability of electron attachment the electron becomes attached to a neutral molecule within a very short time, perhaps after only a hundred collisions. If, therefore, a gas having a negligible probability of electron attachment is used, and measurements are performed only on the effects due to the motion of the electrons, the maximum permissible particle rate could be increased a thousandfold. This can be done quite easily, as the voltage pulse from such an ionisation chamber consists of an initial rapid rise due to the motion and collection of the electrons followed by a much slower rise due to the motion of the positive ions. If this

pulse is then differentiated with a time constant long compared with the transit time of the electrons and short compared with that of the positive ions an output pulse is obtained whose height is proportional to the electron component.

Under these conditions the output pulse is also a function of the initial distribution of the ionisation. The effect can be reduced by using non planar electrodes or can be eliminated by introducing a third electrode into the system so as to screen the anode from the effects of the positive ions.

The main drawback of the ionisation chamber is its low sensitivity. The lower limit of measurement in a typical case corresponds to an energy dissipation of about 60 KeV in the chamber. This means that in order to measure the ionisation loss of a relativistic μ-meson in a gas, the ionisation chamber must either be large or the gas filling must be under pressure.

A large chamber is necessarily associated with a high particle rate (of cosmic rays) making electron collection essential, and thereby introducing the complications alluded to above. In addition the high particle rate increasesthe difficulty of identifying the output pulse that is associated with a particular event. Alternatively if the gas pressure inside the chamber is increased, the dimensions can be reduced for the same stopping power, but this restricts its usefulness. In both cases high operating potentials are necessary to reach "saturation". The simple ionisation chamber is therefore not suitable for a detailed investigation of the ionisation loss

of relativistic particles under a variety of conditions. All these disadvantages can be overcome, however, by operating a smaller chamber with a potential difference between the electrodes greater than that necessary for saturation and sufficient for gas multiplication to occur.

9.1.2. Gas Multiplication

In an ionisation chamber the electrons and positive ions do not acquire more than a very small fraction of the energy expended upon them by an electric field. Most of it is lost in collisions with the molecules of the gas. Under the conditions apertaining in an ionisation chamber all the collisions are elastic ones and electrons reach a form of equilibrium in which, on the average, they gain as much energy from the field between successive collisions as they lose in the collisions. If the field is increased sufficiently, however the electrons can gain enough energy between collisions to undergo inelastic collisions and cause ionisation and excitation of the gas molecules. The secondary electrons produced will, in turn, undergo further inelastic collisions and the initial amount of ionisation will be considerably enhanced. If the degree of this gas multiplication is independant of the amount of initial ionisation, the device is said to be operating in the proportional region and is known as a proportional counter.

The simple parallel plate system of electrodes used for the ionisation chamber is not the most suitable arrangement for a proportional counter. The size of the output pulse will be a function of the charge distribution, as the degree of gas

multiplication will depend on the number of mean free paths traversed by any electron from its point of origin to the anode and also the potential difference necessary to provide the greater electric field may be excessive. Both of these difficulties are overcome by using a non-planar electrode system consisting in its simplest form of a hollow cylinder down the centre of which is stretched a wire. With this electrode geometry the field falls rapidly $\left(E = \frac{V}{\ln b/a} \cdot \frac{1}{r}\right)$* with distance from the central wire and if this is the anode no gas multiplication takes place outside a distance of a few wire radii from the centre. This region is very small compared with the whole counter, so that for all practical purposes all the electrons produced by the passage of an ionising particle undergo the same degree of multiplication and the induction effects at the anode caused by the motion of the positive ions will be due almost entirely to the ions formed (in this secondary process) within the sensitive region both by means of the rapid change in field with distance from the centre and by virtue of their greater numbers compared with that of the initial positive ions. This will ensure a constant multiplication factor throughout the whole volume and, by the choice of a sufficiently thin anode, gains of the order of hundreds can be obtained with quite moderate operating potentials.

The limit to which the gas multiplication can be pushed depends on the gas filling. If a gas as pure argon is used gas gains up to the order of a hundred can easily be obtained, but at gains of a few hundred counter operation becomes very difficult and the multiplication factor varies rapidly with changes in applied

* a is radius of wire, b radius of cylinder.

voltage if indeed the discharge remains stable at all. This is due to the action of photons produced in the multiplication process. As in this instance the counter contains only a pure gas the photons cannot eject photoelectrons from the unexcited gas molecules, but they can do so from the material of the cathode where the work function is only a few voltage e.g. 4.33 volts in the case of copper compared with e_r = 11.57 volts for argon. These photoelectrons then multiply in the same manner as before and as the time elapsing between emission of a photon and ejection of an electron from the cathode is only $\sim 10^{-8}$ second and the transit time of the electrons is quite short ($< 1\mu$ sec.) the successive avalanches follow each other so rapidly that their effects are additive. This process can increase the gain considerably. If A is the gain with negligible photo-effects and γ the probability of emission of a photoelectron per ion pair produced in the avalanche then the overall gain from both causes becomes $\frac{A}{1-A\gamma}$ and if $A\gamma \to 1$ the gain becomes very large indeed, $A\gamma > 1$ being interpreted as a continuous discharge.

Further delayed production of electrons may also occur when the positive ions strike the cathode, but in this case as the transit time is of the order of milliseconds the danger is not that the gain will be increased, but that these secondary electrons will be recorded as separate genuine events. A similar effect will also occur if a molecule in a metastable state returning to the ground state emits a photon which ejects a photoelectron from the cathode, the time delay in this case will be of the

order of milliseconds.

9.1.3 Gas Mixtures

A different state of affairs exists if a mixture of gases is used, because by virtue of the different energy levels existing in the two types of molecule various exchange phenomena can occur in collisions between the two, and it is possible by appropriate choice of gases to eliminate many of the disadvantages of the single pure gas.

One of the common mixtures of gases that is used is a noble gas, e.g. argon or neon, and a smaller amount of an organic gas or vapour, e.g. methane or ethyl alcohol. The ionisation potential of the methane molecule is 12.2 volts compared with 15.7 volts for argon and in addition the methane molecule has broad energy bands which lie below those of the excited states in argon. In fact the absorption spectrum of methane is a continum below 1630 Å (7.5 eV). This is due to the ability of the methane molecule to convert energy it has absorbed into energy of vibration or rotation of the molecule as a whole and because of this three important effects result.

1. The photons produced in the avalanche multiplication processes are absorbed.

2. Argon metastables can revert to the ground state by inelastic collisions with methane molecules, the excess energy being converted into rotational energy.

3. Positive argon ions colliding with the methane molecules have a high probability ($\sim$ 0.1) of undergoing charge exchange,

with the result that the ion sheath consists almost entirely of methane ions when it reaches the cathode. When the ions are neutralised they lose their excess energy by dissociating, so that no further electrons are ejected from the cathode to re-start the process. The argon molecule remaining after the charge exchange may be in an excited state from which it reverts by emitting a photon, but this too is absorbed by the methane.

Using argon and methane and similar gas mixtures gas multiplication factors of several thousand can be obtained before the counter ceases to operate in the proportional mode. The upper limit is set by space charge effect. The space charge created by one avalanche significantly reduces the effective field at the wire and interferes with the formation of successive avalanches formed by other electrons from the original group of ion pairs. Because of this the effective gain falls as the degree of initial ionisation increases. In extreme cases other mechanisms become important and the discharge instead of being localised spreads along the wire and the space charge formed is sufficient to "choke off" the discharge, with the result that the same amount of charge separation occurs whether the initiating particle is a relativistic electron or an alpha particle at the end of its range. Such behaviour is characteristic of the Geiger-Muller counter.

9.1.4 Characteristics of the Pulse From a Proportional Counter

Tha shape of the output pulse from a proportional counter is similar in character to that from an ionisation chamber, but the

mechanism is different. The secondary electrons from the avalanches are produced very close to the wire so that their contribution to the pulse is quite small and the initial rapid rise of the pulse is due almost entirely to the movement of the positive ions in the intense field in the neighbourhood of the wire. This quickly falls off and the pulse rise flattens off. The shape of the pulse profile is independent of the amount of initial ionisation and it is again possible to obtain a measure of the amount of ionisation from the height of the pulse after differentiation. Although excessive differentiation must again be avoided if loss in pulse height is not to be excessive.

9.2. Factors Affecting the Accuracy of Ionisation Measurement

9.2.1. The Factors

The degreee of reliability of measurements with a proportional counter depend on

a). The constancy of the gas multiplication factor. Its independence of time, position, distribution and magnitude of initial ionisation and the statistical uncertainty in its actual value.

b). The linearity and constancy of the gain of the associated amplifiers.

c). The accuracy of amplifier output pulse height measurements.

d). The accuracy with which the output pulse height can be interpreted in terms of the initial ionisation.

Items (b) and (c) are functions of the particular amplifying equipment used and a discussion of these factors is postponed until a later chapter when the amplifying and recording apparatus is considered in some detail.

9.2.2 The Constancy of the Gas Multiplication Factor With Time

There are four quantities which may vary with time and cause changes in the gas multiplication factor. These are the temperature, the gas filling, the counter E.H.T., and the electrical insulation of the counter.

Variations in temperature, unless of a large magnitude will cause negligible changes in the actual physical dimensions of the counter. The pressure inside the counter will vary with temperature, but the mass of the gas will necessarily remain constant. The kinetic energy of the gas molecules will increase with temperature and this will influence the length of the mean free path of the electrons between collisions with neutral molecules and thereby alter both the critical radius at which multiplication starts and the number of ionising collisions per unit path length. However, this effect is expected to be very small for the temperature changes envisaged i.e. a few degrees.

Another effect of temperature variations is to alter the concentration of the quenching gas by varying the amount that becomes adsorbed on the walls of the counter. This effect, fortunately, is not important for a gas such as methane used at room temperatures, but it does become so for counter quenched

with ethyl alcohol which are operated at temperatures below 5°C. The size and nature of the counter walls will also influence the magnitude of the effects.

The gas multiplication factor is very dependent on the counter E.H.T. voltage. In a typical case a change of E.H.T. of a few percent produces a change in gain an order of magnitude greater. It is essential therefore to maintain a very stable E.H.T. supply.

The gas filling may change with time due either to a leak in the counter or to the effect of successive discharges in the counter. If there is a leak and the pressure inside the counter is greater than atmospheric the resulting decrease in pressure will lower the "stopping" power of the counter and at the same time increase the gas multiplication factor. However, for a particle that loses only a fraction of its energy in the counter these two opposing effects will not cancel out, as the variation in the former case is roughly proportional to the pressure while in the latter it varies as a higher inverse power.

If, on the other hand, the pressure inside the counter is less than atmospheric, molecules of oxygen and water vapour in the air leaking in will provide very effective electron traps and even small amounts, of the order of ten parts per million, of counter gas will affect the operation of the counter. The electron trapping is not "permanent" as in the case of a condensed medium, but the negative ions formed have such a small velocity compared with that of the original electrons (about 10^{-3} of the electron velocity)

that they are effectively removed from the discharge.

The fraction of the electrons produced at a distance r_o from the anode that survive to reach the critical region (radius r_c) is given by:

$$\exp - \int_{o}^{r_o - r_c} \frac{dx}{\delta}$$ (see for example Sharpe, 1955).

or approximately $\exp - \int_{o}^{r_o - a} \frac{dx}{\delta}$ since $r_c \simeq a$

Where $\delta = \frac{W^2 \times 7 \times 10^{-16}}{\varepsilon/p \; C p h}$ is the mean free path against capture.

in a gas at pressure p containing a concentration C of contaminant of electron capture probability h, and W is the mean drift velocity when ε is the field strength.

$$W \sim \mu_- \left(\frac{\varepsilon}{p}\right)^{1/2}$$

Where μ_- is the electron mobility which is $\sim 10^5 \text{ cm}^{3/2} \text{ V}^{-1/2} \text{ sec}^{-1} \text{ atm}^{1/2}$ for many gases. Also $h \sim 10^{-4}$ so that δ reduces to $\sim \frac{7 \times 10^{-2}}{Cp}$ cm. For the counters in this experiment C is $\sim 10^{-5}$ for oxygen contamination and p is 0.53 atmospheres.

Then:

$$\exp - \int_{o}^{r_o - a} \frac{dx}{\delta} \text{ is } \sim \exp - \int_{o}^{5.5} 7.5 \times 10^{-5} \, dx$$

Therefore only about .04% of the electrons are lost by electron capture which is negligible.

In every discharge a certain amount of the quenching gas is dissociated. For a vapour such as ethyl alcohol the dissociation is permanent and its concentration gradually falls with time (of operation). Fortunately in a proportional counter the losses

when using ethyl alcohol or a similar quenching agent are not serious. For example a counter of the type used in the experiments to be described is subject to bombardment by cosmic ray particles at a rate of about 100 particles per second. If they each dissipate 6 KeV in the counter and the counter gain is 10^3 this will produce 2×10^7 ion pairs/sec. Assuming that the quenching mechanism is 100% perfect this will also be the number of molecules of alcohol that are used up per second, so that in a year 6×10^{14} molecules or about 10^{-9} mole of alcohol will be removed. In comparison with this the counter contains $\sim 10^{-2}$ mole of alcohol so that loss of quenching gas by dissociation is not likely to be of any importance.

Variations in insulation resistance of the proportional counter are due almost entirely to changes in climatic conditions. In an ionisation chamber, where it is often necessary to measure currents down to 10^{-14} amp., or to collect small quantities of charge over appreciable periods, the degree of insulation between anode and cathode must be very high indeed under all conditions.

In a proportional counter the response of the system to direct currents and low frequencies is zero and a steady small leakage of current between anode and cathode will not affect the pulse shape or size unless the leakage current is sufficiently large to produce a significant voltage drop in the network decoupling the counter from the E.H.T. supply. It may, however, conceivably lead to a further distortion of the electric field in the neighbourhood of the wire support (See 9.2.3c). The flow of current will alter

the d.c. level of the pulse amplifier, if, as in this experiment, the cathode of the counter is at a high potential and the anode is grounded through the grid resistor of the first valve. The change in bias level may make the amplifier response non linear and will increase the noise level, because not only will the valve be operating under conditions different from those selected to give minimum noise, but the leakage current flowing through the grid resistor will, because of its particle nature, be subject to random fluctuations.

The degrees of insulation required to minimise these two effects can be estimated. In the d.c. level case an additional bias of 0.1 volt could certainly be neglected, and if the grid resistor were 10^7 ohms and the E.H.T. supply 1 Kv this would require an insulation resistance of 10^{11} ohms. This can be relatively easily obtained and in the warm atmosphere of a room containing electrical apparatus dissipating several kilowatts this can easily be maintained.

The noise induced by random fluctuations in the leakage current is given by:

$$Vg = \left[\frac{eIg}{2C^2} \quad \frac{T_1^2}{T_1 + T_2}\right]^{\frac{1}{2}} \quad \text{volts (r.m.s.) (See chapter 10).}$$

where e is the electronic charge, I_g the leakage current, C the total grid capacity and T_1 and T_2 are time constants that express the bandwidth of the amplifier.

Using the values associated with this experiment V_g will be equal to 10 μ volts for a leakage current of $\sim 10^{-7}$ amps.

i.e. an insulation resistance of 10^{10} ohms.

9.2.3. Constancy of Gas Multiplication Factor With Position, Distribution and Amount of Ionisation

(a) Amount of ionisation. If space charge effects are not negligible the gas multiplication factor will vary with the amount of initial ionisation, becoming smaller as the ionisation increases. In any quantitative work therefore the counter must be checked for linearity over the range of ionisation expected.

(b) Equal quantities of ionisation, but different track lengths. The effect of columnar recombination will be more severe in the short dense track than in a long, less dense one. In addition, the spread in transit time of the electrons moving from their points of origin to the critical region may be sufficiently great in a large counter to give a faster rising output pulse from the shorter track and the amplifier being frequency dependent will respond differently to the varying rise times and introduce an additional uncertainty.

(c) Equal quantities of ionisation and equal track lengths. Variations in the gas multiplication factor may occur both along and across the counter. Variations along the length of the counter result from variations in the diameter of the anode wire or from the effect of field distortion caused by the finite length of the counter and the supports for the wire. The variations in wire

diameter become more important as the diameter decreases and this together with the increasing fragility of the wire, limited the smallest size that can usefully be employed. Apart from mechanical defects, changes in the effective wire diameter along its length may be caused by the presence of dust particles on the wire, so that when constructing a counter great care has to be taken to exclude dust and also to avoid introducing any further mechanical defects as might result from kinking the wire when it is being mounted.

The effect of the finite length of the counter and the wire supports is localised at the ends of the counter and the field is reasonably constant to within a few cathode radii of the ends. This holds when the wire is fastened directly to metal supports of sufficient diameter to reduce the gas gain to unity and the length of the counter is defined as the length of the wire. If the wire is terminated instead in insulating sleeves the length of the uniform response part of the counter will be more uncertain as an additional field distortion may result from the build up of static charges on the surface of the insulators.

The problem of indefinite length can be overcome either by using guard electrodes at the ends of the wire with the same diameter as the wire or by the more direct method of restricting the flux of particles to the central uniform field section of the counter allowing a suitable safety

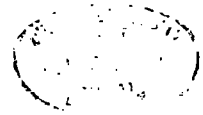

margin at either end. The latter is easily put into practice in cosmic ray measurements, because by using a simple Geiger counter telescope array those particles passing through the uniform region are selected.

Variations in gas multiplication factors across the width of the counter are due to a variety of causes. These are the effects of electron attachment, the effect of the radially asymmetrical electric field resulting from the rectangular cross section of the counter necessary to ensure constant track length (for vertical trajectories) and also the misalignment of the anode wire.

The effect of the presence of gases with high electron attachment probabilities is equivalent to a reduction in the gain of the counter. This effective gain will differ not only for long and short tracks, but also for two equal tracks, one of which passes close to the wire and the other which passes close to the walls of the counter, because the distance the electrons travel to reach the critical region will be different in the two cases and so also, therefore, will the probability of "Trapping". An additional difference may also arise because of the effect of transit times on the rise time of the output pulse, as mentioned above, although in the case of equal track lengths the effect will be smaller.

The radially asymmetrical field will have two effects; firstly, electrons equidistant from the wire may take different times to reach it, and secondly the critical region will

not be circular in cross section, so that the gas gain will vary with angle.

The additional asymmetry introduced by the displacement of the wire from the central position occurs both in the case of cylindrical and rectangular counters. In a cylindrical counter the magnitude of the effect is indicated by:

$$\frac{dE}{E} \simeq \frac{4a\Delta}{b^2}$$ (See Rossi and Staub, 1949).

where a and b are the anode and cathode radii respectively, E is the mean field strength in the neighbourhood of the wire and dE is the difference in field strength for directions on either side of the wire when it is displaced a distance Δ along this direction.

Smith (Private communication, 1959) has determined the form of the electric field configuration inside a rectangular counter both with the wire central and with it slightly displaced. Using the dimensions of the present apparatus it is found that the departure from a radially constant field in the case of zero displacement is negligible at distances of the order of the critical radius, and that the effect of displacing the wire is given to a good approximation by the expression for the cylindrical case on using a geometric mean of the dimensions for b.

The expected maximum displacement of the wire, taking into account the predicted sag under gravity, does not exceed 1 mm and using the value of $\frac{dA}{dV}$ (rate of change of gain

with E.H.T.) obtained for these counters the maximum spread in pulse height from this cause is less than 0.1% which is negligible.

9.2.5. Statistical Variations in the Gas Multiplication Factor

Even if the perfect proportional counter could be made and all the uncertainties described above eliminated there would still remain the spread in the gas multiplication factor due to the statistical nature of the multiplication process itself. The extent of this spread has been evaluated by Curran et al (1949) for the case where the gain is much greater than one. Then, if the initial number of electrons is N, and $\bar{M}$ is the mean multiplication factor, the probability that M will lie between M and M + dM will be given by:

$$\frac{M}{\bar{M}}^{(3/2N-1)} \quad e^{-3/2N\left(\frac{M}{\bar{M}}-1\right)} \quad dM.$$

The fractional statistical deviation of this curve is $(\frac{2}{3}N)^{\frac{1}{2}}$ This spread was shown to be approximately equal to that introduced by the spread in the mean value of the average energy loss per ion pair formed, so that the total factional standard deviation of a pulse distribution from a perfect counter will be $(4/3N)^{\frac{1}{2}}$. An energy dissipation of 5 KeV in argon will therefore give an output pulse whose fractional standard deviation in height will be $(\frac{4}{3 \times 200})^{1/2}$ i.e. ~ 8%.

9.2.6. The Relationship Between Pulse Height and Energy Dissipation

When the inaccuracies and variations in response of the

proportional counter and its associated amplifier and display equipment have been reduced to a minimum there remains the problem of determining the numerical relationship between an output pulse height, measured in volts (or cm) and an initial expenditure of energy, measured in ev. It is not practicable to obtain this relationship by determining the relevant factors in the chain of processes, i.e.

(a) The average amount of energy required to form an ion pair.

(b) The gas multiplication factor of the counter.

(c) The gain of the amplifier.

and performing the necessary calculations. This is so, because it is not possible to calculate (b), the gas multiplication factor, given the dimensions of the counter, details of the gas filling and the E.H.T. voltage. This means that it must be determined experimentally and the method used to do this can by a slight modification be used to calibrate not just the counter, but the system as a whole, thereby enabling one to obtain the relationship between final pulse height and energy loss directly.

The way in which the gas multiplication factor can be measured is to expose the counter to radiation, e.g. α— particles or X-rays so that the entire energy of the particles or photons is given to the gas. The output pulse height is then measured under normal conditions and then with the E.H.T. reduced to give a gain of unity. This is a satisfactory procedure for low gains, but not for high where the large amount of ionisation necessary for the measurements with no gas multiplication may be subject to space charge effects under

normal conditions which seriously reduce the measured value of the gain, whereas for the amounts of ionisation that the counter is expected to measure these effects may be completely negligible.

A better method is to irradiate the counter with X-rays of known energy, comparable to the expected energy losses under investigation, and to measure as before the pulse height corresponding to the total absorption of individual photons. This then yields the calibration factor directly.

Originally the X-rays were produced by irradiating a sheet of a selected metal with γ -rays from a radioactive source, but with the appearance of easily available radio-isotopes it became possible to use instead K-capture X-ray sources. This method was pioneered by Rothwell et al (1950) in their work on the calibration of proportional counters and their application to energy loss problems notably that of the ionisation loss of relativistic electrons.

The method is a very convenient and powerful one, because not only can the counter pulse be calibrated directly, but by using a number of different X-ray sources the linearity of the system can be checked and by calibrating the counter with a single source placed in different positions the constancy of the gas multiplication factor along and across the counter can be verified. The only restriction on this is that it is necessary to provide a thin calibration window in the counter walls. Mica is often used for this purpose. If this is not done and a large source is used instead, the low energy ($\sim$ 10 KeV) calibration X-rays are excessively attenuated in comparison with the higher energy ($\sim$ 1 MeV) X-rays which are also

emitted by the sources. The high energy X-rays have a much smaller probability of losing all their energy in the counter, but they give rise to electrons and photons extending over a wide energy range and the contribution from the calibration X-rays is lost. It is important to note that this method of calibration may be subject to a small systematic error. This arises from the fact that the photoelectrons produced by the K-capture X-rays have a range in the gas of only a few millimetres, whereas the ionisation under investigation is produced along a path of 11 cm. These differences in track length can lead to difference in output pulse height for the same initial amount of ionisation, for the reasons discussed above (section 9.2.3. (b)). The affect is expected to be small, however, it will be considered again in Chapter 12 when the results of the ionisation experiment are analysed.

9.3. The Construction of the Proportional Counters

The constructional details of the proportional counters are shown in Figure 9.3.1. The cathodes were made from a section of copper waveguide roughly sawn to length and then accurately milled. The two holes for the calibration window were drilled and the ends of the counter polished with fine emery paper ready for the brass end pieces to be soldered in place. These brass end pieces were machined to shape, drilled and tapped to take the feed-through insulators, screening caps and the brass gas inlet pipe. The inlet pipe was brazed on, the edges of the brass plates tinned and the completed end pieces soldered onto the copper waveguide. A rinse with carbon tetrachloride was then given to remove traces of oil and grease.

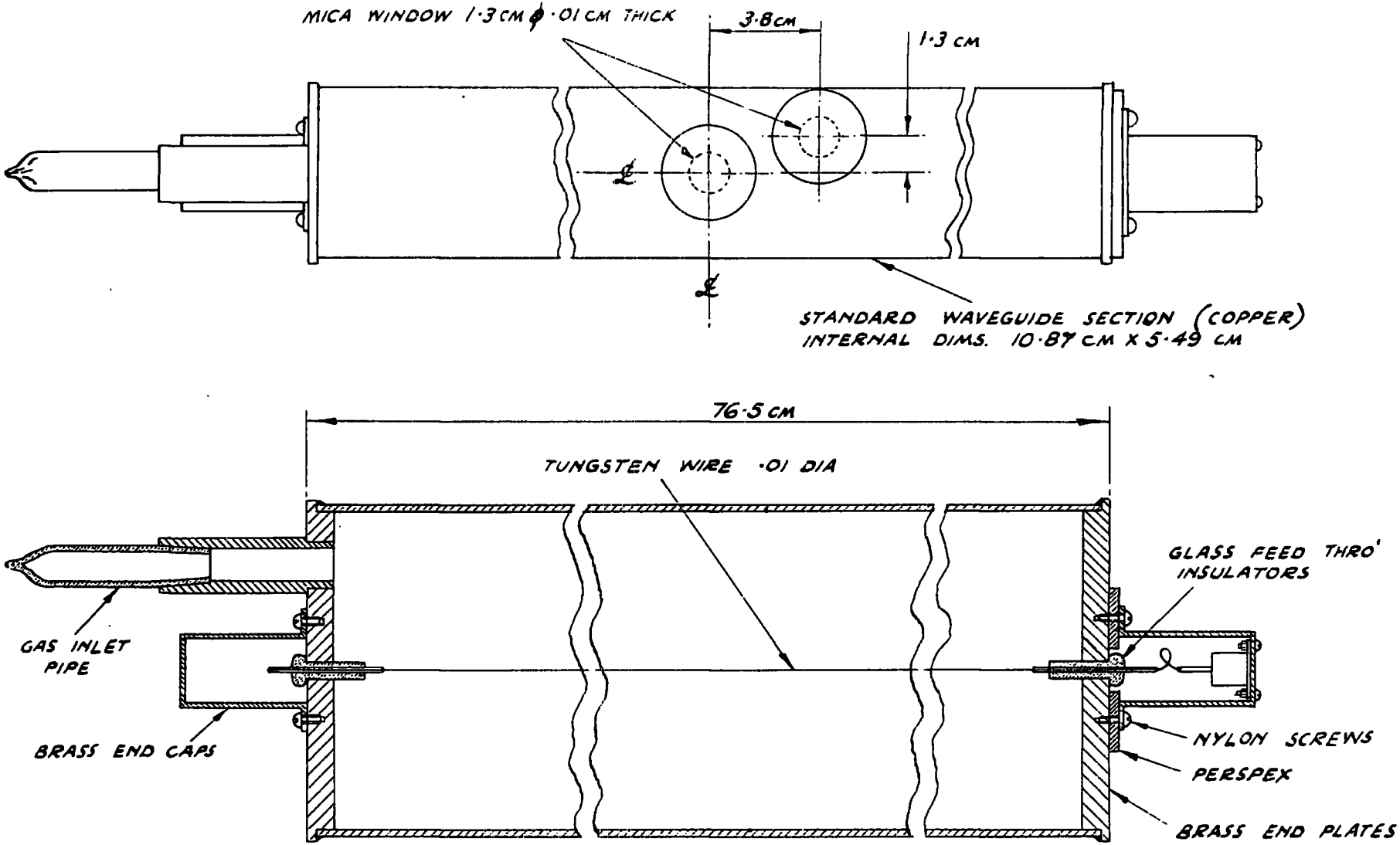

FIG. 9.3.1. SKETCH OF PROPORTIONAL COUNTER

The central tungsten wire was passed through the holes in the brass end plates using a thick (14 SWG) copper wire as a lead and the glass feed-through insulators threaded onto the ends of the tungsten wire. 'Araldite' was then used to fasten the insulators, wire and glass inlet pipes in position. In order to prevent the wire from sagging the 'Araldite' was allowed to set with the counter supported vertically and with the wire stretched by a 200 gm weight. When it was certain that the 'Araldite' had set hard the counters were rinsed out with water and detergent, tap water, distilled water and finally with acetone. They were then allowed to drain and the remaining traces of acetone removed by evacuating them.

The mica windows were fastened on with 'Araldite' and a layer of 'Araldite' painted over all the soldered joints as a precaution against possible pin-holes. The constructional work was then completed by putting on the screening cans as shown in the diagram. The connection to the anode was made by binding the tungsten wire to its supporting metal tube with tinned copper wire and soldering the latter in position. The completed counters were then sealed on to the vacuum system, pumped down and tested for leaks. After flushing out with 1 cm. of Neon and re-evacuating, the counters were filled with 2.9 cm of methane and 40.1 cm of Neon at 20^{o}C. Each counter was then given a preliminary test using cosmic rays as a source of ionisation and were found to operate satisfactorily in the same voltage region.

CHAPTER 10

THE ASSOCIATED ELECTRONIC CIRCUITS

10.1. General features

A block diagram of the proportional counter and its associated electronic circuits is shown in Fig. 10.1.1. The pulses from the counter, which are of the order of a few hundred microvolts for relativistic particles, are amplified about five hundred times by a head amplifier mounted close to the counter and pass from there via several metres of screened cable to the main amplifier and recording equipment. Each counter has its own head amplifier, but the output pulses from all the units are mixed and fed into one common main amplifier. The system is designed for a maximum of four separate counter chains.

10.2. The Stabilised E.H.T. Supply

This is based on an A.E.R.E. design and is capable of supplying up to 2.5 kv. The output from this unit, which has its own integral coarse and fine output controls, is connected to the counters via a 25 step potentiometer chain and a decoupling network consisting of 100K ohm resistor and a 0.5 μF condenser. The resistance to ground of this condenser and the associated feed through insulators was better than a few times 10^{10} ohm at 2 kv, so that relative changes in the E.H.T. could be conveniently monitored

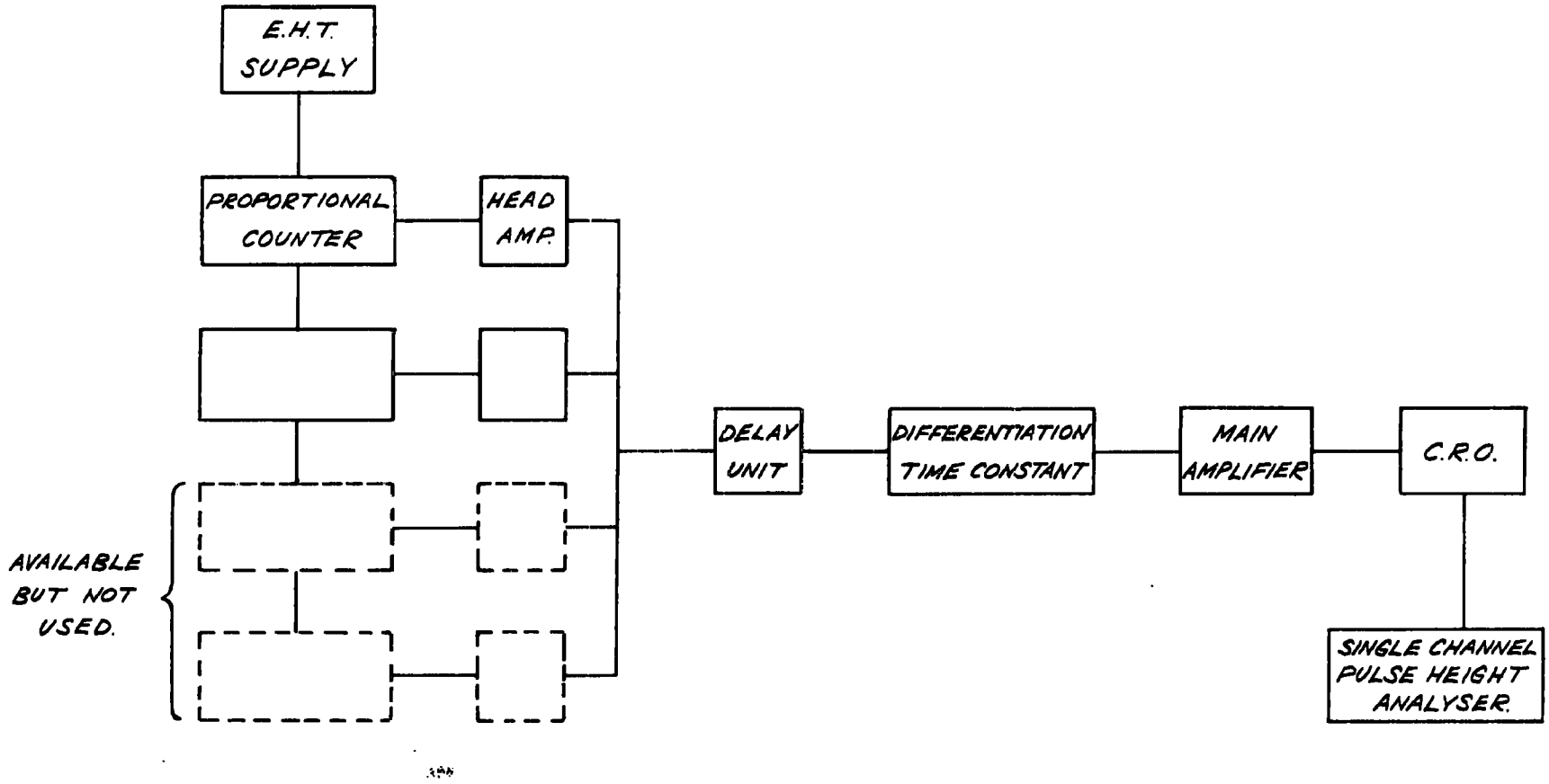

FIG. 10.1.1. BLOCK DIAGRAM OF PROPORTIONAL COUNTERS & ASSOCIATED AMPLIFIERS.

at the output terminals of the E.H.T. pack instead of directly across the counters.

The E.H.T. was monitored by comparing a fraction of it with the E.M.F. of a standard cell using a Pye 'Scalamp' galvanometer as null indicator. With this arrangement the sensitivity was such that the lowest limit of measurement of 1 part in 6000 was imposed by the number of decades on the resistance box rather than by the minimum detectable shift of the galvanometer light spot.

A typical set of day to day E.H.T. readings is shown in table 10.2.1.

Table 10.2.1.

	E.H.T. (mult. by const.)
Sunday	5954
Monday	5952
Tuesday	5954
Wednesday	5950
Thursday	5948
Friday	5950
Saturday	5950

A study of the gas multiplication factor versus E.H.T. curves for typical proportional counters (Rossi & Staub, 1949) indicates that for small voltage changes a given fractional change in E.H.T. can produce a change in gas gain an order of magnitude higher.

This was subsequently borne out by experiments on the actual counters used in this experiment (see Chapter 12 for details). If therefore results are to be consistent to within ± 1% over a run the E.H.T. supply should be stable to at least one part in a thousand in order to remove any uncertainty as far as it is concerned. Table 10.2.1. shows that the E.H.T. pack satisfies this criterion.

10.3. The head amplifier

This is based on the well known ring of three circuits, and is shown in fig. 10.3.1. The first three valves are the amplifier proper with the negative feedback loop connected between the cathode of V_3 and the cathode of V_1. The fourth valve is a cathode follower providing a low output impedance for the pulses which have to be fed to the main amplifier via several metres of cable. V_4 is necessary even if, as was done originally, the signal is taken from the very low impedance point at the cathode of V_3 instead of from the relatively high impedance at its anode. This is so, as in the former case the output impedance is not purely resistive, but includes an inductive component which causes the amplifier to oscillate when loaded by the capacity of a few metres of cable (see for example Elmore & Sands, 1949).

The changeover to the present system was prompted by the fact that the ordinary cathode follower can only handle satisfactorily fast rising pulses of positive polarity and also

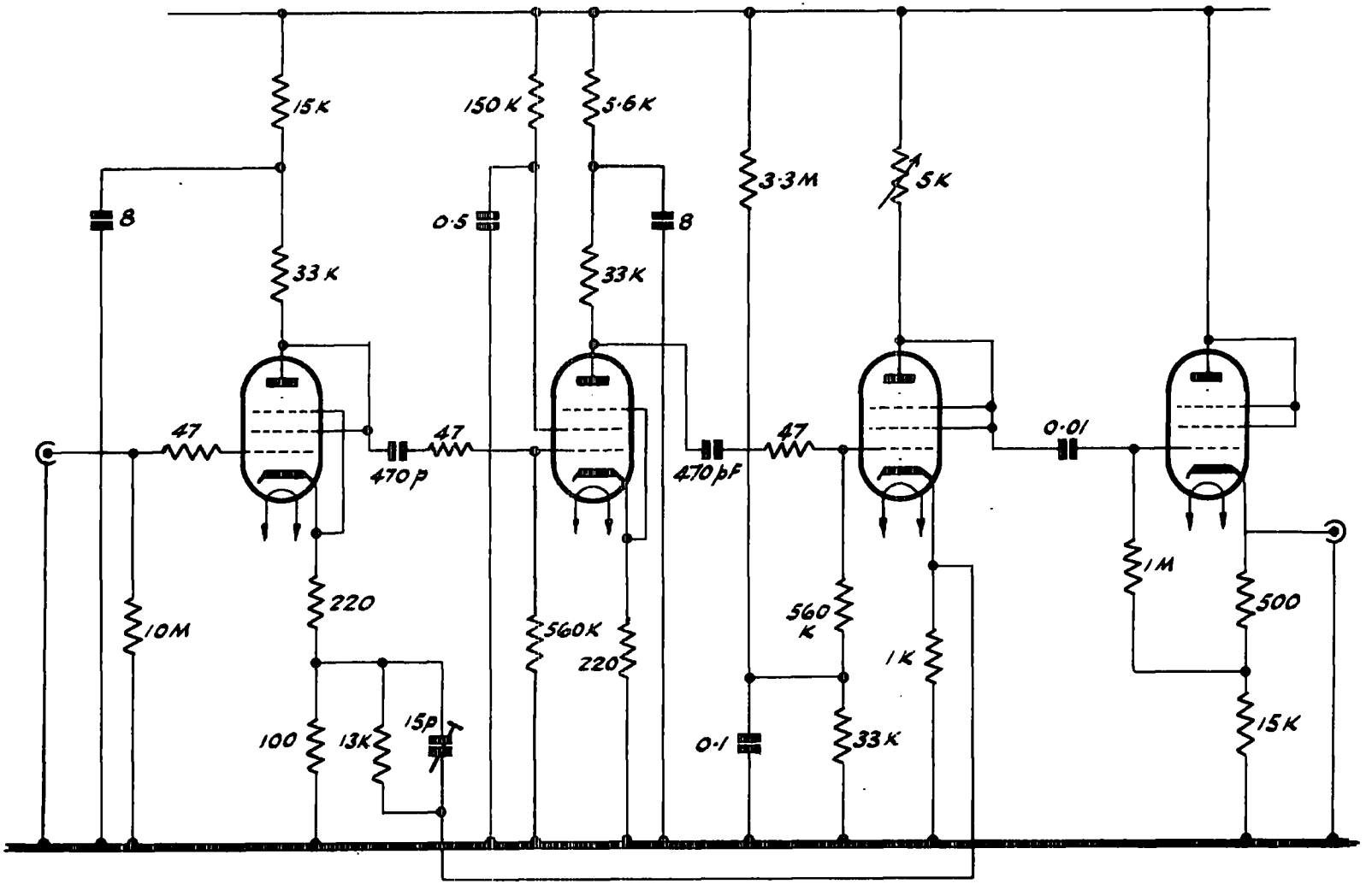

FIG. 10.3.1. HEAD AMPLIFIER

by the need for increased and easily controllable gain. In this way the gain of the individual head amplifier could be adjusted to counterbalance the variations in gas multiplication among the proportional counters when they were operated at the same E.H.T.

In operation the gain of each head amplifier was set approximately correctly. The negative feedback condenser C was adjusted for no overshoot on a fast rising test pulse and the gain readjusted to the required value. The problem was made easier by the decision, prompted by the amount of time available and the relative collecting efficiencies of the counters, to use only two of the four available counters. The gain of the amplifier associated with the counter with the lower gas multiplication factor was then set at maximum and the head amplifier of the other counter adjusted accordingly. The gain in the maximum position is $\sim$ 500.

10.4. The lower limit of pulse measurement

The lower limit of pulse size measurement is set by the noise level of the amplifier and as there is a limit to the amount of gas multiplication that can be obtained from a proportional counter without passing outside the proportional region, it is necessary to consider the steps that can be taken to reduce the amplifier noise and to keep the signal to noise ratio as high as possible.

The sources of noise can be divided into three categories. These are:

(1) Mechanical. External mechanical shocks or vibration set up vibration in the components of the amplifier which can cause electrical oscillations of considerable magnitude. This is particularly true for valves.

(2) External sources of electrical interference. In this category are included electromagnetic disturbances picked up by the signal leads, mains-borne interference and mains ripple on the power supplies.

(3) Inherent electrical noise in the amplifier, particularly the input network of the first stage, and in the first valve.

The effect of mechanical vibrations can be much reduced by first of all making sure that all components are rigidly fastened to the amplifier chassis and then supporting the whole amplifier in such a way that its period of natural oscillation is very long. Any induced vibration which in general will be of much shorter period will then be heavily damped. Vibrations of period comparable with that of the natural period of oscillation are not likely to occur, but these can be controlled by additional mechanical damping and in any case the response of the amplifier to such low frequencies, of the order of a few cycles per second, is very small indeed.

External sources of electrical interferences are reduced by using adequate electrical screening, multiple if necessary, by avoiding wherever possible multiple earth returns, by using d.c. supplies for the heaters of the valves and by adequate smoothing and decoupling for all power supplies.

The inherent electrical noise of the amplifier and its input circuit is the source of noise over which least control can be imposed and in general it sets the lower limit of signal detection. When, as in this case, the first stage of the amplifier produces appreciable amplification of the signal, only noise produced in its input stage and within the first valve are important.

The main sources of noise in the first stage of the amplifier are:

(1) Thermal noise due to the thermal motion of electrons in the input resistor of the amplifier.

(2) Shot noise arising from the random emission of electrons from the cathode or from the electron cloud surrounding it, depending on whether the valve is operating under temperature or space charge limited conditions.

(3) Grid current noise due to the random motion of the current carriers in the grid current through the grid resistor.

(4) Flicker noise due to the random appearance of impurity centres on the cathode surface.

The noise level appearing at the output of the amplifier is a function of the frequency response of the amplifier. The limits of the pass band can be reasonably specified in terms of a single integrating time constant T_1, and a single differentiating time constant T_2 corresponding to the upper and lower half power frequencies.

It is convenient to specify the noise level in terms of the equivalent input noise for an amplifier of infinite bandwidth and constant gain. The total r.m.s. equivalent noise level can then be shown to be (see for example Gillespie, 1953):

$$v^2 = \frac{kTe}{C^2R}\left(\frac{T_1^2}{(T_1 + T_2)}\right) + kTe\ \frac{2.5}{gm}\ \frac{T_1}{T_2\,(T_1 + T_2)}$$

$$+ \frac{eIg}{2C^2}\left(\frac{T_1^2}{(T_1 + T_2)}\right) + \frac{10^{-13}\,T_1^2}{(T_1^2 - T_2^2)}\,\frac{Ia}{gm}\,\frac{T_1}{T_2}\ \text{volts}^2$$

where the successive terms represent the contributions from thermal, shot, grid current and flicker noise respectively, and k is Boltzman's constant, T_e the absolute temperature, R the grid resistor, C the total input capacity including strays, e the electronic charge, I_a the anode current, gm the mutual conductance and I_g the sum, regardless of sign, of the positive and negative components of the grid current.

In the case of a pentode first stage the shot noise term becomes

$$kT \frac{2.5}{gm} \left(\frac{I_a}{I_c}\right) \left(1 + 8 \frac{I_s}{gm}\right) \frac{T_1}{T_2(T_1+T_2)}$$

due to the effect of the division of the cathode current I_c between the anode current I_a and the screen current I_s.

Not all of these terms are of equal importance. R is generally chosen to make the thermal noise negligible in comparison with the grid current noise and the latter is reduced by increasing $-V_g$ and decreasing V_a. This reduces the number and kinetic energy of the electrons, and by so doing decreases the positive grid current due to the positive ions produced when the electron stream collides inelastically with residual gas molecules. This process cannot be carried very far however, since the gm is also reduced and the shot noise is increased. In most cases shot noise is the predominant term and under these conditions it is advantageous to use a triode input stage.

10.5. The Signal to Noise Ratio

In order to evaluate the signal to noise ratio, S/N, it is necessary to specify the form of the input pulse. For the ionisation chamber and proportional counter this can be reasonably approximated by a pulse with an initial linear rise of period T to a plateau of much longer time period (see Gillespie, 1953) and using Gillespie's treatment it can be shown that the S/N is

a maximum for $T_1 = T_2$ for all values of X from 0.5 to ∞ where X is defined by $(T_1 T_2)^{\frac{1}{2}} = XT$.

A similar analysis shows that this condition also gives the least variation in amplifier gain for variations in the pulse rise time.

The size of the single differentiating time constant that limits the low frequency response of the amplifier and its position in the amplifier chain are important for a variety of reasons. It controls to a large extent the ability of the amplifier to deal with pulses which follow in close succession to one another. For this purpose the time constant should be small compared with the transit time of the positive ions in the counter, but not smaller than the initial rapid rise time of the counter pulse, otherwise the pulses will be unduly attenuated without any appreciable gain in resolving power.

If pulses from the counter arrive so rapidly, and their length is such, that the leading edge of one falls on the tail of the previous pulse, 'pile up' occurs which can, if of sufficient magnitude, drive the amplifier off the linear part of its characteristic. The probability of this happening increases with successive stages as the pulse height increases. It would therefore seem advisable to introduce the differentiating time constant as early as possible in the amplifier chain and in fact this could

be done simply by using a comparatively small load resistor, e.g. 10^5 ohm on the counter, so that the time constant consists of this resistor and the total input capacity of the amplifier, counter and strays. It is known, however, that to reduce thermal noise to the minimum this load resistor should be as large as possible and it would seem better from this point of view to put the small time constant later on in the chain. This would have the additional advantage that the effects of microphonics and a.c. pick-up would be much reduced and in practice the small time constant is placed after the first few stages of amplification where the pulses are too small for 'pile up' to be important in the applications envisaged. A suitable position is after the head amplifier.

In the amplifying system used in this experiment, the differentiating time constant was 5 μsec. The upper frequency 'limit' was determined by the constants of the head amplifier and no additional integrating time constant was introduced. The upper half power frequency determined from a series of gain v. frequency measurements corresponded to a value of T_1 of approximately 2 μsec. In view of the slow variation of S/N with the ratio of T_1/T_2 in the neighbourhood of $T_1 = T_2$ this was considered adequate.

The noise level in the first valve was kept down by connecting it as a triode and by suitably adjusting the grid voltage, but no attempts were made to specially select valves for the first

stage or to investigate the effects of operating at reduced anode voltage. This was because it was found possible to obtain a good S/N without these elaborate precautions, but if at a later date investigations were carried out with different counter fillings and lower gas gains it might prove necessary to take these precautions.

Experiments showed that S/N was approximately 20 for the most probable pulse height under the conditions of this experiment.

10.6. The main amplifier and recording equipment

The pulses from the head amplifier are mixed by connecting the outputs in parallel, so that the cathode followers in each of the head amplifiers have a common cathode load as far as A.C. signals are concerned. The 'mixed' pulse is then delayed by about 5 μsec., differentiated by passing through a 5 μsec. CR coupling and fed into the main amplifier and from thence into an oscilloscope for display or photographic recording. The oscilloscope is triggered by a pulse from the coincidence circuits which select the cosmic ray particles and the delay introduced into the proportional counter pulse enables the 'bright-up' pulse to reach maximum despite delays introduced by the coincidence circuits and also puts the counter pulse beyond the initial non-linear section of the time base sweep. A few milliseconds after the initial sweep the timebase is again triggered and the second

sweep used to provide a base line from which measurements can be made.

The coincidence circuits and the cycling system for the cameras etc. are considered in the next chapter.

CHAPTER 11

THE EXPERIMENTAL ARRANGEMENT

11.1. The Geometrical Arrangement

The four proportional counters are mounted side by side at a distance 31 cm. above tray B in the spectrograph, with their longest dimension in a direction at rightangles to the direction of the magnetic field. This is shown in fig. 11.1.1. The geiger counters designated T, which are mounted above and below each proportional counter, are connected to form a set of four, two-fold telescopes and in conjunction with the spectrograph select the cosmic ray particles.

The proportional counters, the geiger counters, their associated quenching units and the four head amplifiers are mounted on a trolley which can be moved in and out of the 'beam' of the spectrograph so as to facilitate tests and to enable other experiments to proceed. The proportional counters, supported at either end on insulating blocks, are contained in an aluminium box for screening purposes and are connected by short lengths ($\sim$15 cm.) of coaxial cable to their respective head amplifiers. These are supported from the trolley framework by stretched rubber strings to reduce the effects of microphony.

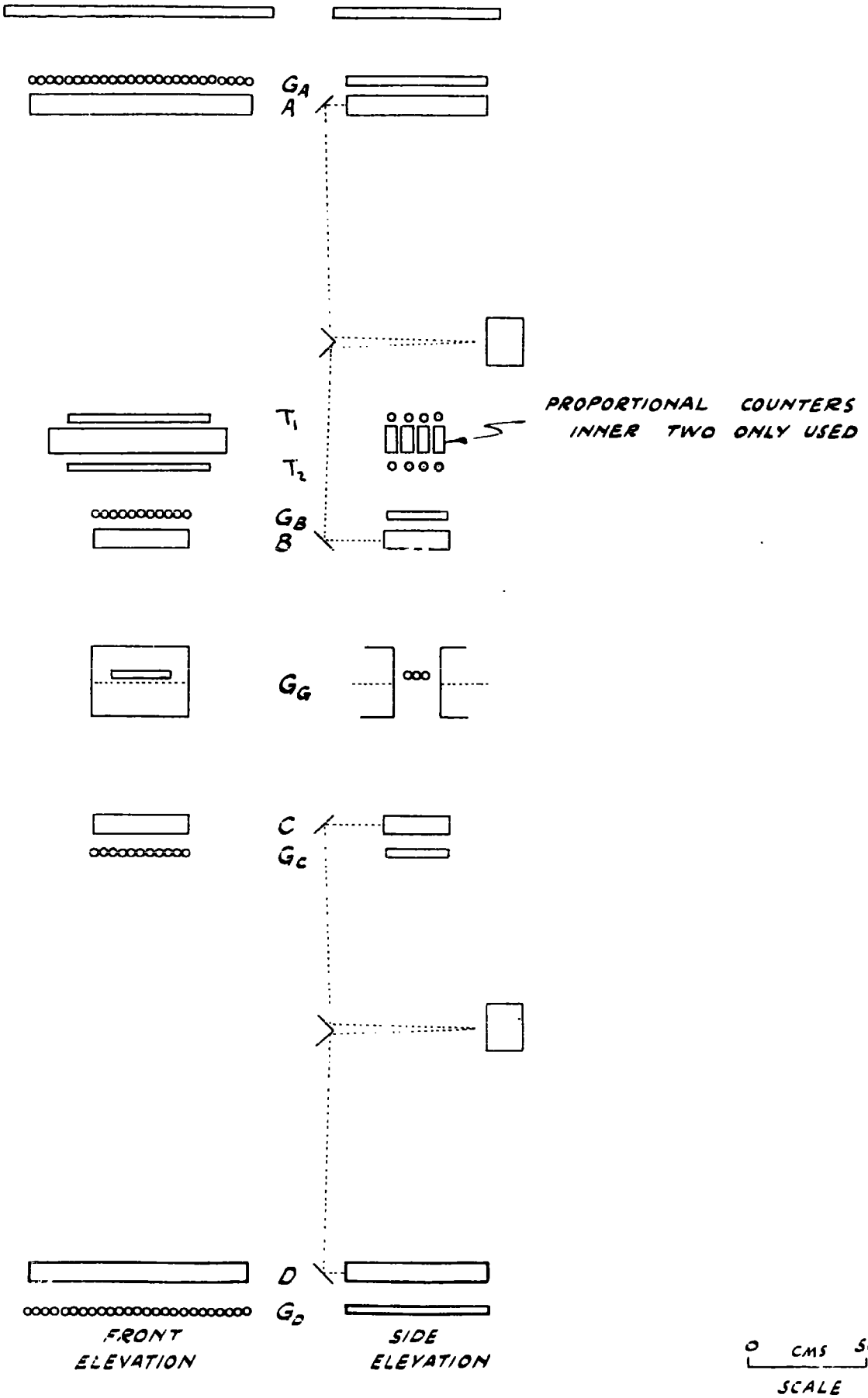

FIG. II.1.1. PROPORTIONAL COUNTERS IN THE SPECTOGRAPH

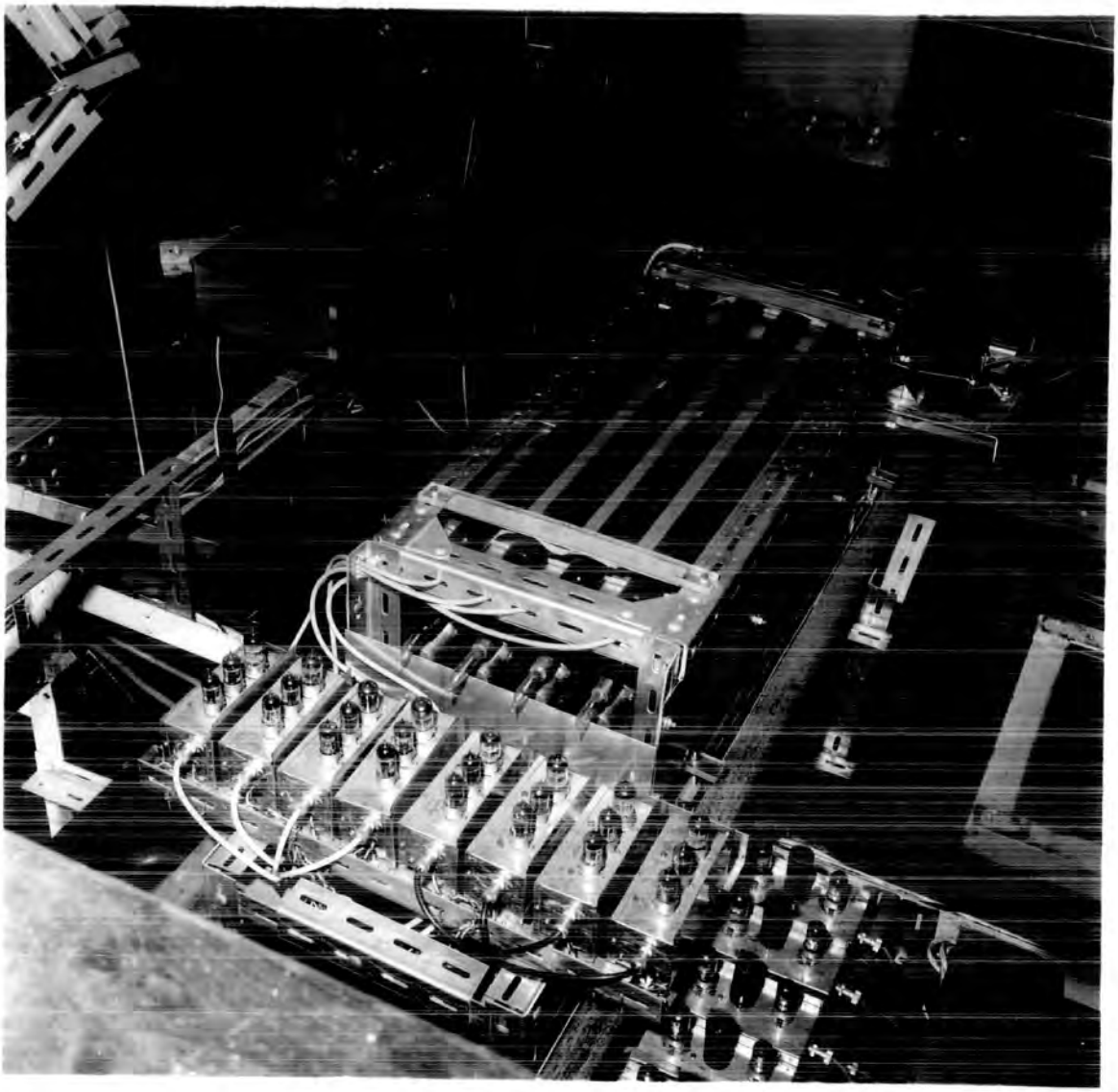

PLATE II.1. PROPORTIONAL COUNTER ASSEMBLY

The trolley is shown in plate 11.1. Part of the screening has been removed to show the proportional counters. The framework supporting the top four geiger counters is hinged and lifts up to enable a radioactive source to be placed on one of the calibration windows.

11.2. Particle selection

The particle beam through each of the proportional counters is defined by the geiger counters in the spectrograph and by the individual two-fold telescopes. The spectrograph defines the useful length of the proportional counters and the two-fold telescope the useful width. The useful length is 52 cm. compared with the actual length of 76 cm., so that end effects can be safely neglected. The useful width is approximately 60% of the total.

The particle momentum is determined in the same way as in the spectrum measurements, but the accepted particles have to satisfy the additional criterion of discharging one of the four 2-fold telescopes. This is ensured by mixing the outputs from the four 2-fold coincidences units and feeding the common output pulses into one of the channels of the main Rossi coincidence circuit which is then operating in 6-fold coincidences. The other five channels being operated by pulses from the five trays of G.M. counters as in the spectrum measurements. The master coincidence pulse from the Rossi unit is then used:

(a) to trigger both the momentum analyser oscilloscope and the proportional counter oscilloscope.

(b) to trigger the camera cycling systems.

(c) to gate the unit which determines the proportional counter through which the particle has passed.

11.3. Correlation of the film records

It is necessary to adopt some method of correlating the information recorded on the two oscilloscope films, i.e. the momentum of the particle and the amount of ionisation it produces and also to correlate these records with the data obtained from the flash-tube cameras if in use. In principle it should be possible, having started the oscilloscope cameras together, to number the frames mentally from the start, but the necessity of counting up to several hundred frames with absolute certainty and the possibility of lost or doubtful frames due to accidental fogging or faults in development renders the method highly unsatisfactory. The method used here is to label some of the pairs of corresponding frames with the flashes from a set of neon bulbs. The bulbs are arranged inside the camera cones as close to the actual oscilloscope screen as possible taking care not to obstruct the view of the trace. The 'ionisation' camera sees nine bulbs altogether. Four of these indicate which of the proportional counters is involved in a given event. Two more, together with a corresponding pair associated with the momentum

analyser camera, are arranged to flash and label every 5th frame. One flashes for every 5th frame and two for every 25th frame. The remaining three bulbs are arranged to perform a similar function in conjunction with the flash tube array except that in this case one bulb flashes for every event in which the flash tubes are pulsed and two bulbs indicate a 5th frame and three bulbs a 25th.

11.4. Electronic Circuits for particle selection and record correlation

A block diagram of the complete system is shown in fig. 11.4.1. All the units except for the 2-fold coincidence units, the cycling system and the hodoscope unit have been described in detail elsewhere. The remainder will now be described.

The 2-fold coincidence unit

The circuit is shown in fig. 11.4.2. The basic 2-fold units are four short suppressor base pentodes V_{1-4} biassed off by both g_1 and g_3. The two coincident signals are applied to these grids and the output signals from all units mixed by virtue of the common anode load R. V_5 inverts the negative coincidence pulse and by appropriate choice of the values of its associated circuit elements also discriminate against the small non coincident break through pulses due to capacitative coupling between g_3 and anode. V_6 is the output cathode follower.

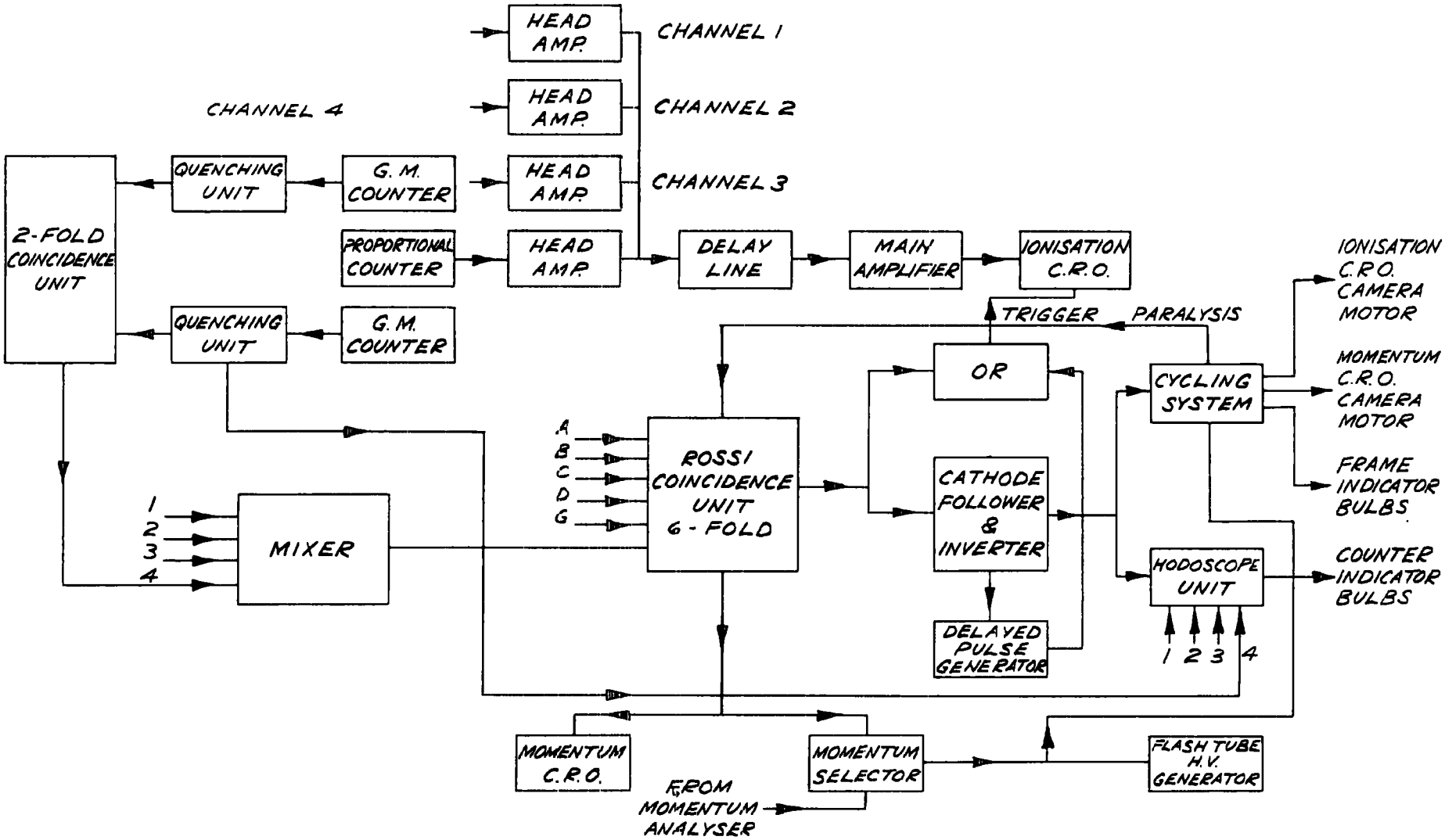

FIG. II.4.1. BLOCK DIAGRAM OF IONISATION EXPERIMENT LAYOUT

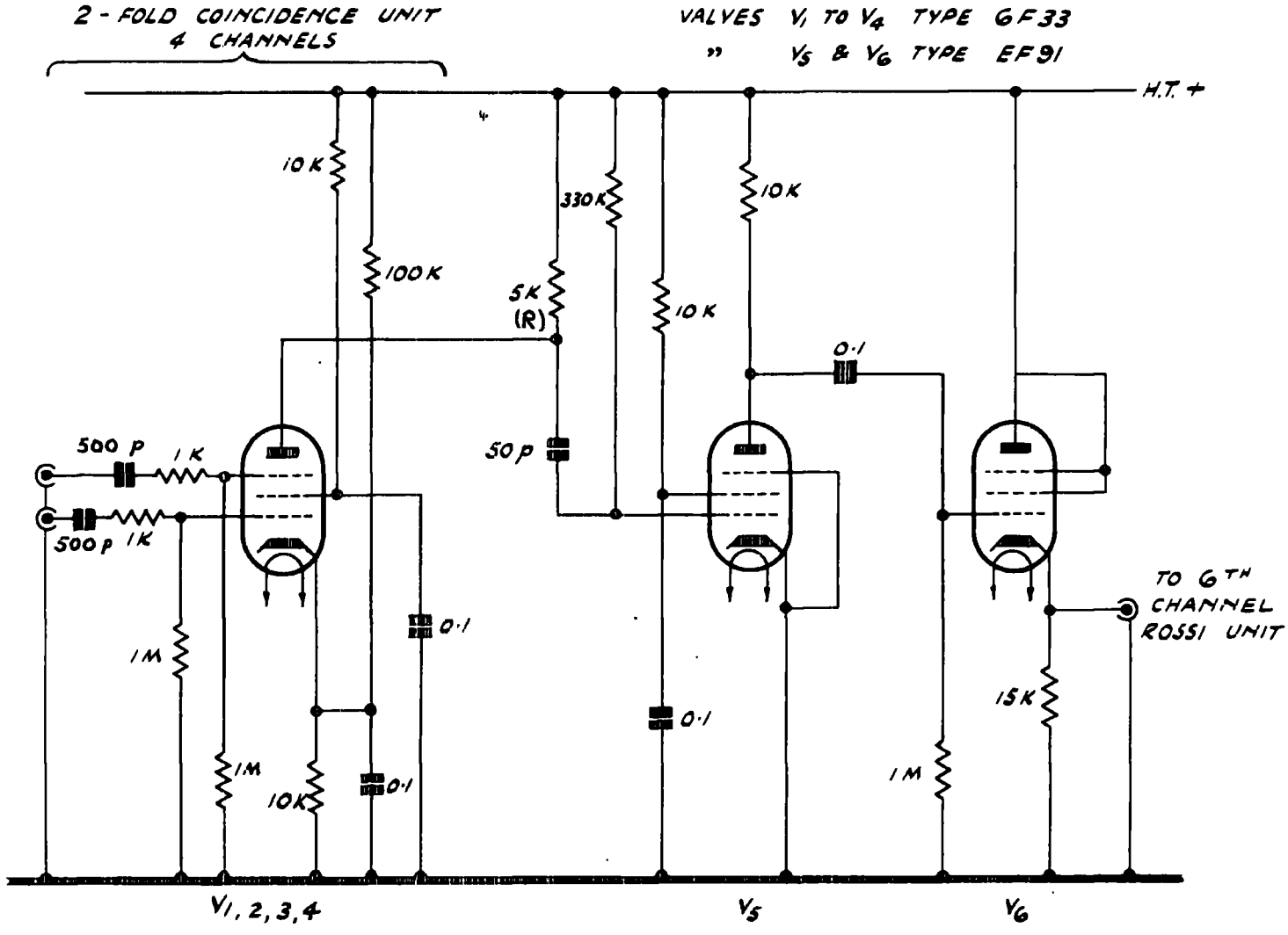

FIG. II. 4. 2. 2 - FOLD COINCIDENCE UNITS & MIXER STAGE

The Cycling System

The circuit is shown in fig. 11.4.3. The relays and uniselectors are actuated by pulses from the Rossi coincidence unit and by pulses from the momentum selector (flash tube trigger pulses) applied to the two univibrators V_3 and V_4 respectively. V_1 and V_2 serve to isolate the univibrators from the input circuits and prevent any spurious pulses generated at the end of the univibrator pulse from being fed back into the Rossi or momentum selector circuits. It is helpful to consider the action of the two sets of univibrators and associated relays etc. separately.

(a) The Rossi unit section

This part of the circuit performs three functions.

1. It paralyses the Rossi circuit during the cycling period.
2. It 'counts' the number of events and flashes the correlation bulbs at the appropriate frames.
3. After a delay ($\sim$200 ms) to allow the bulbs to flash the two cameras are moved on.

Mode of operation

Normally V_{3a} is non conducting and V_{3b} is hard on. When the univibrator is triggered V_{3a} is switched hard on and relay RL_1 energised. The contacts K_{11} close paralysing one of the channels of the Rossi coincidence unit by shunting

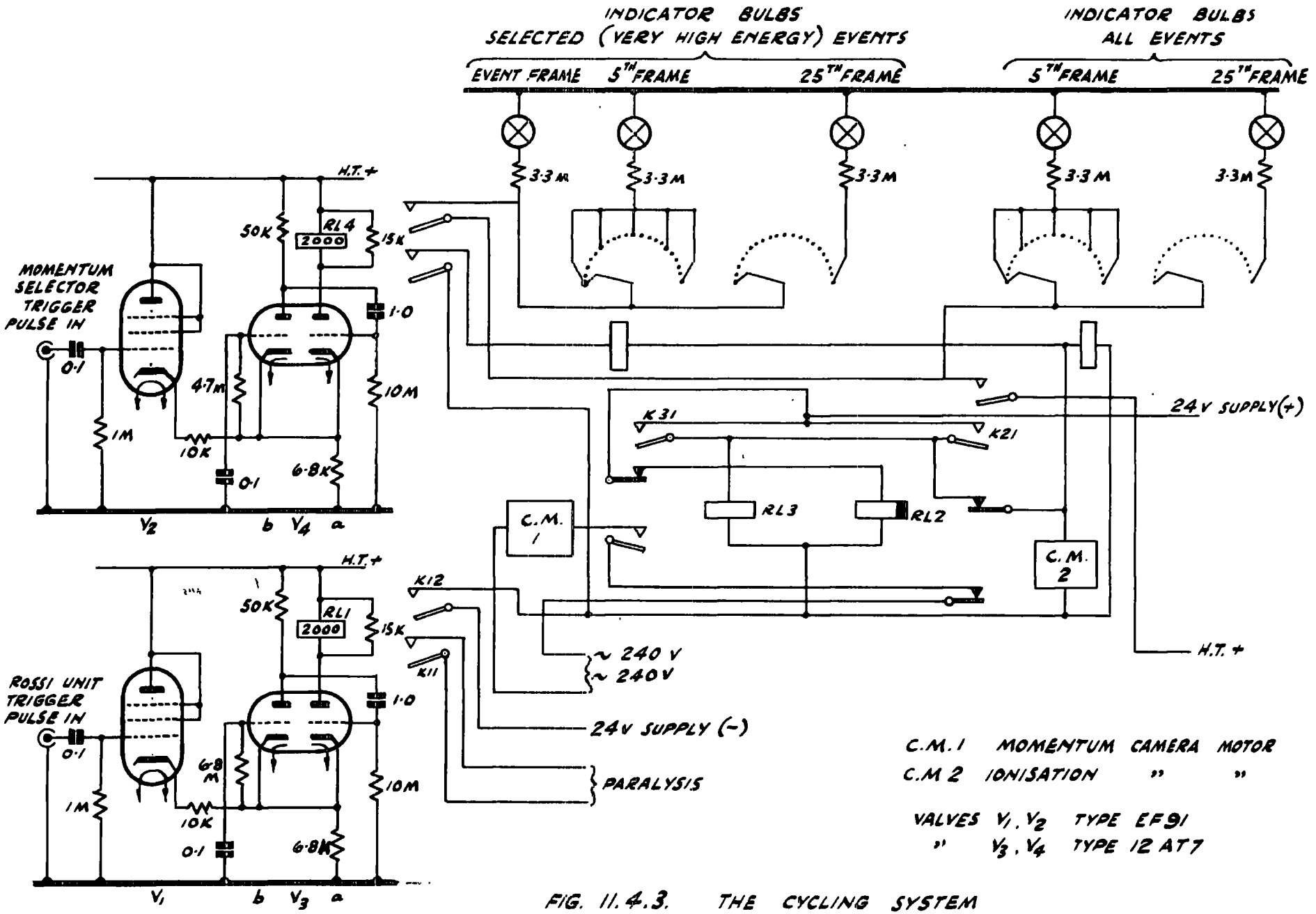

FIG. 11.4.3. THE CYCLING SYSTEM

a control grid of one of the inverters to earth. Contacts K_{12} also close, energising the relay system RL_2 and RL_3. From the circuit diagram it can be seen that RL_2 operates first, switching on RL_3, which in turn switches off RL_2, remaining on itself until the end of the univibrator period by virtue of K_{31} which is in parallel with K_{21}. Relay RL_2 controls the period of flashing of the bulbs used to correlate the film records. The period is lengthened by use of an eddy current slug on RL_2 and the period can be controlled by altering the position of a screw in the armature. The camera and uniselector are controlled by contacts on both relays. They operate only when RL_3 is on and RL_2 is off, so that the camera and uniselector, which move on together, cannot do so until the bulbs have been switched off. The uniselector, which has 25 positions, 'counts' the number of frames and determines whether the bulbs flash or which bulbs flash depending on the setting of the uniselector at the end of the previous cycle.

(b) <u>The momentum selector section</u>

This section controls the bulbs correlating the ionisation CRO film and the flash tube data films. Essentially, the bulbs and frame-counting uniselector are switched by RL_2 and RL_3 as for the other set of bulbs and uniselector, but their power supplies are also routed via the contacts on relays

RL_4 in V_{4a} anode lead. The period of this univibrator is made slightly less than that of the other univibrator to ensure that the paralysis time is longer than the former's period.

The Hodoscope Unit

The proportional counter through which the particle has passed is identified by determining which of the four 2-fold counter telescopes has been traversed and by means of associated electronic circuits causing one of four neon bulbs located inside the ionisation camera cone to flash. This is done by detecting 2-fold coincidences between pulses from the quenching units associated with the top four geiger counters (T_1) and master Rossi coincidence pulse. The circuit is shown in fig. 11.4.4. V_1 acts as isolator and phase splitter for the positive Rossi trigger pulse. V_{2-5} are 2-fold coincidence units the output pulses from which trigger the associated cathode coupled univibrators V_{6-9}. The neon hodoscope bulbs are directly coupled to the cathode of these valves and flash for $\sim$30 ms.

The isolator valve V_1 also supplies inverted (negative) Rossi pulses to the delayed trigger unit which triggers the 'ionisation' oscilloscope a few milliseconds after the main event so providing a base line from which measurements can be made. This unit (see fig. 11.4.5.) is merely a modified quenching unit. The positive univibrator pulse from V_{1b} anode is

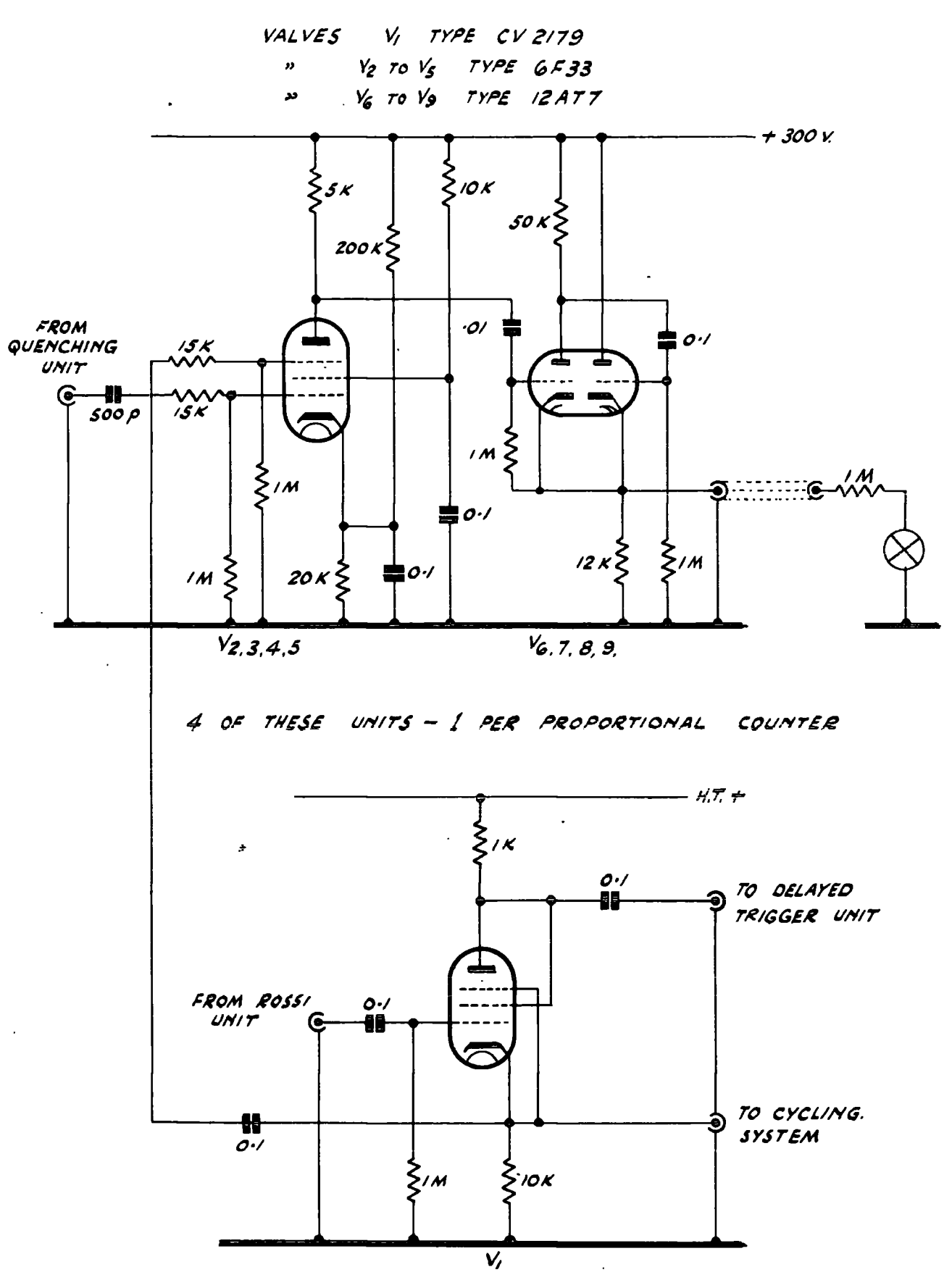

FIG. 11.4.4. NEON HODOSCOPE

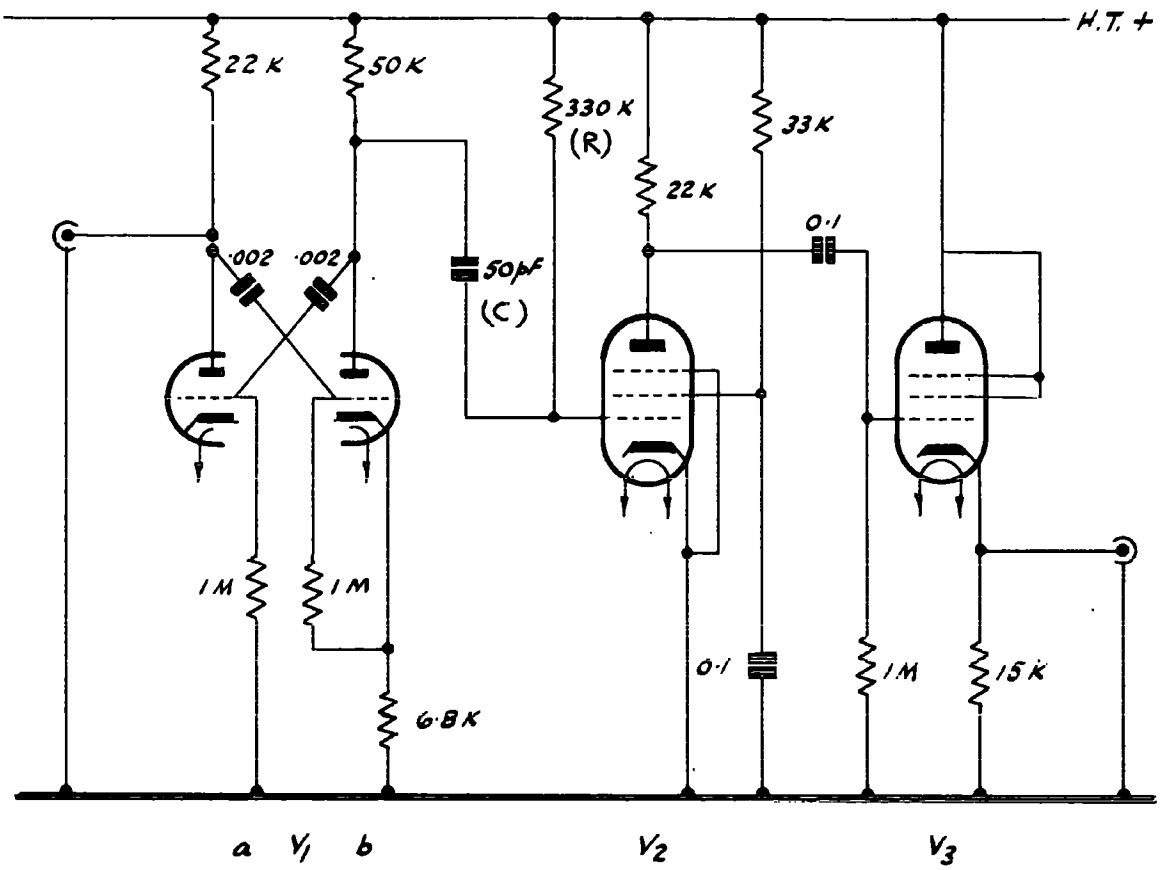

VALVES V_1 TYPE 12 AT 7

" V_2 & V_3 TYPE EF91

FIG. 11.4.5 DELAYED PULSE UNIT

differentiated by C and R and fed to the inverter V_2 which only responds to negative going pulses. The unit therefore produces a positive output pulse at the falling edge of the univibrator pulse.

CHAPTER 12

THE EXPERIMENTAL RESULTS

12.1. The linearity of response of the amplifiers and proportional counters

Prior to the main part of the experiment a series of tests were carried out to investigate the performance of the amplifiers and proportional counters. These measurements were performed using a simplified amplifier chain. This consisted of one head amplifier, the main amplifier and a single channel pulse height analyser.

The linearity of the amplifying system was first checked by feeding suitably attenuated pulses into the head amplifier and measuring the height of the output pulses from the main amplifier with the single channel pulse height analyser. The result for one such combination of head amplifier and main amplifier is shown in fig. 12.1.1. The deviation of the input pulses from their nominal values does not exceed 1% and the deviation from linearity of the output pulses over the range 0 to 10 arbitrary input units corresponding to an energy range in the following experiments of 0 to 29 KeV is $\leq$1.6%. (Minimum ionisation corresponds to 5.1 KeV).

The performance of the counter was then tested using the k-capture x-rays from Zn65 (8.05 KeV) and Sn 113 (24.2 KeV). These sources were prepared by evaporating a drop of the radioactive salt solution on a small tray (2-3 cm. diameter), giving a source strength of $\sim$0.1μC. The trays, aluminium in the case of

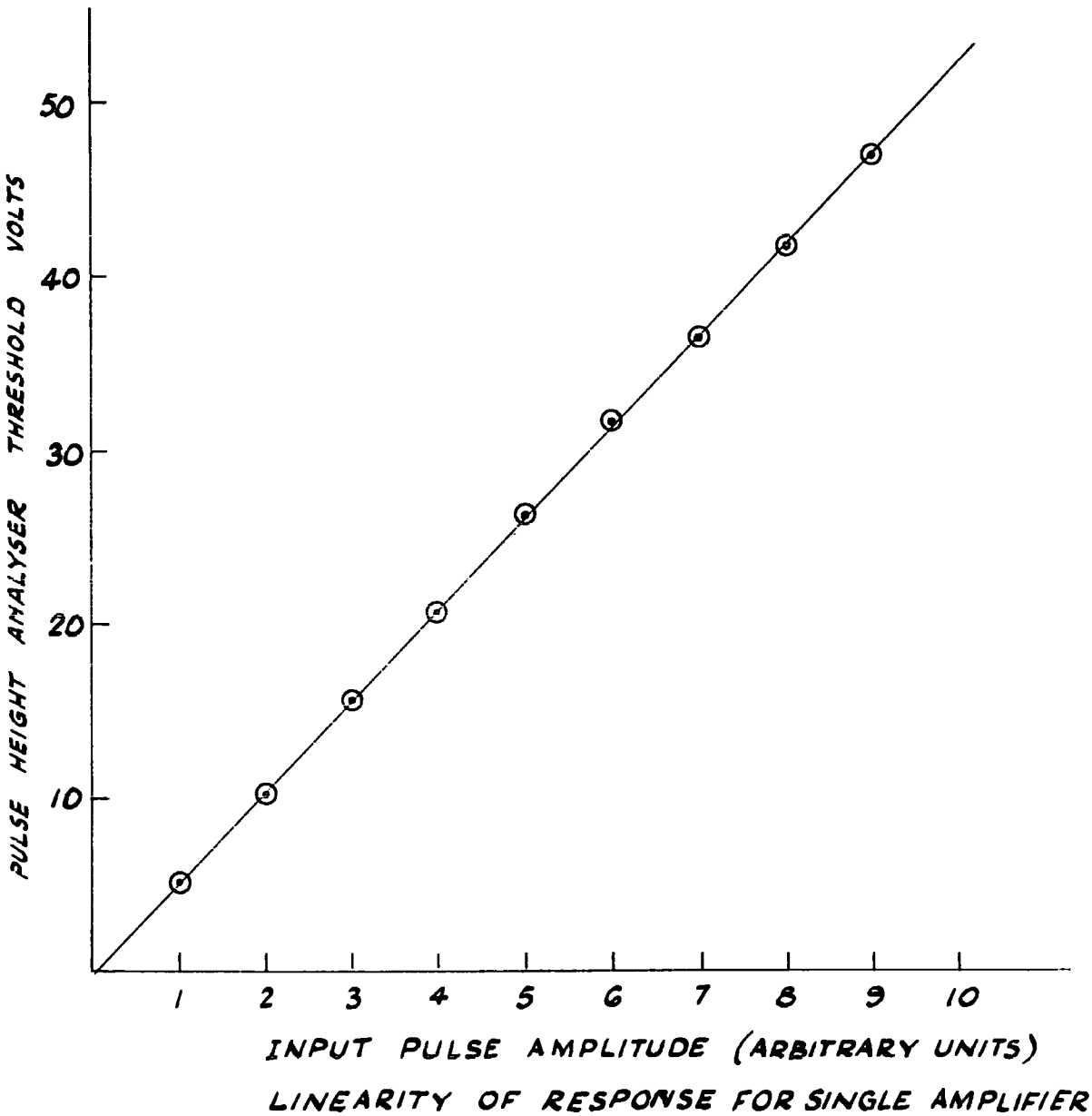
PULSE HEIGHT ANALYSER THRESHOLD VOLTS
50
40
30
20
10
1
2
3
4
5
6
7
8
9
10
INPUT PULSE AMPLITUDE (ARBITRARY UNITS)
LINEARITY OF RESPONSE FOR SINGLE AMPLIFIER

FIG. 12.1.1.

Zn 65 and polythene in the case of Sn 113 (since Sn_2Cl_2 soln. contains free HCl), were then covered with a layer of 'cellotape' to protect them and in use were inverted in turn over one of the mica windows in the counters.

The k-capture x-ray photons from these sources are absorbed by photoelectric processes, as Compton scattering is of negligible importance at these energies. The energy absorption takes place in several stages, the electron ejected at the first stage carrying an amount of energy:

$$e = h\nu - \varepsilon_i$$

where $h\nu$ is the energy of the photon and ε_i is the energy required to remove the electron from the atom. The photoelectron is then slowed down by molecular collisions giving up its energy and producing further ionisation and excitation.

If the electron has been ejected from an inner shell of the atom, electron rearrangement takes place between the shells to fill the vacancy. The energy released in this process is removed either by the emission of a photon or by the ejection of an electron from the ion (the Auger effect). When the latter occurs the energy of the electron is absorbed in the usual manner, but if a photon is emitted there is an appreciable probability that it will escape from the counter, so that a monoenergetic photon source will give rise to more than one peak in the pulse height

spectrum. These peaks are a main peak corresponding to the total energy of the photons $h\nu$ and a subsidiary escape peak or peaks of energy $h\nu - h\nu'$, where $h\nu'$ is the energy of the photon that is emitted when, for example, an electron drops from the L shell to fill a vacancy in the K shell.

The probability that the excess energy is removed by emission of a photon rather than an electron depends on the atomic number of the gas, the probability increasing with increasing atomic number. In the heavier gases, such as xenon, this probability, the so-called fluorescence yield, is high and may give rise to a certain amount of confusion in the interpretation of complex energy spectra, but in the lighter gases it is of much less importance. In argon for example, it is only 9% and in neon it is even less, so that the escape peak is completely negligible in comparison with the main peak and no difficulty arises.

The efficiency with which the photon energy is converted into the equivalent number of ion pairs is determined almost entirely by the probability for the initial photon interaction in the counter. This is so, because the energy of the primary photoelectron cannot exceed that of the photon and since for a 10 KeV electron the range in the counter gas is only a few millimetres the probability that most of them are absorbed by the counter gas is very high, whereas on the other hand the photon absorption process gives a very low conversion efficiency. For example, in the case of 10 KeV x-rays and for a vertical path through the counter 40%

of the radiation is absorbed by the mica window and only 2.0% by the gas.

The tests that were performed with the sources were:-

(a) A determination of the pulse height distribution corresponding to the 8.05 KeV photons using the central calibration window. The result obtained is shown in Figure 12.1.2. The width expressed in terms of the standard deviation (assuming an approximately normal distribution) is 7.6%. This compares favourably with the value 7% obtained using Curran's (1949) expression, i.e. $\sigma = (4/3N)^{1/2}$. Where N is the number of ion pairs formed initially.

(b) A second determination for the other calibration window that lies 1.3 cm off the centre line of the counter, and a comparison with the previous measurments to see if the gas multiplication factor varies across the counter. The result showing the two distributions is given in Figure 12.1.3. It is seen that within the limits of accuracy of the experiment the two distributions are the same, and no variation in gain across the counter can be detected.

(c) A determination of the positions of the peaks of the pulse height distributions obtained with the x-rays from Zn 65 and Sn 113. The expected ratio between the positions of the two peaks is 24.2/8.05 i.e. 3.01. The measured ratios for the

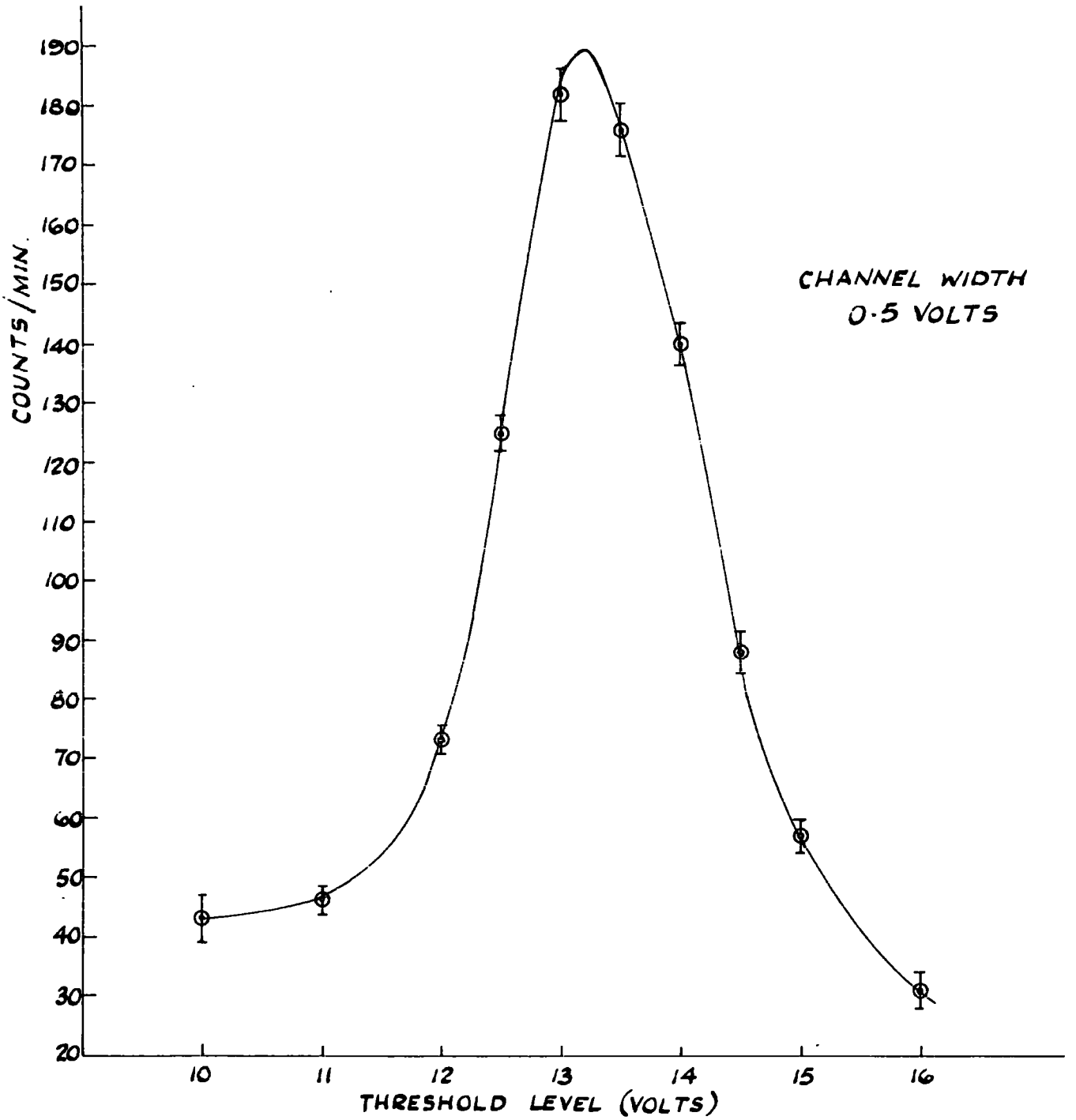

FIG. 12·1·2 PULSE HEIGHT DISTRIBUTION FOR 8·05 keV X-RAYS FROM Zn 65

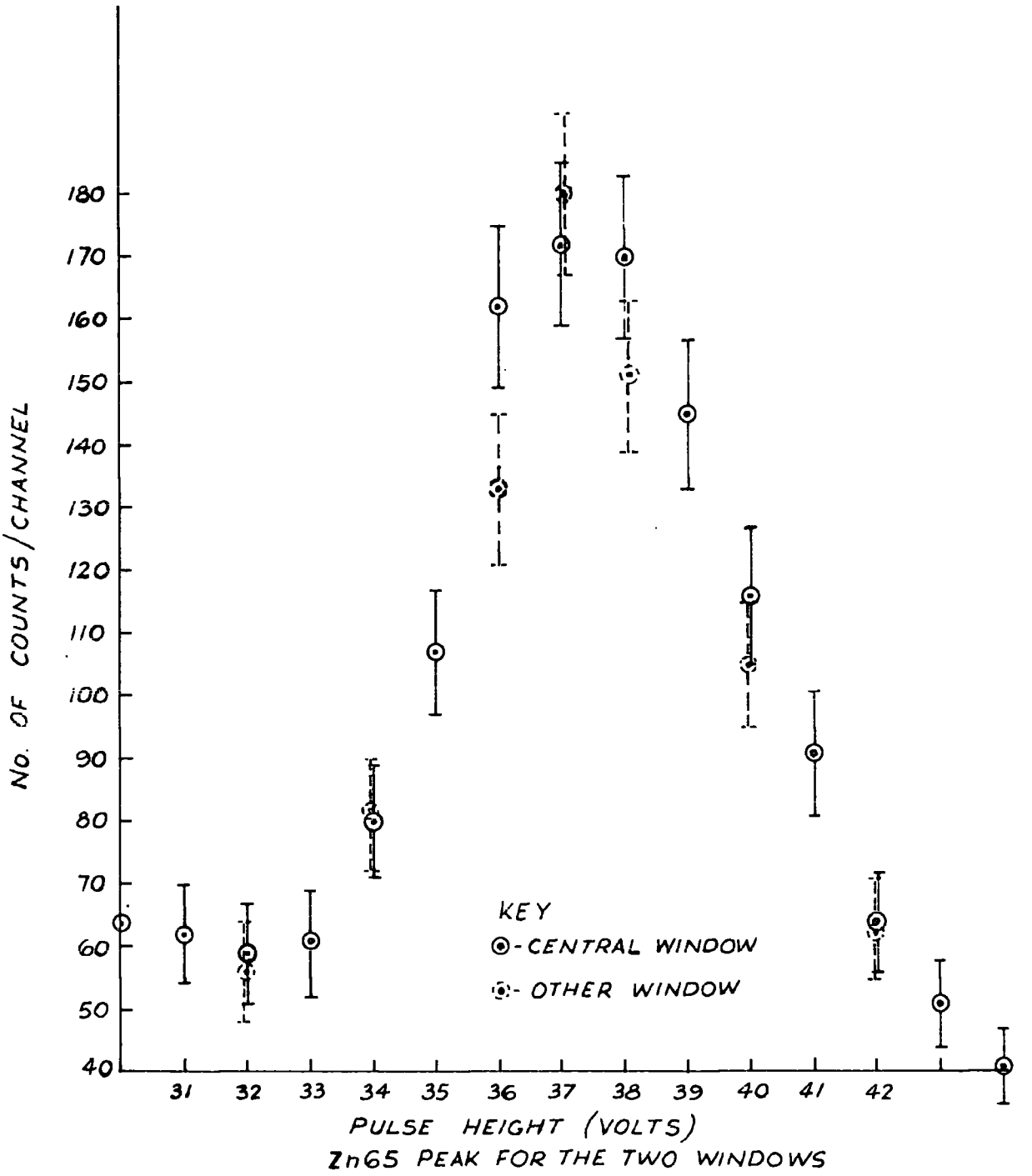
No. OF COUNTS / CHANNEL
180
170
160
150
140
130
120
110
100
90
80
70
60
50
40
31
32
33
34
35
36
37
38
39
40
41
42
KEY
⊙ - CENTRAL WINDOW
⊙ - OTHER WINDOW
PULSE HEIGHT (VOLTS)
Zn65 PEAK FOR THE TWO WINDOWS

FIG 12·1·3

two counters were 3.08 ± 0.06 and 2.99 ± 0.06 from which it may be concluded that the results are not inconsistent with a linear counter response up to at least 24.2 KeV.

It could be argued that two such determinations do not provide conclusive evidence for this, but it is difficult to conceive a mechanism that would yield a non linear relationship between energy and pulse height and still pass through the two experimental points and the 'origin'. This is especially so in view of the fact that experiments in the past with proportional counters using several calibration sources have indicated no such non-linear relationships, but only the saturation that sets in at higher energies.

(d) A determination of the variation of multiplication factor with counter E.H.T. The position of the peak corresponding to 8.05 KeV photons was determined for three values of the E.H.T. At the normal operating E.H.T. 970 volts and at ± 25 volts from this value. This gave a value for $\frac{\delta A}{A} \Big/ \frac{\delta V}{V}$ of 11, i.e. 1% change in E.H.T. will result in a change of 11% in gain. This is of the magnitude to be expected and since the day to day variation in E.H.T. is only of the order of 1 part in several thousand the stability of the E.H.T. power pack is quite adequate for the present purpose.

In the main experiment the amplifier system was changed to that described in an earlier chapter. The two counters were used simultaneously, the outputs of the head amplifiers strapped together and the common output fed into the main amplifier. The output pulses from the main amplifier were then displayed on a cathode ray tube and could simultaneously be measured with a single channel pulse height analyser. The system was adjusted for approximate equality of response from both counter chains using a calibration source, as described in chapter 10 and the linearity of the amplifiers tested using a pulse generator. The amplifier linearity in this case was found to be slightly below the previous standard, but to be still sufficiently linear.

The figures for one of the amplifier chains were as follows:

Equivalent energy range 0-17.5 KeV Max. deviation from linearity 1.4%

Equivalent energy range 0-20 KeV Max. deviation from linearity 5.6%

12.2. The experimental procedure

When these tests had been completed and it was certain that the counters and amplifiers were operating satisfactorily the main experiment was started and the proportional counters on their trolley pushed into the 'beam' of the spectrograph.

Originally, it had been intended that at least 10,000 events should be accumulated, but shortage of time enabled only some 1,500 events to be recorded.

During the experiment tests were performed daily to check on the constancy of the gain of the amplifiers and proportional counters and also to provide calibration points for subsequent analysis.

The routine daily checks were:

1. The E.H.T. supply voltage was measured.
2. The overall response of each counter chain was checked with the single channel pulse height analyser using the Zn 65 source.
3. A series of pulses from a pulse generator were fed into each head amplifier in turn and the height of the corresponding output pulses recorded photographically from the oscilloscope and also measured directly on the pulse height analyser. In this way the Zn 65 calibration measurements made with the pulse height analyser could be converted at a later date into the corresponding pulse height on the oscilloscope display.

The stability of the system was found to be perfectly adequate as no significant change in the position of the Zn 65 calibration peak for one counter chain could be detected over the period of the complete run and only an overall change of $\sim 4\%$ in the other. If the mean position of the latter is taken for the purpose of calculation the effects of this already small drift will tend to cancel out and it can safely be ignored.

12.3. Analysis of results

12.3.1. The basic data

Each run yields two film records. The momentum analyser film and the proportional counter oscilloscope film. Between them they contain information on the momentum category number, its sign, the height of the proportional counter pulse and the counter involved for each particle that is recorded, and also a photographic record of the calibration tests. Pairs of typical frames are shown in plates 12.3.1. and 12.3.2.

Both films were projected and measured. The estimated accuracy of each pulse height measurement from the proportional counter record was better than 2.5% and the departure from linearity for the two amplifier chains as measured on the film record as distinct from the pulse height analyser measurements were as follows:

Amplifier No. 1

Equivalent energy range	0-17.5 KeV	Max. deviation from linearity	1.0%
" " "	0-20 KeV	" " " "	5.2%

Amplifier No. 2

Equivalent energy range	0-17 KeV	Max. deviation from linearity	1.1%
" " "	0-20 KeV	" " " "	2.1%

The results were divided up into groups defined by counter number and momentum category number. The ratio between the Sn 65 peaks for two counters was only 1.15, and the two sets of results were combined without introducing appreciable error by multiplying

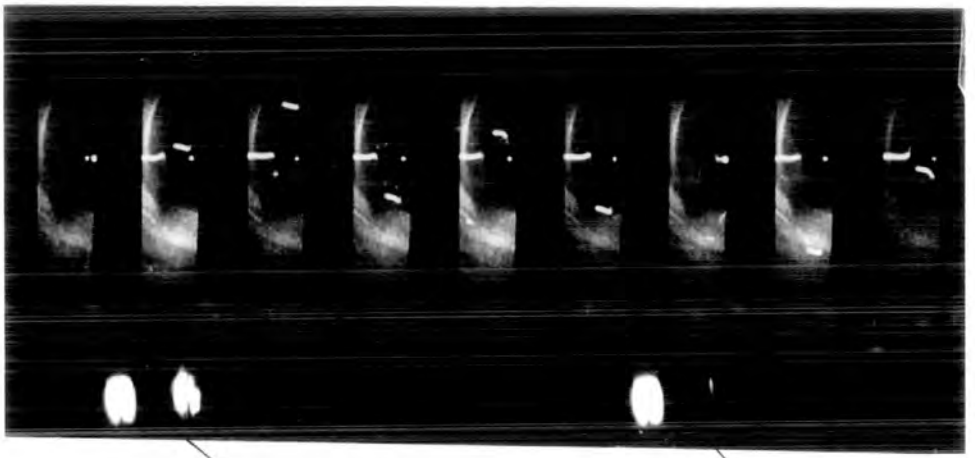

PLATE 12.3.1. MOMENTUM

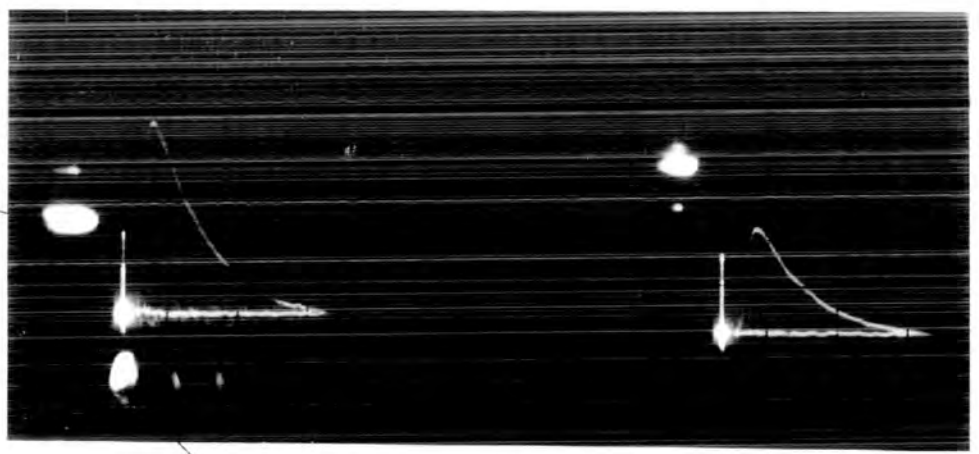

PLATE 12.3.2 IONISATION

one set by this ratio. From considerations of momentum cell size and number in each cell the results were then grouped as follows:

Table 12.3.1.

Cat. Nos.	No. in cell
0	71
1	241
2	256
3	218
4	171
5	130
6 & 7	182
8 & 9	96
10, 11, 12, 13 & 14	108

12.3.2. Determination of the most probable ionisation

Once the grouping of table 12.3.1. was decided upon a variety of methods were available for determining the most probable value of each distribution, but in view of the relatively small number of results in each group it was decided that a complete analysis along the lines of the Behren's curve fitting method (1951) or the

Hammersley and Morton method (1955) was hardly justified. Some discussion of these methods will, however, be given on account of the importance of this topic.

Both of these methods start with a master curve which is known to be of the same form as the distribution curves to which the histograms of the results tend as the number of results is increased and the cell widths are decreased. The master curve is normalised to the data in question and is then fitted to the histogram by suitable adjustment of the curve width and mode. The two methods differ in the manner in which the latter step is carried out.

Eyeions (1955) obtained a master curve by combining all the individual histograms corresponding to the different momentum bands. This was possible, because it was found that the width of each distribution was sensibly constant from one to another and a master histogram was plotted using all the results, but referring each to an origin based on the median value of the individual group from which the particular result was drawn.

Eyeion's method of obtaining a master curve was obviously attractive, since if the shapes of the individual distributions after normalisation were all the same a master curve obtained in this manner could be fitted to each in turn by eye alone. This method would lack the objective approach obtainable by purely mathematical means, but for the number of results available would prove quite adequate.

This method was tried but was not entirely successful, because there was found to be a noticeable decrease in the width of the distribution with decrease in momentum. However, a master curve based on the results corresponding to momentum categories 1, 2, 3 and 4 was calculated and fitted to the various groups. 'Normalisation' of the curves being conveniently carried out by plotting the results on semi-logarithmic graph paper.

In the case of the lower momentum group, i.e. higher momentum category numbers the fit was not too good but this could be improved by either slightly distorting the master curve or by plotting the results on logarithmic paper to obtain a more symmetrical distribution whose width varied little from group to group.

12.3.3. Determination of the error in the mode

It is difficult to obtain a meaningful estimate of the error to be attached to the value of the mode of an asymmetrical distribution. If by analogy with the normal distribution one calculates the 'distance' from the origin (mode) of imaginary boundaries within which is contained a certain fraction of the total distribution one is lead to the possibility that the error has two different magnitudes depending on its sign.

The work of Hammersley & Morton (1955) which is probably the most extensive in this field shows, however, that this is not the case, so that if the error is to be estimated without recourse to a complete mathematical treatment it will be necessary to introduce an element of symmetry into the problem.

One possible approach is to fit a normal curve to the leading edge of the distribution so that the origin of the normal curve passes through the mode and the positive half of the normal curve is a reflection of the leading edge of the distribution in a vertical line through the origin. The number of events contained in the area enclosed by the normal curve is then estimated and the standard error of the mean calculated in the usual manner.

This method cannot lead to a gross inaccuracy in the error, since although the width of the actual distribution is greater than the normal distribution this will be compensated for to a certain extent by the reduced number of events considered when the standard error of the mean of the normal curve is deduced from the standard deviation.

However, when the error corresponding to a particular set of results was calculated by this method it was found to give a smaller value than that which one would expect from comparison with the results of Eyeions et al and other experimenters. This is obviously of importance if any quantitative comparisons are to be drawn between these results and those of other workers.

An easier and better way to estimate the error is to use Eyeion's results to derive an empirical relationship between the error and the width of the distribution and the number of events. This was done and the errors calculated on this basis for each set of results.

The distribution curves for the groups are shown in Figs. 12.3.1. to 12.3.9. In each case the value of the mode of the distribution is given together with the estimate of the statistical error involved.

The errors quoted in these results are derived from the shapes of the frequency distributions of the events in each momentum group. The extent of the spread in value in each distribution is determined by several factors. These are :-

1. The inherent statistical spread of the type treated by Landau.
2. The spread introduced by the statistical nature of the gas multiplication process.
3. The additional spread introduced by variations of the gas multiplication factor throughout the counters.
4. The spread introduced by variations in the overall gain of the system throughout the experiment.
5. The spread due to errors in pulse height analysis etc.
6. The spread due to the finite momentum cell width.

Of all these factors the first is by far the most important.

The error calculated does not include the systematic error due to non linearity in the amplifying system. This, as measurements have shown, is small and can safely be neglected.

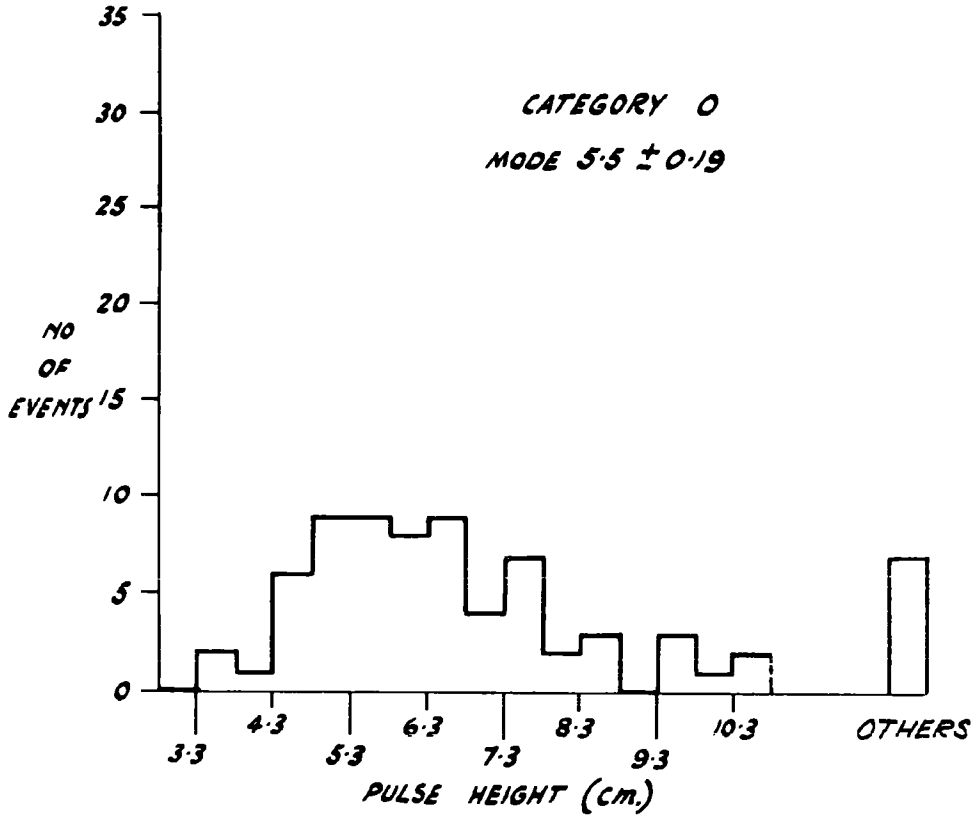

FIG. 12.3.1.

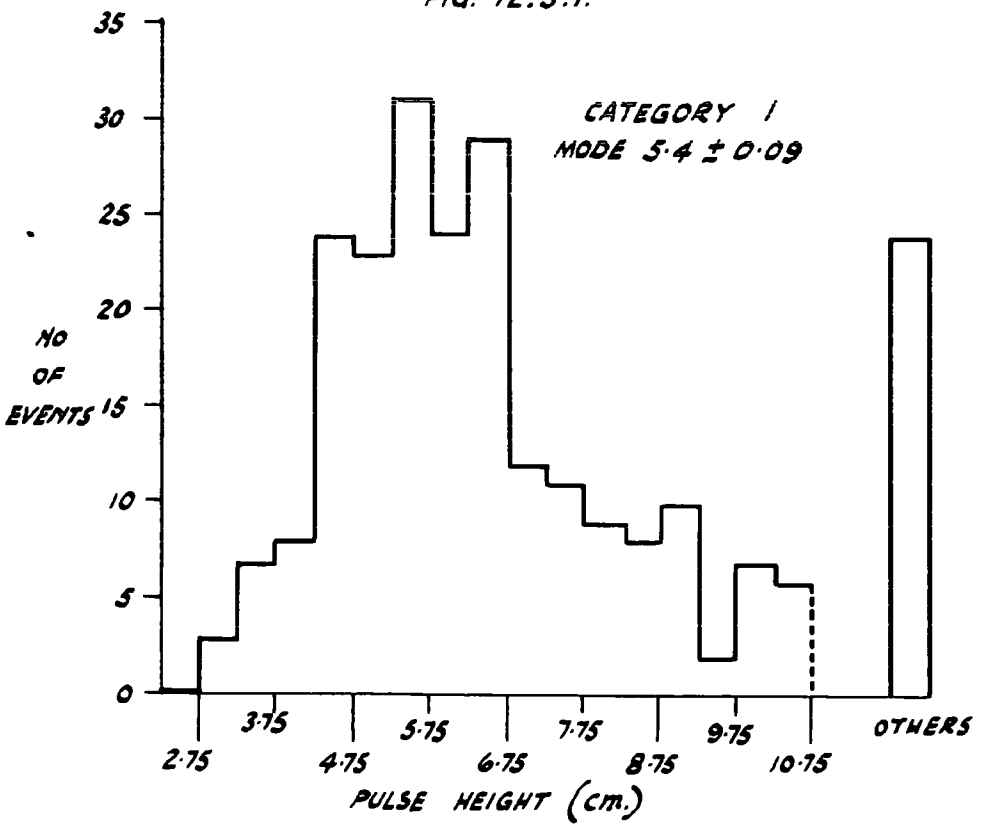

FIG. 12.3.2.

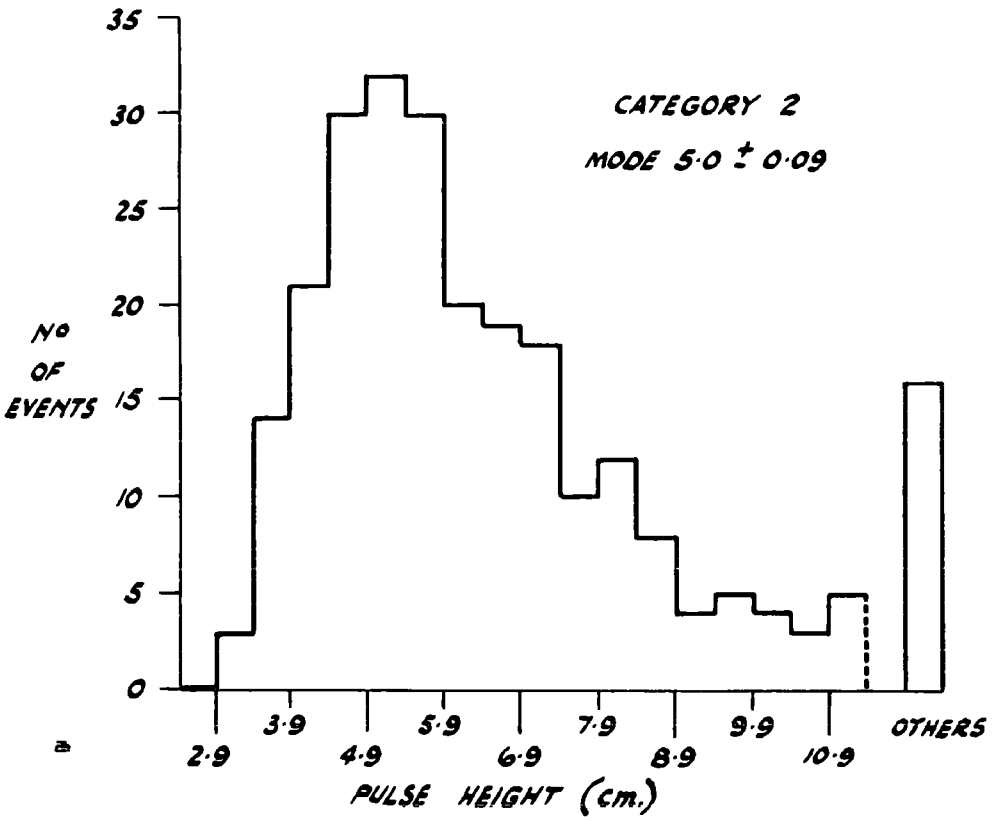

FIG. 12.3.3.

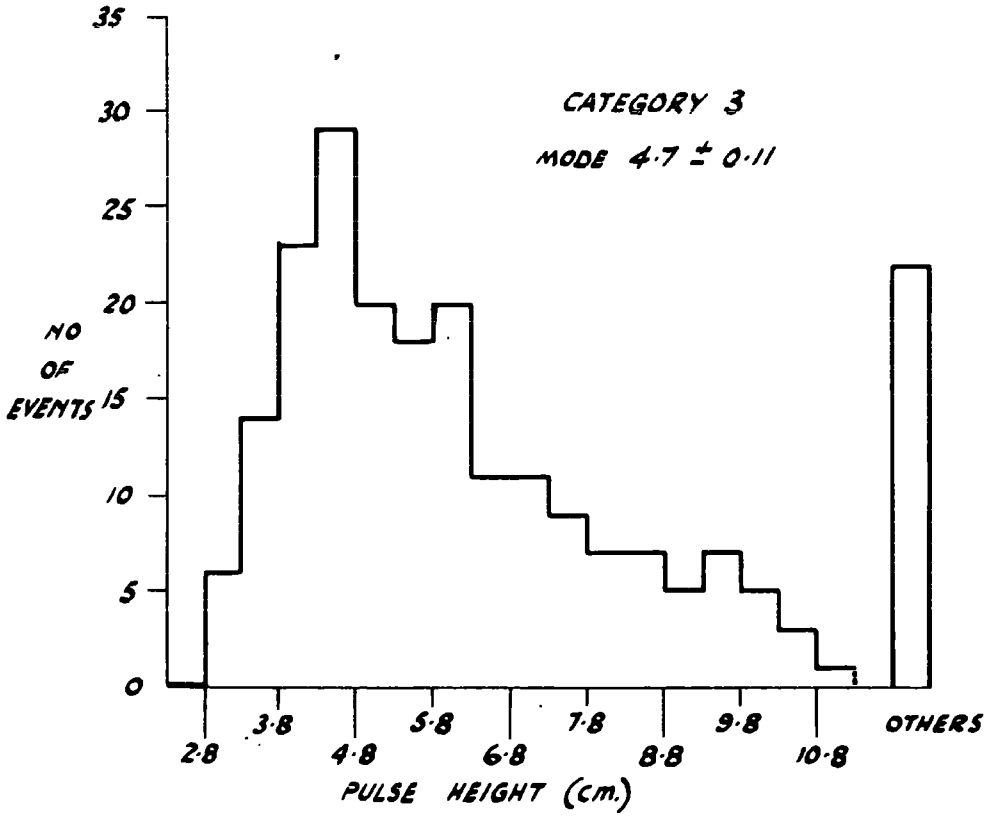

FIG. 12.3.4.

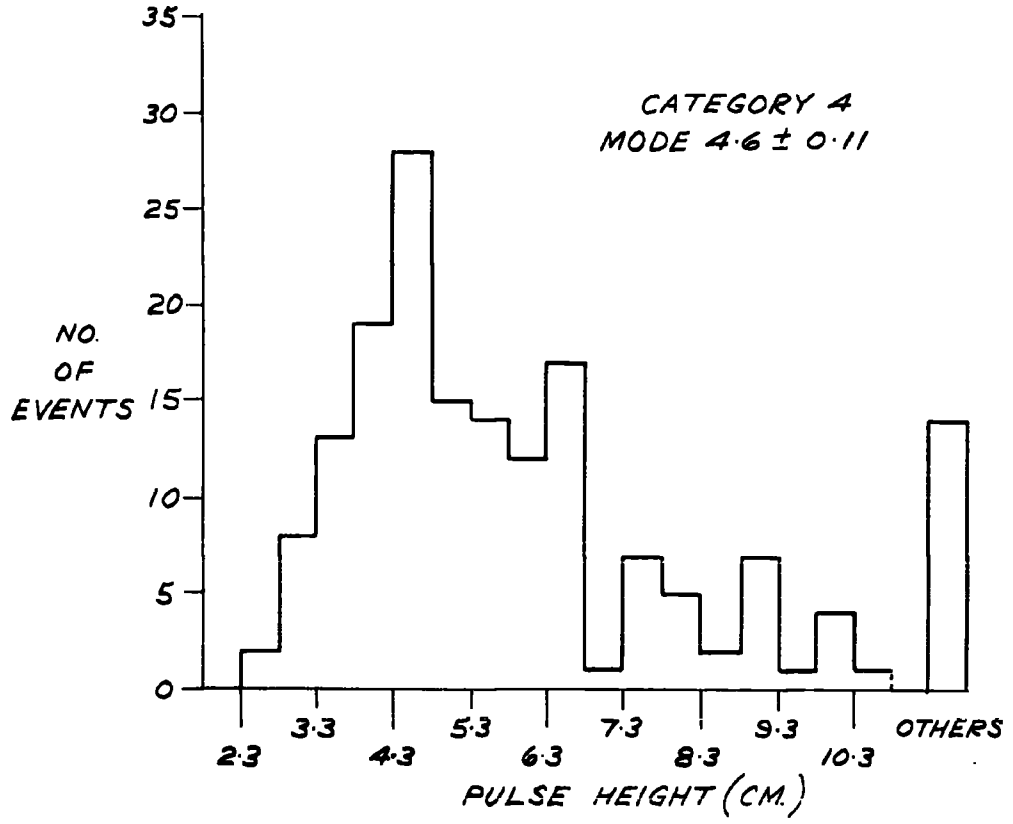

FIG. 12.3.5

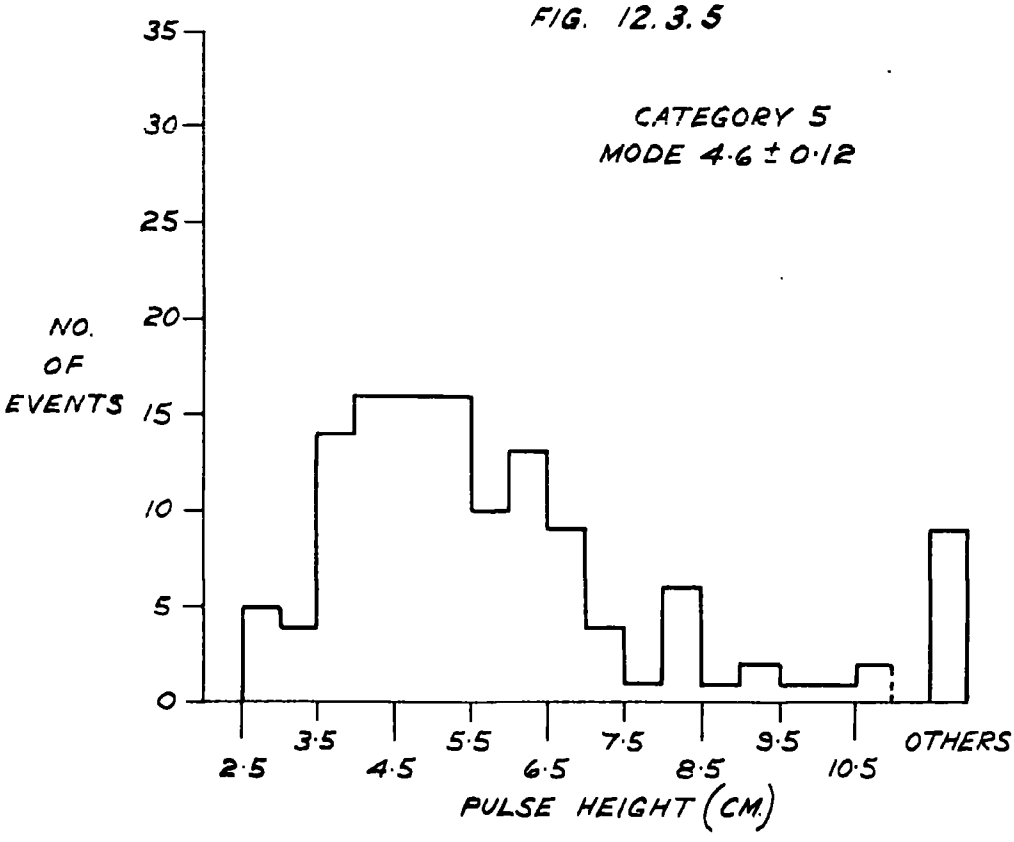

FIG. 12.3.6.

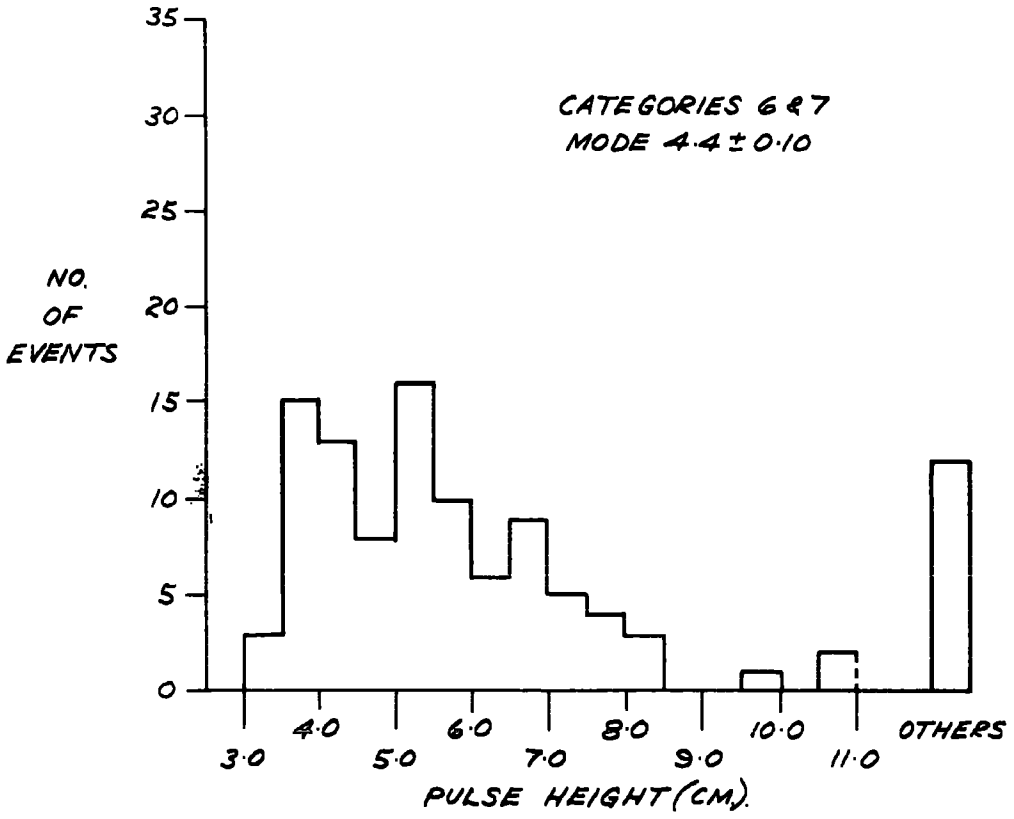

FIG. 12.3.7.

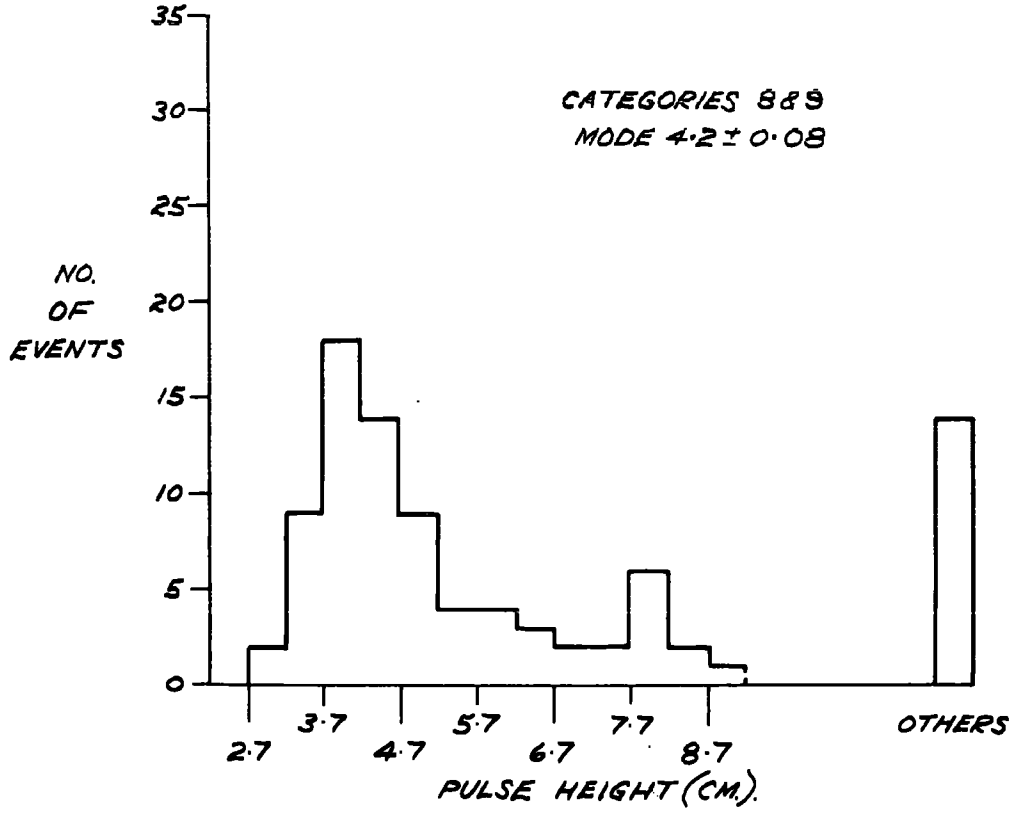

FIG. 12.3.8.

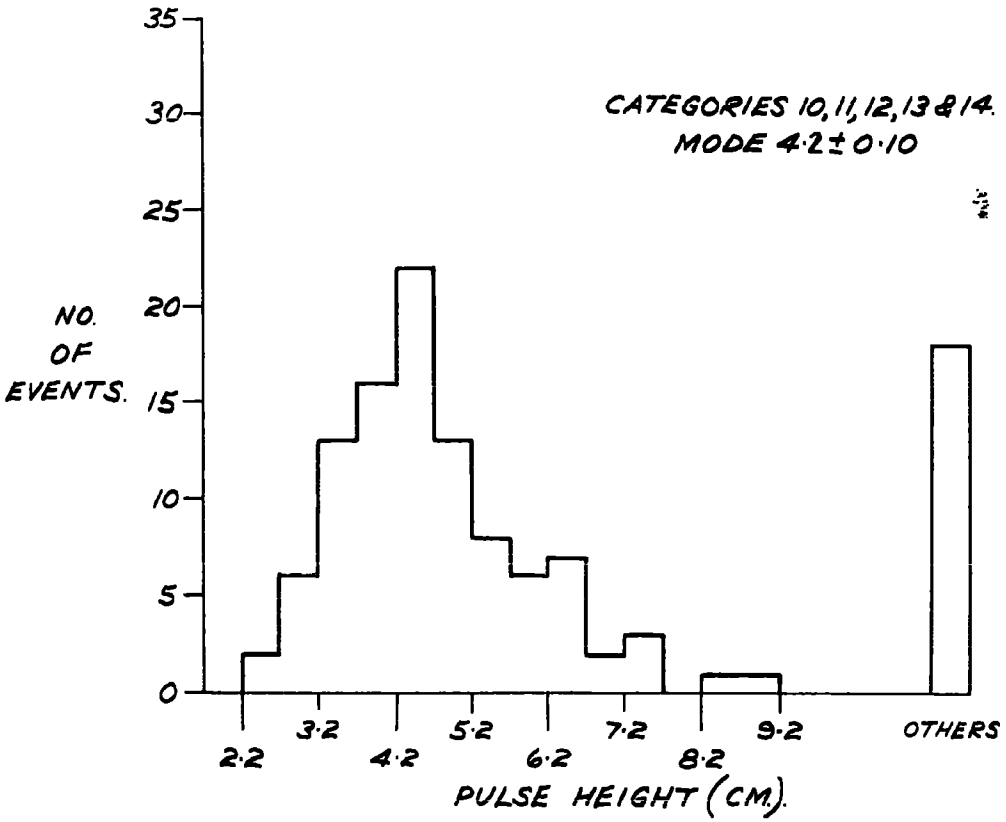
CATEGORIES 10, 11, 12, 13 & 14.
MODE 4·2 ± 0·10
NO. OF EVENTS.
35
30
25
20
15
10
5
0
2·2
3·2
4·2
5·2
6·2
7·2
8·2
9·2
OTHERS
PULSE HEIGHT (CM).

FIG. 12.3.9.

The results as they stand are in the form of pulse heights measured on an arbitary scale and although satisfactory for a relative determination the form of the variation of ionisation with momentum are not directly suitable for comparison with the theoretically predicted values.

12.3.4. Determination of Absolute Values

The conversion of the pulse heights to absolute values of ionisation loss was carried out using the Zn 65 calibrations as follows.

The results of the film record of the pulse height calibrations obtained using a pulse generator were plotted against the corresponding results for the single channel pulse height analyser as shown in Fig. 12.3.10. This relationship was then used to convert the voltage reading on the analyser corresponding to the 8.05 KeV x-ray from Zn 65 into the equivalent pulse height on the film record. The result of this was that 1 cm. pulse height was equivalent to an energy loss of 1.27 ± 0.03 KeV.

12.3.5. The effective mean momenta for the groups

The effective mean momenta for each momentum group was found by :-

1. Calculating the momentum spectrum corresponding to each category or group of categories. This was done as explained in Chapter 3 by taking the sea level momentum spectrum and multiplying it by the acceptance function of the category or categories.

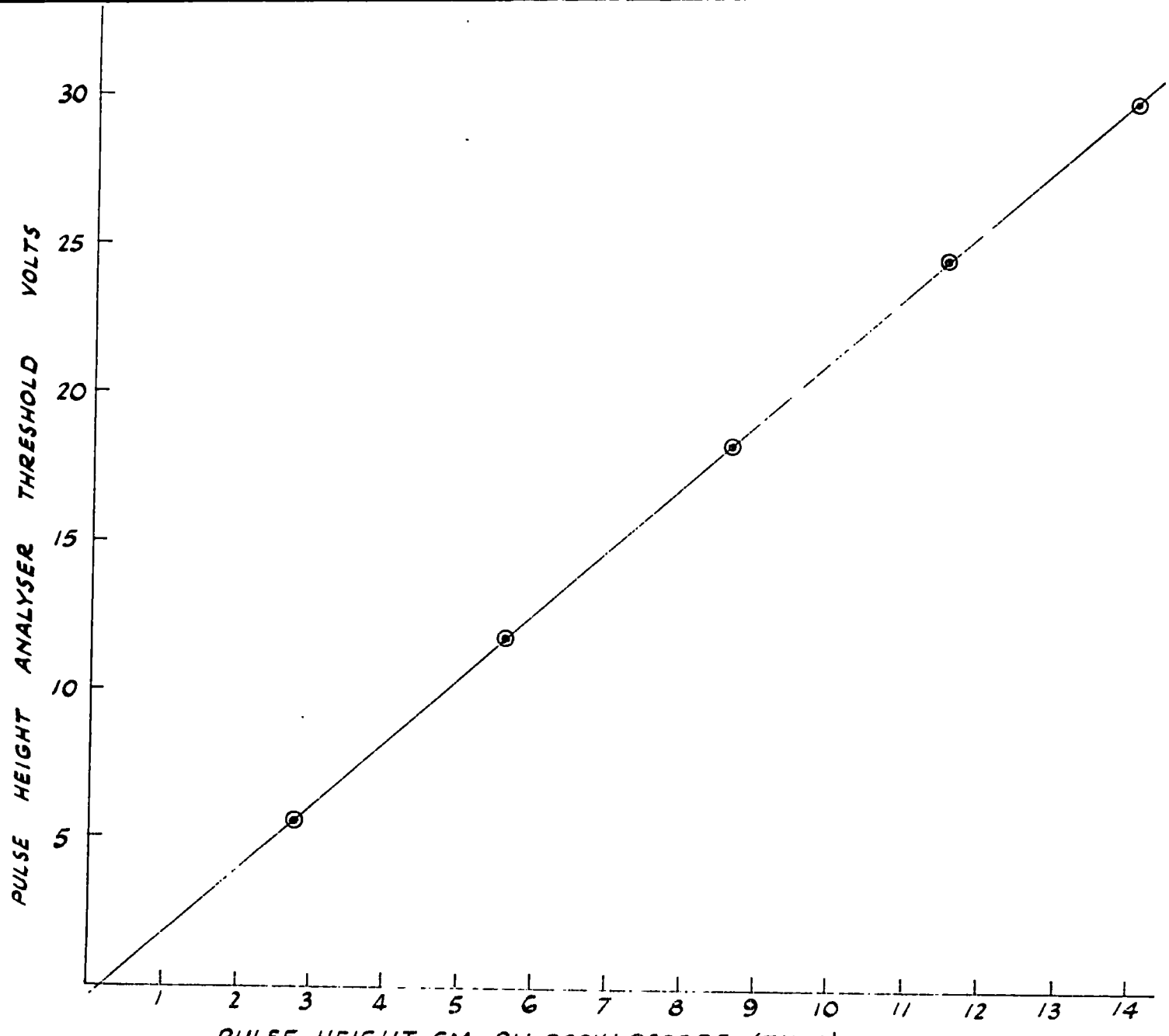

FIG 12·3.10. HEIGHT ANALYSER

2. Weighting this resultant spectrum in terms of the expected variation of ionisation predicted by theory and calculating the mean momentum, i.e. I(p) is the most probable ionisation loss of a particle of momentum p and N(p)dp is the relative number of particles of momentum p→p + dp then the mean momentum $\bar{p}$ is given by:

$$I(\bar{p}) = \frac{\int_0^\infty N(p)\, I(p)\, dp}{\int_0^\infty N(p)\, dp}.$$

which theory is used to predict I(p) is not very important in this instance, since it only introduces a second order uncertainty. If more experimental results were available, and hence higher statistical accuracy, it might be necessary to calculate I(p) by means of successive approximation, but there is no justification for it in this case.

The mean effective momentum for each of the selected groups was calculated by a colleague Mr. R. West, using Sternheimer's theory for the ionisation loss process. This gives for the energy loss the expression:

$$-\frac{1}{\rho_0}\frac{dE}{dx} = \frac{A}{\beta^2}\left[B + 0{\cdot}69 + 2\ln\frac{p}{\mu c} + \ln T_{MeV} - 2\beta^2 - \delta\right]$$

where $A = \frac{2\pi n e^4}{mc^2\rho_0}$, $B = \ln\left[\frac{mc^2}{I^2}(MeV)\right]$, ρ_0 is the density,

& T_{MeV} = the maximum energy transfer in a single collision.

$$= \frac{E^2 - \mu^2 c^4}{\mu c^2\left[\frac{\mu}{2m} + \frac{m}{2\mu} + \frac{E}{\mu c^2}\right]}$$

I = 9.56, A = 0.0761 and B = 17.23 (Rydberg units)

δ = density effect correction.

$$= 4.606\,X + C + a(X_1 - X)^m \quad \text{for } X_0 < X < X_1$$
$$= 4.606\,X + C \quad \text{for } X > X_1$$

$$X = \log_{10}\left(\frac{p}{\mu_c}\right)$$

Neon. $-C = 11.72$, $a = 0.258$, $m = 3.18$, $X_1 = 4$ & $X_o = 2.14$

CH_4 $-C = 9.56$, $a = 0.0552$, $m = 4.22$, $X_1 = 4$ & $X_o = 1.55$

The final results are given in Table 12.3.

TABLE 12.3

Category No.	Mean Momentum (GeV/c)	Most Probable Ionisation Loss (KeV)
0	19.35	6.98 ± 0.28
1	9.2	6.86 ± 0.18
2	4.58	6.35 ± 0.17
3	3.06	5.97 ± 0.18
4	2.29	5.84 ± 0.18
5	1.83	5.84 ± 0.19
6, 7	1.44	5.59 ± 0.17
8, 9	1.09	5.34 ± 0.15
10, 11, 12, 13 & 14	0.82	5.34 ± 0.17

The results are shown graphically in Figure 12.3.11 (open circles) together with the theoretical relationship according to Sternheimer.

The experimental points are seen to all lie below the theoretical curve, the discrepancy being of the order of 5%. As this could be due to systematic error in the calibration process (See Figure 9.2.3) the results have been normalised to fit the theoretical curve at the point for categories 8 and 9 and the normalised values plotted

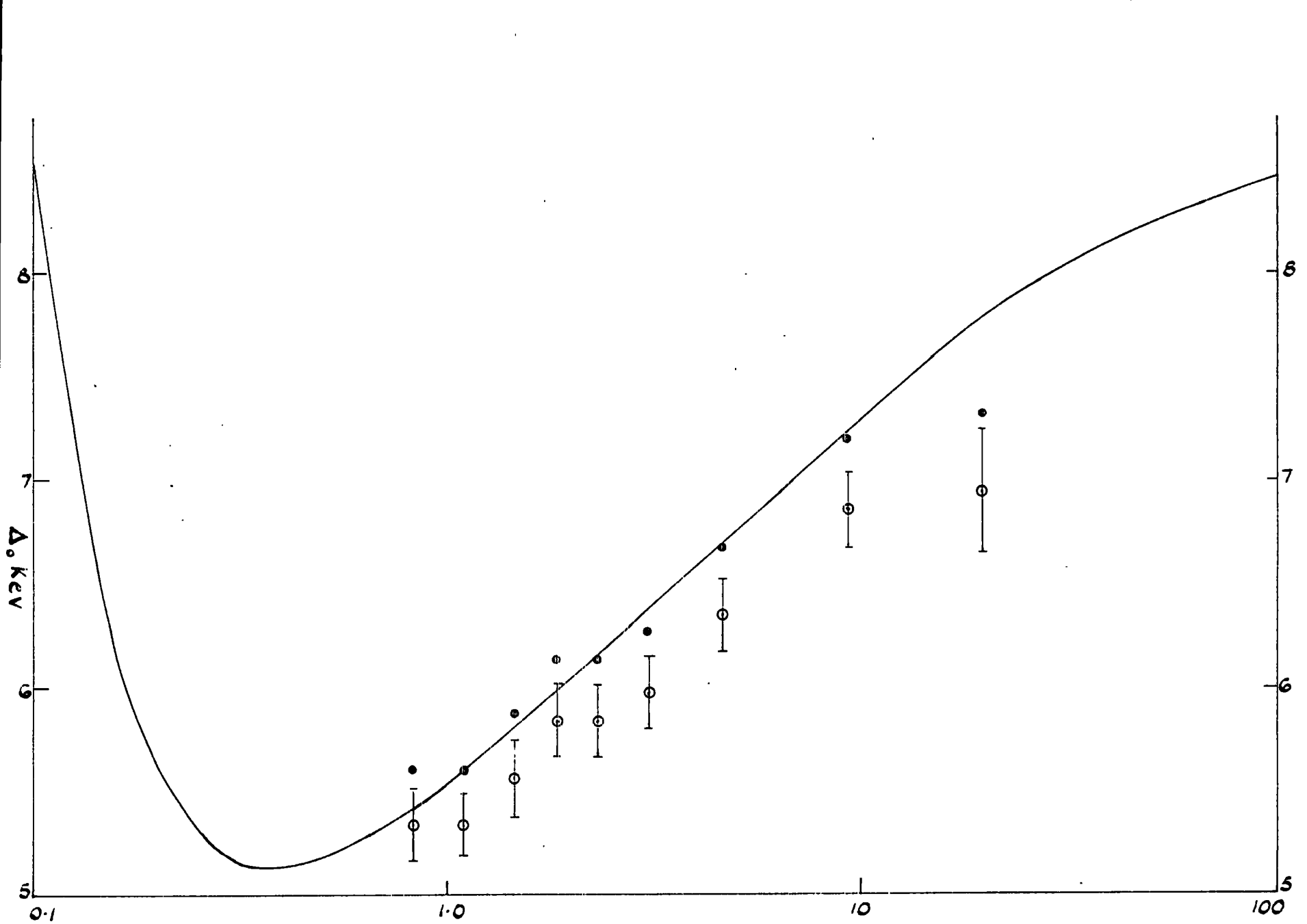

FIG. 12.3.11. MOMENTUM p GeV/c (μ MESONS)

as closed cicles in Figure 12.3.11.

Differences of this nature between the experimental results and the theoretical curve have been noted before and the normalisation procedure is standard practice. The justification for it is that by choosing the normalisation point near to the region of minimum ionisation any uncertainty in the theoretical value of the density correction becomes unimportant.

Systematic errors may enter into the calibration measurements in two ways.

1. There is no experimental evidence to show that the average energy required to form an ion pair in neon of any gas is sensibly constant up to particle energies of ~10GeV. Measurements so far have only been extended up to 340 MeV.
2. The effect of the difference in track length of the ionisation produced by the μ-mesons and that of the photoelectrons produced in the gas by the calibration x-rays. This may lead to an error, as explained in chapter 9, because of the higher probability of re-combination in the denser track and also, because of the shorter time spread in arrival at the critical region of the electrons from the shorter track.

12.4 Conclusions

12.4.1. Ionisation Loss Measurements

Figure 12.3.11 shows that there is good agreement between the normalised results of the present experiment and the theoretical curve of Sternheimer. The statistical accuracy of the results is, however, insufficient to detect an earlier

fall off in the relativistic rise of the form indicated by the results of Eyeions et al (1955) but the results do show that there is no gross discrepancy between experiment and theory in the case of neon as was found, for example, by Kepler et al (1958) in the case of xenon.

In conlusion some comments will be made on the performance of the apparatus.

12.4.2. Performance of the Equipment

The equipment behaved satisfactorily. The slight drift that occurred in one counter chain was due to variation in gain of the head amplifier and was almost certainly caused by changes in resistance of the preset potentiometer used to vary the gain. Replacement of the component should cure this fault.

The work carried out with the equipment suggested a few points which require further investigation and improvement.

These are:

1. A reduction in calibration time. This is mainly concerned with the time taken to determine the position of the Zn 65 peak and the problems can be tackled in two ways. Firstly by replacing the single channel analyser by a multichannel machine and secondly by investigating the possiblity of using stronger sources. At present an order of magnitude increase in source strength is sufficient to spoil the resolution of the spectrum. The transport times in the counter are of importance in this connection,

but so are the differentiating and integrating time constants in the amplifier and adjustment of these may enable a further decrease in waiting time to be obtained.

2. An increase in accuracy of the method for determining the linearity of the amplifying system. In the present instance the measured departures from linearity in the important region are not inconsistent with the errors involved in the measurement. This has not been important so far since the statistical error involved in the measurement of the most probable ionisation loss is so much larger.

3. A more detailed study of the proportional counters. This to include a measurement of the gas multiplication factor along the length of the counter and an accurate measurement of the magnitude of the end effects. The precautions taken in the present experiment with regard to the latter are no doubt adequate. Any remaining effect can only lead to a slight broadening of the pulse height distributions, but broadening due to end effects and imperfections in the anode wire would invalidate any experiments that might be made on the fluctuations in the ionisation loss process and it would be singularly unfortunate if the one central calibration window were situated above an imperfection in the wire. That this is not the case with the counters in this experiment is known from the degree of agreement that exists between the results obtained between the central window and the window that lies 1.3 cm. off centre

and at a distance 3.8 cm along the axis of the counters.

Finally it is considered that the apparatus modified in the way described above, would be suitable for resolving between the different theoretical distributions if an extended series of measurements is made with it.

ACKNOWLEDGEMENTS

The Author wishes to thank Professor G.D. Rochester F.R.S. for his support and interest. He is greatly indebted to him both for allowing an extension to the period of research and for assistance in obtaining an additional grant to cover part of this period.

The Author is deeply indebted to his supervisor, Dr. A.W. Wolfendale for his guidance, help and unfailing encouragement both during his period of research and during the writing of this thesis.

He would like to thank Mr. G. Martin, Reader in Radio-Chemistry at Durham, for considerable help and advice in the preparation and use of radio-active sources for calibration purposes.

He would also like to thank Dr. Smith of the Mathematics Department at Durham for his help with solving some of the problems arising from the use of rectangular shaped proportional counters.

The Author is grateful to his colleagues for their co-operation and for helpful discussions and suggestions.

He wishes to thank Mr. Threadgill and his workshop staff for their considerable assistance both in the construction of apparatus and in the practical solution of some problems that arose during the course of this work.

The Author is indebted to D.S.I.R., for the award of a Research Studentship for the period 1956 - 1959 and for a temporary Research Assistantship from October - December, 1959.

REFERENCES

Ashton, F., Brooke, G., Gardner, M., Hayman, P.J., Jones, D.G., Kisdnasamy, S., Lloyd, J.L., Taylor, F.E., West, R.H., and Wolfendale, A.W., 1960 Nature, 185, 364.

Bakker, C.J., and Segrè, E., 1951, Phys. Rev., 81, 489

Barber, W.C., 1956, Phys. Rev., 103, 1281

Becker, J., Chanson, P., Nageotte, E., Treille, P., Price, B.T., and Rothwell, P., 1952, Proc. Phys. Soc. A, 65, 437

Behrens, D.J., 1951, A.E.R.E. Report T/M50 (H.M. Stationery Office, London, Code Number 70-674-0-42).

Bethe, H.A., 1932 Z Phys. 76, 293; 1933 Handb. der Phys., 24, 515

Blackett, P.M.S., 1937 Proc. Roy. Soc. A159, 1.

Bloch, F., 1933, Ann. Phys. Lpz., 16 285; 1933, Z Phys. 81, 363

Bohr, N., 1915, Phil. Mag., 30, 581; 1948, Det. Kg;. Dans. Vid. Sels., 18, 8

Bradley, E.F., 1955, Proc. Phys. Soc. A68, 549

Budini, P., 1953, Nuovo Cim., 10, 236

Budini, P., and Taffara, L., 1956 Nuovo Cim., 4, 23

Budini, P., Taffara, L., and Viola, C., 1960, Nuovo Cimento 5, 864

Caro, D.E., Parry, J.K., and Rathgeber, H., 1951 Aust. J. Sci. Res. A, 4, 16

Chase, R.L., and Higinbotham, W.A., 1952, Rev. Sci. Inst., 23, 34

Conversi, M., and Gozzini, A., 1955 Nuovo Cim., 2, 189

Coxell, H., and Wolfendale, A.W. 1960, Proc. Phys. Soc. 75, 378

Curran, S.C., et al 1949, Phil. Mag. 40, 939

Elmore, W.C., and Sands, M., 1949, Electronics (McGraw Hill, New York).

Eyeions, D.V., Owen, B.G., Price, B.T., and Wilson, J.G., 1955, Proc. Phys. Soc., A, 68, 793

Fano, U., 1953, Phys. Rev., 92, 328

Fermi, E., 1939 Phys. Rev., 56, 1242; 1940 Ibid., 57, 485

Fowler, G.N., and Jones, G.M.D.B., 1953, Proc. Phys. Soc. A, 66, 597

Gardner, M., Kisdnasamy, S., Rossle, E., and Wolfendale, A.W., 1957 Proc. Phys. Soc. B, 70, 687

Gillespie, A.B., 1953, Signal, Noise and Resolution in Nuclear Counter Amplifier (Pergamon Press, London).

Glaser, D.A., Hamermesh, B., and Safonov, G., 1950, Phys. Rev., 80, 625

Ghosh, S.K., Jones, G.M.D.B., and Wilson, J.G., 1952 Proc. Phys. Soc. A, 65, 68; 1954 Ibid., 67, 331

Gray, L.H. 1944, Proc. Camb. Phil. Soc., 40, 72

Halpern, O., and Hall, H., 1940, Phys. Rev., 57, 459; 1948 Ibid., 73, 477

Hammersley, J.M., and Morton, K.W., 1955 Proc. Phys. Soc. A 68, 793

Hines, K.C., 1955, Phys. Rev., 97, 1725

Holmes, J.E.R., Owen, B.G., Rodgers, A.L., and Wilson, J.G., 1955 Conference on Recent Developments in Cloud Chambers and Associated Techniques, Univ. College, London.

Huybrechts, M., and Schonberg, M., 1952, Nuovo Cim., 9, 764

Hyams, B.D., Mylroi, M.G., Owen B.G., and Wilson, J.G., 1950, Proc. Phys. Soc., A, 63, 1053

Kepler, R.G., Andlau, C.A., Fretter, W.B., and Hansen, L.F., 1958 Nuovo Cim., 7, 71

Landau, L., 1944, J. Phys. U.S.S.R., 8, 201

Messel, H., and Ritson, D.M., 1950 Phil. Mag. 41, 1129

Moroney, J.R. and Parry, J.K., 1954 Aust. J. Phys. 7, 423

Nash, W.F. and Pointon, A.J., 1956. Proc. Phys. Soc. A, 69, 725

Owen, B.G. and Wilson, J.C., 1951 Proc. Phys. Soc. A, 64, 417

Owen, B.G., 1950 Proc. Phys. Soc. A, 63, 1074

Parry, J.K. Rathgeber, H.D., and Rouse, J.L. 1953, Proc. Phys. Soc. A, 66, 541.

Price, B.T., 1955, Rep. Prog. Phys. 18, 52

Puppi, G., 1956, Prog. Cosmic Ray Physics, Ed. Wilson, J.G. Vol. III (North Holland Publ. Co.,)

Rodgers, A.L. 1957nPhd. Thesis (University of Manchester).

Rossi, B., 1952, High Energy Particles (New York : Prentice Hall)

Rossi, B., and Staub, H., 1949 Ionisation Chambers and Counters (McGraw Hill).

Rothwell, P., and West, D., 1950, Proc. Phys. Soc. A, 63, 539

Sharpe, J., 1955 Nuclear Radiation Detectors (Methuen Monograph)

Sternheimer, R.M., 1952, Phys. Rev., 88, 851; 1953 Ibid. 89, 1148, 1953, Ibid, 91, 256; (errata, see Ibid., 1954, 93, 1434); 1954, Phys. Rev., 93, 351; Ibid., 1956, 103, 511

Swann, W.F.G., 1938, J. Franklin. Inst., 226, 598

Valentine, J.M., and Curran, S.C., 1958, Rep. Prog. Phys. 21, 1.

Wick., G.C., 1941 Ric. Scient. 11, 273; 1943, Nuovo Cim., 1 302

Wilson, J.G., 1946, Nature, 158, 415

Wilson, J.G. 1951, The Principles of Cloud Chamber Techniques.
(Cambridge O.U.P.)